Analysis of DNA - ligand interaction in a parallel force-based assay

Katja Maria Limmer

Dissertation
an der Fakultät für Physik
der Ludwig–Maximilians–Universität
München

vorgelegt von
Katja Maria Limmer
aus München

München, den 11.11.2013

Erstgutachter: Prof. Dr. Hermann E. Gaub
Zweitgutachter: Prof. Dr. Dieter Braun
Tag der mündlichen Prüfung: 17.12.2013

Zusammenfassung

Biomolekulare Wechselwirkungen, zum Beispiel zwischen DNA und Proteinen, sind sehr vielfältig. Ihre Charakterisierung erfordert hochgradig parallele und universal einsetzbare Untersuchungsmethoden. Kraftmessungen an einzelnen Molekülen können die Wechselwirkungen unterschiedlicher molekularer Komplexe auch in dichten Medien quantifizieren ohne die molekulare Bindung durch eine Farbstoffmarkierung zu beinflussen. In den meisten Fällen haben diese Methoden allerdings einen sehr geringen Durchsatz. Die Technik des *Molecular Force Assay* (MFA) umgeht diesen Nachteil, indem zwei molekulare Bindungen miteinander verglichen werden. So können tausende molekulare Wechselwirkungen parallel untersucht werden, ohne dass die Messung den Einzelmolekül-Charakter verliert. Ziel dieser Arbeit war eine Weiterentwicklung des MFA, um dessen Anwendbarkeit auf aktuelle biologische Fragestellungen zu erweitern.

Als erstes wird ein Aptamer-Sensor für die Charakterisierung kleiner Moleküle beschrieben. Aptamere sind Oligonukleotide, die spezifisch einen bestimmten Liganden binden. Eine Aptamersequenz als Teil einer der beiden molekularen Komplexe führt zu dessen Stabilisierung durch die Bindung mit dem Liganden, so dass das bindende Molekül auch in komplexen Flüssigkeiten analysiert werden kann. Dieser kraftbasierte Nachweis der Aptamer-Ligand Wechselwirkung ermöglicht auch eine Charakterisierung von kleinen oder nur schwach bindenden Molekülen, da auf zusätzliche Techniken zur Signalverstärkung oder Waschprozeduren verzichtet werden kann. Die Dissoziationskonstante kann dank des Parallelformats in einer einzigen Messung bestimmt werden. Ein kraftbasierter Aptamer-Sensor ist somit ein vielversprechendes Instrument für eine schnelle Charakterisierung kleiner Moleküle in dichten Medien.

Des Weiteren wird gezeigt, dass sich der MFA zur Suche RNA-bindender Moleküle eignet, die gleichzeitig das Protein Dicer inhibieren. Dicer spielt bei der RNA Interferenz, ein Mechanismus der Genregulation mit Hilfe kurzer Stücke nichtkodierender RNA, eine entscheidende Rolle, indem er lange, doppelsträngige RNA in kurze Segmente von 19-22 Basenpaaren schneidet. Diesen Vorgang gezielt zu verhindern ist ein vielversprechender Ansatz bei der Entwicklung neuer medizinischer Therapien. Der MFA kann sowohl verlässlich die Dicer-Aktivität messen als auch die Dissoziationskonstante des RNA-Liganden bestimmen. Werden die molekularen Komplexe des MFA mit dem RNA-bindenden Molekül und Dicer inkubiert, kann eine gezielte Hemmung von Dicer beobachtet werden, die mit der Konzentration des Liganden korreliert. Dies zeigt, dass der MFA eine effektive Methode zur Suche von RNA-bindenden Molekülen ist, die gleichzeitig das Protein Dicer an der Produktion kleiner RNA Segmente für die RNA Interferenz hindern.

Als drittes wird die Eignung des MFA zur Quantifizierung von Protein-DNA Wechselwirkungen untersucht. Um den komplexen Vorgang der Transkription zu verstehen, ist es unabdingbar, die Wechselwirkungen der beteiligten Proteine mit der DNA im Nukleus genau zu bestimmen. Durch die große Zahl von Wechselwirkungen sind Methoden mit hohem Durchsatz unerlässlich. In einer Weiterentwicklung des MFA kann die Bindungsstärke eines Zinkfinger-Proteins mit drei verschiedenen DNA-Motiven durch den Vergleich mit zwei unterschiedlichen Referenzen in einer einzigen Messung quantifiziert werden. Dieses Experiment zeigt eindrucksvoll das Potential des MFA, zum Verständnis des komplexen Mechanismus der Transkription beizutragen.

Zusammenfassend präsentiert diese Arbeit drei Anwendungen des MFA, die zur Lösung sehr unterschiedlicher biologischer Fragestellungen beitragen können.

Summary

Biomolecular interactions like protein-DNA binding are very diverse. Their analysis requires highly parallel assays that are easily adaptable for the characterization of various molecular complexes. Single-molecule force measurements can quantify the interaction of different molecules even in complex ambients without disturbing the molecular bond by labeling, but are in most cases low throughput. The technique of the Molecular Force Assay (MFA) overcomes this drawback by comparing two molecular bonds with each other. It allows the analysis of thousands of molecular interactions in parallel without losing the single-molecule character. The objective of this thesis was to adapt the technique of the MFA for new applications that have the potential to contribute significantly to the solution of current biological problems.

First, a force-based aptamer sensor for the characterization of small molecules is described. Aptamers are oligonucleotides that are selected for their ability to bind a certain ligand with high specificity. Implementing an aptamer into one of the bonds of the MFA enables the detection of its ligand even in complex fluids by a strengthening of this bond upon ligand binding. The force-based detection of the interaction between aptamer and ligand enables the characterization of low affinity binders or small molecules without relying on signal amplification or stringent washing requirements. The parallel format allows the determination of the dissociation constant in a single measurement. Thus, a force-based aptamer sensor is a promising analytical tool for a fast characterization of analytes in complex fluids.

Second, the application of the MFA as a screening tool for RNA binders that selectively inhibit the protein Dicer is demonstrated. Dicer is a fundamental part of the RNA interference mechanism that regulates gene expression with small non-coding RNA sequences. Dicer matures the small RNAs by cutting the precursor molecules into pieces of 19-22 base pairs. The selective inhibition of Dicer by a ligand that binds specifically to a certain precursor molecule has a great potential for future medical therapeutics. The MFA can reliably detect Dicer activity and characterize possible RNA binders by determining the dissociation constant. If both the ligand and Dicer are added to a MFA sample, Dicer is clearly inhibited upon ligand binding in relation to the ligand concentration. Hence, the technique of the MFA is a valuable tool to screen for RNA binders that selectively hinder Dicer from maturing the precursor molecule upon ligand binding.

Third, the MFA is applied to quantify DNA-protein interactions by measuring their binding strength. In order to understand transcription, identifying how strong a protein binds to the genomic DNA is essential. Due to the huge number of DNA-protein interactions that participate in transcriptional regulation, high throughput methods for the analysis of these interactions are highly desirable. As a proof-of-principle, the MFA quantifies the interactions of a zinc finger protein with three DNA motifs by comparing them to various reference bonds within a single measurement. Further miniaturization can easily extend the setup's capacity in terms of multiplexing. This illustrates the potential of the MFA to quantify protein-DNA interactions in a highly parallel format in order to contribute to the understanding of transcriptional regulation.

Conclusively, this thesis demonstrates the various applications of the Molecular Force Assay in biological sciences by means of three distinct examples that cover a wide area of biological problems.

Contents

List of Figures

Chapter 1

Introduction

Biological processes are very complex due to the multitude of involved molecules and molecular interactions. Examples are cell division, photosynthesis or the interplay of cells in multicellular organisms. Signals from the environment are absorbed and converted into actions like movement in a certain direction or the synthesis of certain proteins to metabolise a new nutrient. Understanding these processes and, one step further, influencing them is the aim of biological sciences. A combination of techniques and perspectives, biological, chemical, but also physical or computational, offer the greatest chance to achieve this aim. This has already been proven in the past with the human genome project as the most prominent example. Between 1990 and 2003, several institutes and reasearch groups from multiple countries and with different scientific background combined their efforts and techniques to decipher the human DNA code. In April 2003, a consortium presented 99 % of the sequence of the 20600 human genes. Additionally, the human genome project deciphered the genomes of several model organisms and, importantly, led to the development of new and the improvement of existing sequencing techniques (for more information see [1]). Some of these methods and developments are based on physical principles, for instance gel electrophoresis or fluorescence-based sequencing techniques. The application of physical knowledge in biology has a far-reaching tradition of several decades. A prominent example is the discovery of the helical structure of double-stranded DNA molecules by x-ray diffraction [2][3][4]. Today, structural analysis of biological molecules like proteins by x-ray diffraction or nuclear magnetic resonance is a standard method and has helped to elucidate the binding properties of many molecular complexes.

Another physical application that has made a great contribution to our understanding of biological processes is the development of the atomic force microscope (AFM) by Gerd

Binnig et al. in 1986 [5]. This technique enables the measurement of very small forces (piconewton) between a surface and a cantilever tip and was developed to image surfaces by scanning the very sharp tip over the sample while the interaction force between surface and tip is measured via cantilever deflection. If the interaction force is held constant, it can be used to create a topographical image. For biological systems, the stability and interaction forces between single molecules are of utmost importance. Those quantities can be determined by attaching the molecule or molecular complex under investigation between surface and tip. Removing the tip from the surface, the molecule is loaded with a force that is measured by monitoring the cantilever deflection. Additionally, the distance between surface and tip is determined. The resulting force-extension-curve is analyzed for information like the elasticity of a molecule, the unfolding of single molecular domains or the most probable rupture force. The ability to characterize a single molecule or bond renders this application of the AFM especially powerful as it offers the possibility to detect rare events, transient phenomena, conformational changes and molecular heterogeneity, aspects that are not accessible in bulk measurements. Examples for the successful investigation of biological structures and processes by AFM are the analysis of DNA melting [6][7][8], ligand and receptor pairs [9][10][11], protein unfolding[12] or cell adhesion[13][14]. Furthermore, the AFM can also be applied to position single DNA molecules or proteins with nanometer precision [15][16][17]. Despite the unprecedented insights into biological systems and the great potential, AFM suffers from some severe drawbacks. One is the limited force resolution (around $10pN$) that is determined by the size of the cantilever [18]. This problem can be partly circumvented by measuring forces with optical or magnetic tweezers. But these two techniques come with other limitations. Optical tweezers operate in a very small force range of $0.1pN - 100pN$ and the optical trapping itself might heat or photodamage the sample. Magnetic tweezers can apply forces over a broad range but those forces are only constant in a very small area due to the steep gradient of the magnetic field. In addition, a force control similar to AFM requires sophisticated technical components [19]. But the most severe limitation for all force spectroscopy techniques is the great effort necessary to measure and analyze unbinding forces that makes them unsuited for large-scale investigations. In contrast, biological processes might follow common principles but the individual interplay of molecules differs greatly in the details. Examples are protein-protein interaction or DNA-protein binding. Furthermore, force-based techniques offer unique advantages like probing the molecule or molecular interaction itself without labeling or being sensitive to complex backgrounds. In addition, quantification of the binding strength between

molecular complexes cannot be accessed by other methods. Hence, force-based techniques that are compatible with high-throughput systems are highly desirable.

A possible realization for a parallel, force-based technique is the Molecular Force Assay (MFA). In the MFA, the macroscopic force transducer, the cantilever or bead, is replaced by a molecular bond, in most cases a well-characterized DNA duplex which acts as reference bond. This reference bond is connected in series with the sample bond, the molecular complex in question. If a force is applied to this whole construct of sample and reference bond, the weaker one will rupture with a higher probability and a fluorophore attached to the linker polymer between the two bonds will indicate the intact molecular complex. Thus, the MFA does not record forces or extensions, but compares the two molecular bonds with each other. As the binding strength of the two complexes are of the same order of magnitude, very small differences in molecular stability can be resolved. A skillful choice of sample and reference complex enables a good characterization of the sample bond. The molecular construct of sample and reference bond is connected to two surfaces that are separated in order to apply a force to the bonds. Since every sample bond is only compared to its own reference without being disturbed by other molecules attached nearby to the surfaces, thousands of molecular constructs can be tested within several square micrometers. Hence, the statistics of a single measurement already allow to draw valid conclusions. Depending on the technical implementation, several sample bonds can be tested against multiple references so that a single experiment enables the characterization of the molecule under investigation. So far, the MFA was applied to detect single nucleotide polymorphism [20], study differences in antibody/antigen interactions [21], investigate the chiral binding selectivity of small peptides [22][23] and analyse the interaction of the proteins EcoR1 and p53 with different DNA sequences [24][25].

The objective of this thesis was to adapt the MFA for further applications in biological science that have the potential to contribute significantly to the solution of current biological problems. This was achieved for very different biological problems. Publication P1 demonstrates the characterization of an analyte in a complex background by the implementation of a split aptamer into the sample bond. An aptamer is an artificial oligonucleotide that is selected from a random pool for its specificity to its ligand. Here, an adenosine-selective aptamer was integrated into the sample bond. Its ligand was reliably detected by the stabilization of the sample bond upon ligand binding. Furthermore, the measurement is not affected by complex ambients and does not require stringent washing steps that often makes it difficult to detect transient interactions and low affinity binders. Varying

the ligand concentration allowed the determination of the dissociation constant in a single MFA measurement. Techniques that can capture analytes in complex fluids and quantify their concentration are highly desirable for diagnostic purposes. P1 describes a proof-of-principle for the detection and characterization of a small molecule by an aptamer in a force-based assay. The parallel design allowes to extend the assay easily for the analysis of multiple small molecules by the integration of additional aptamers.

The RNA interference mechanism is the motivation for publication P2. Small RNA duplexes are matured by the protein Dicer that cuts double-stranded RNA into pieces of 19-22 base pairs independently of their sequence. One of the matured RNA strands is integrated in a protein complex known as RNA-induced-silencing-complex that binds to messengerRNA at least partly complementary to the small RNA strand and, in most cases, hinders protein translation [26]. Several classes of small RNAs exist that differ in their origin and function, for instance short-interfering RNA (siRNA) or microRNA (miRNA). Number and kind of the naturally occuring miRNAs in a cell depend on the stage of the cell cycle and health status. The quantity of some miRNAs is greatly increased in connection with severe illnesses like cancer [27]. Hence, the selective inhibition of single microRNA precursors might be a first step in the development of a new generation of medical therapeutics. Here, the application of the MFA comprised a screening assay for RNA ligands that selectively inhibit Dicer from cleaving and, thus, maturing the small RNA precursor. The activity of the protein Dicer can easily be detected in a force-based assay as it greatly destabilizes the sample bond by cutting off about 20 basepairs in comparison to a DNA reference that Dicer cannot process. As a proof-of-principle, a RNA aptamer for the aminoglycoside paromomycin was integrated into the RNA duplex and a selective inhibition of Dicer processing upon ligand binding was detected by means of the MFA. Additionally, the dissociation constant of paromomycin to its aptamer was measured. Hence, the MFA can be applied to screen for and analyze miRNA ligands that selectively hinder Dicer from cleaving. The parallel format of the MFA offers the possibility to screen for several ligands or multiple miRNAs within a single experiment.

A great part of gene expression is regulated at the transcription stage by protein-DNA interaction. These transcription factors bind to some DNA sequences with high affinity, to others with only low affinity or not at all. Recent studies demonstrate that not only strong interactions control transcription but that weak protein-DNA binding contributes significantly to transcriptional regulation [28][29]. In order to understand and influence the regulation network that governs transcription, a quantification of the interaction of the ma-

jority of transcription factors with genomic DNA is of utmost importance. But not only the gigantic number of interactions is a challenge. Low affinity binders might easily be missed, especially by methods that rely on stringent washing procedures. Furthermore, affinity or thermodynamic constants might not be the best quantities to characterize protein-DNA interaction in a nuclear environment, where a transcription factor will probably always be bound to some DNA sequence due to the high concentration of DNA inside the nucleus. Specificity that comprises the discrimination between high and low or no binding sequences is better suited to characterize the binding properties of a protein. Binding strength is a quantity analogous to the specificity and is accessible in force measurements. Manuscript M1 describes an adaptation of the MFA which enables the quantification of the binding properties of a six zinc finger construct against three sample sequences, a high affinity, a low affinity and a no binding DNA sequence in comparison to two reference DNA duplexes in a single measurement. Weak interactions can also be detected without problems since the force measurement is performed under equilibrium conditions. Furthermore, the parallel format of the MFA allows its extension to the testing of additional DNA sequences or proteins within a single experiment. Thus, with further miniaturization and parallelization, the MFA has a great potential to contribute to the understanding of transcriptional regulation.

Conclusively, this thesis demonstrates three new applications for the technique of the Molecular Force Assay in biological science in order to contribute to the understanding of biological processes like gene expression. For this purpose, chapter 2 introduces the relevant biological molecules and processes, while chapter 3 describes the Molecular Force Assay in greater detail. Chapter 4 summarizes the results of the publications P1 and P2 as well as of manuscript M1. A short outlook describes additional possibilities for the application of the MFA in biological science.

Chapter 2

Biological Background

Gene expression can be summarized in the phrase "from DNA to RNA to protein". After a very short introduction into the mechanism of gene expression, this chapter describes the molecules of interest for this thesis, especially the oligonulceotides DNA, RNA and aptamers, and the cellular processes that gave the motivation for the experiments of this thesis.

2.1 Very short introduction into gene expression

The genetic information is stored in the DNA sequence of a cell. In order to use this information, the cell has to translate the genetic code into functional units, the proteins. In a process called transcription an RNA copy of a DNA sequence is produced. This RNA can be translated in an amino acid polypeptide that folds into a three-dimensional structure and forms the functional protein. This flow of information from DNA to RNA to protein is called gene expression and is valid for all living cells. Proteins are the main constituents of a cell and are engaged in nearly every task that is performed in and by the cell, from structure, signaling or transport to metabolism. Different tasks in a cell's life or changing environmental conditions require different proteins so that the regulation of gene expression is of utmost importance for the cell. Especially in multicellular organisms, differentiation between various cell types like muscle or nerve cells arises by the expression of different RNA molecules and proteins. Gene expression can be influenced at every stage from transcriptional initiation to post-translational modifications. Compared to prokaryotes that lack cellular compartments, eukaryotes offer additional possibilites for gene regulation due to their intracellular structure of nucleus and cytoplasma. Differences

in chromatin structures caused by histone modifications change the accessibility of certain DNA sequences. After transcription, modulation of capping, splicing and polyadenylation of the messengerRNA as well as the nuclear export rate or sequestration of the RNA transcript alter the rate of gene expression. Thus, gene expression is an extremely complex mechanism that requires a multitude of molecular interactions.

2.2 Oligonucleotides

The oligonucleotides DNA (deoxyribonucleic acid) and RNA (ribonucleic acid) are also known as the molecules of life and are crucial for the transmission, expression and conservation of genetic information. DNA as the carrier of the genetic information has to be very robust against external influences. RNA is the bridge between the genome and the functional protein. The information stored in the DNA is transcribed into messengerRNA (mRNA), which in turn is translated into a protein. Additionally, non-coding RNA plays a vital role in the processes that regulate transcription and translation.

2.2.1 DNA

A DNA molecule is a polymer chain consisting of nucleotides. A nucleotide is composed of the pentose sugar 2-deoxy-D-ribose, a phosphate residue and one of four different nitrogen heterocyclic bases. Cytosine and thymine are monocyclic pyrimidine derivatives, while adenine and guanine are bicyclic purines (see Figure 2.1 A). Nucleotides are covalently linked together by phosphodiester bonds between the phosphate group attached to the 5' hydroxyl group of the pentose sugar molecule and the 3' hydroxyl group of the next pentose. Hence, a DNA polymer has a 5' end and a 3' end (see [30] for additional information). Typically, two antiparallel DNA strands compose a double helix as was shown in 1953 by J. Watson and F. Crick [4]. The negatively charged sugarphosphate groups constitute the backbone of the helix, while the opposing nucleobases form pairs in the core of the helix (see Figure 2.1 B). In the most stable configuration adenine binds thymine via two hydrogen bonds and guanine pairs with cytosine via three hydrogen bonds. This is known as Watson-Crick base pairing.

Three variants of the double helix are possible, A-form, B-form or Z-form that differ in chirality, tilt and depth of major and minor groove [30]. Under physiological salt conditions, the B-form dominates and is displayed in Figure 2.1 B. These three structures occur in many variations, for example the rise per base pair depends on the sequence. The irreg-

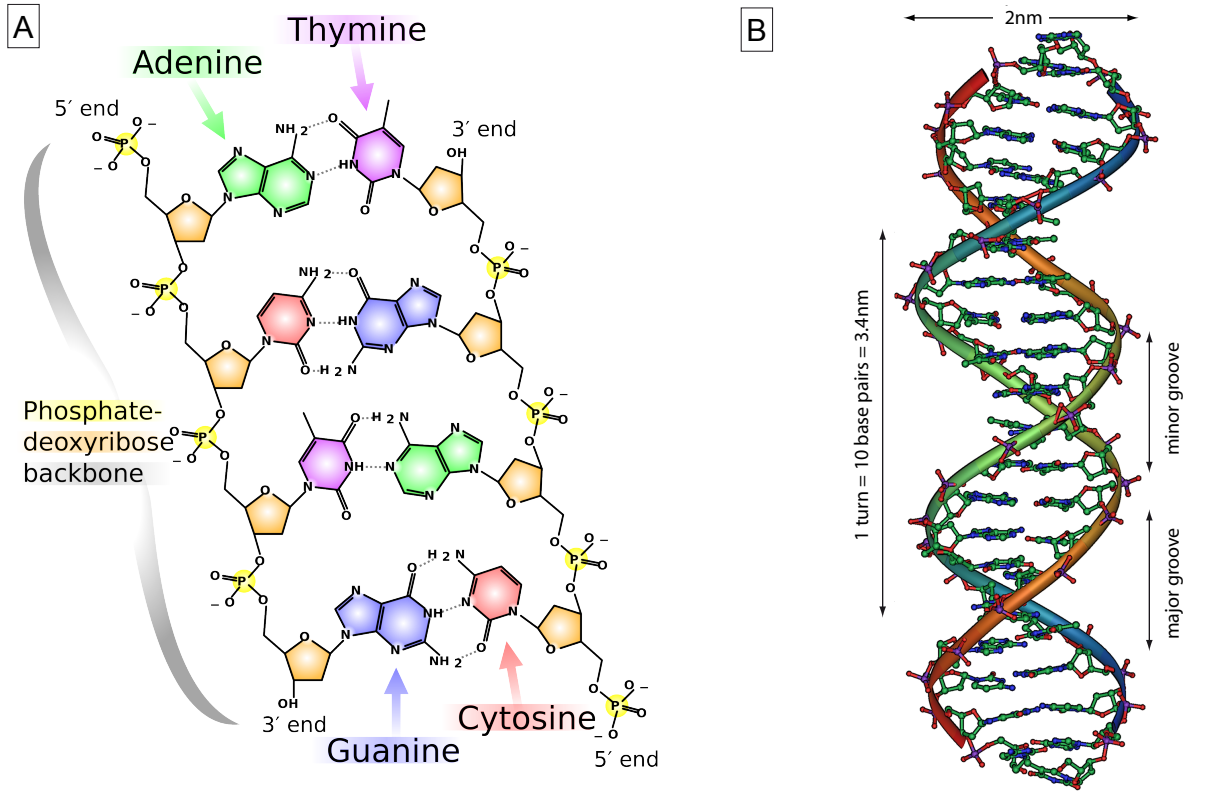

Figure 2.1: Double-stranded DNA. (A) The nucleotides are joined via phosphodiester bonds. Two strands are connected antiparallely by hydrogen bonds between the Watson-Crick base pairs and form a double helix. (B) Depending on the environmental conditions, the DNA duplex can adopt different helical variants. The B-form dominates under physiological conditions (adapted from [31]).

ularities in the double helical structure are assumed to play an important role in protein recognition and binding or in other interactions involved in the process of transcription and replication [30]. Non-Watson-Crick base pairing and base mismatches also alter the double-strand structure and are especially relevant for synthesized oligonucleotides and aptamers described in detail in Chapter 2.2.4.

The specific sequence of the four nucleobases codes the genetic information. This system is very simple but also very versatile since a DNA molecule of n nucleotides can consist of 4^n different sequences. Additionally, the double-stranded nature and the backbone structure account for the robustness of a DNA molecule. These properties, specificity, simplicity and robustness, render the DNA so special and are the reason for its usage in nanotechnological applications. Its ability to build programmable sequence-specific duplexes by self-assembly enables the construction of two and three-dimensional structures, DNA origami, [32][33] and molecular nanodevices [34][35]. Furthermore, DNA duplexes can be applied as force sensors in force-based techniques like the Molecular Force Assay (see Chapter 3).

2.2.2 DNA as a force sensor

Several factors influence the thermal stability of a DNA duplex. Watson-Crick base pairing and stacking interactions [36] between the nucleobases stabilize the DNA structure. Hence, sequences with a majority of CG pairs melt at higher temperatures compared to strands with a majority of AT pairs. Mismatches and bulges disrupt the double-stranded structure and weaken the complex. The negatively charged phosphate backbones reject each other depending on the salt concentration of the buffer system and can have a destabilizing effect. Furthermore, two entropic effects weaken the DNA duplex. First, double-stranded DNA has a persistence length of $50nm$ at a $[Na^+]$ concentration of around $0.1M$ [37] and is, thus, rather rigid. Single-stranded DNA is considerably more flexible and environmental conditions influence its mechanical properties significantly stronger. As a consequence, the persistence length of single-stranded DNA varies from of $0.75nm$ at high salt concentrations to $10nm$ at low ionic strength [35]. Second, the entropy of the solvent also has a destabilizing effect since the hydration shell of a DNA duplex is greater than of two single strands. Both effects counteract the formation of a DNA duplex and reduce its stability. Summarizing, all these effects influence the thermal stability of a DNA duplex and have to be taken into account when analyzing the behavior of DNA under force.

There are two geometries to melt a DNA duplex under force. In shear geometry, the force is applied parallely to the long axis of the DNA helix and all base pairs are stretched

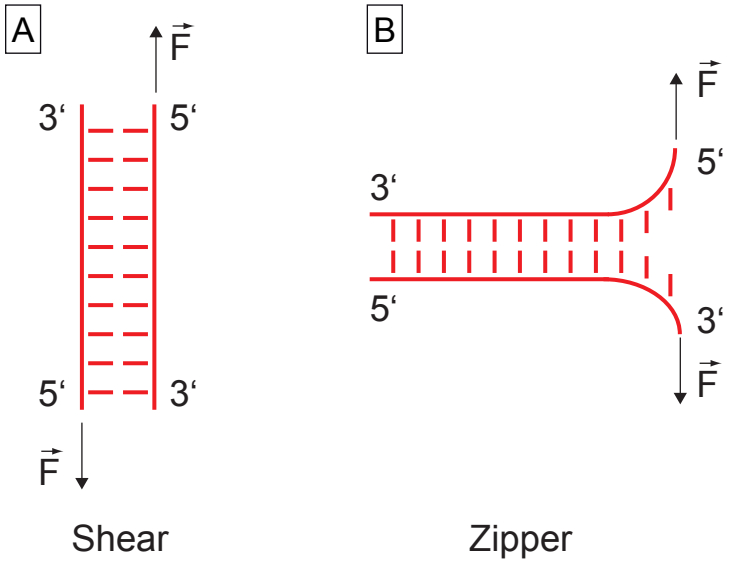

Figure 2.2: Two geometries to melt a DNA helix. (A) In shear geometry the force $\vec{F}$ is applied in the direction of the longitudinal axis of the duplex and the entire helix is loaded. (B) In zipper geometry, the base pairs are melted separately from one end to the other.

simultaneously, as displayed in Figure 2.2 A. Thus, an elongation of the DNA duplex leads to higher rupture forces. Additionally, the rupture force depends on the force loading rate [38]. For this work, DNA sequences between 20 and 40 base pairs were used that melt between $35pN$ and $50pN$ [38]. It is important to notice that the force is applied to either the two 5’ ends or the 3’ ends since the stretching mode of the helix and, thus, the unbinding pathway differs according to the direction the force is applied as was shown by [39]. In zipper geometry, the DNA is melted from one end and one base pair at a time is ruptured (see Figure 2.2 B) in a quasi-equilibrium process. The forces needed to separate the individual base pairs could be determined to $10pN$ for A-T and $20pN$ for C-G and are independent of the force loading rate [7][40]. Consequently, the forces to melt double-stranded DNA depend on the unbinding geometry. This principle is used in a technique known as Single Molecule Cut & Paste (SMC&P) that applies a hierarchical rupture force system in order to position individual molecules with nanometer precision [15][16]. Both unbinding modes can be utilized in the Molecular Force Assay. They are chosen according to the properties of the system to be investigated.

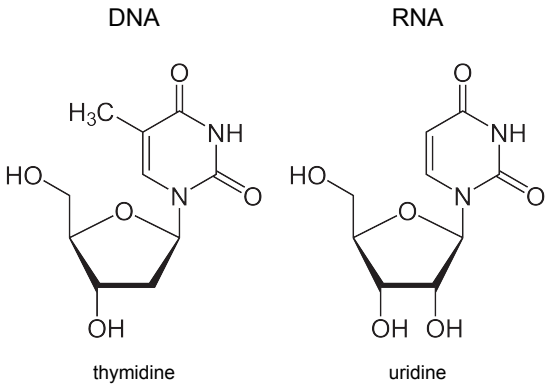

Figure 2.3: Structural differences between DNA and RNA molecules. DNA is composed of 2-deoxy D-ribose, while RNA is built of D-ribose molecules. The base thymine in DNA is replaced by uracil in RNA (adapted from [42]).

2.2.3 RNA

On the molecular level, ribonucleic acid (RNA) differs from DNA in two aspects. Instead of 2-deoxy-D-ribose RNA is composed of the pentose sugar D-ribose and the base thymine in DNA is replaced by uracil in RNA, which, like thymine, forms Watson-Crick base pairs with adenine. Figure 2.3 displays the nucleotides of RNA and DNA in a direct comparison. These structural differences cause RNA to be more susceptible to hydrolysis but are also responsible for a greater diversity in RNA secondary structure, since the extra hydroxyl group can be an additional binding site for forming branched polynucleotides. While for DNA Watson-Crick base pairing and the double-stranded helix inside the cell dominates, base pairing in RNA structures is very diverse. A good overview of these structures is given by Leontis et al. [41]. RNA molecules in the cell are mostly single-stranded, but can be found to form double helices, for which the A-form predominates [30]. Additionally, other structures like bulges, hairpins, loops or pseudoknots appear and are determined by the function of the particular RNA molecule. These conformations can be as diverse as the different tasks RNA can perform.

2.2.4 Aptamers

Aptamers are single-stranded, artificial oligonucleotide sequences that recognize their particular ligand with high affinity and specificity. They were discovered in 1990 independently by Andrew D. Ellington and Jack W. Szostak [44], as well as Craig Tuerk and Larry Gold

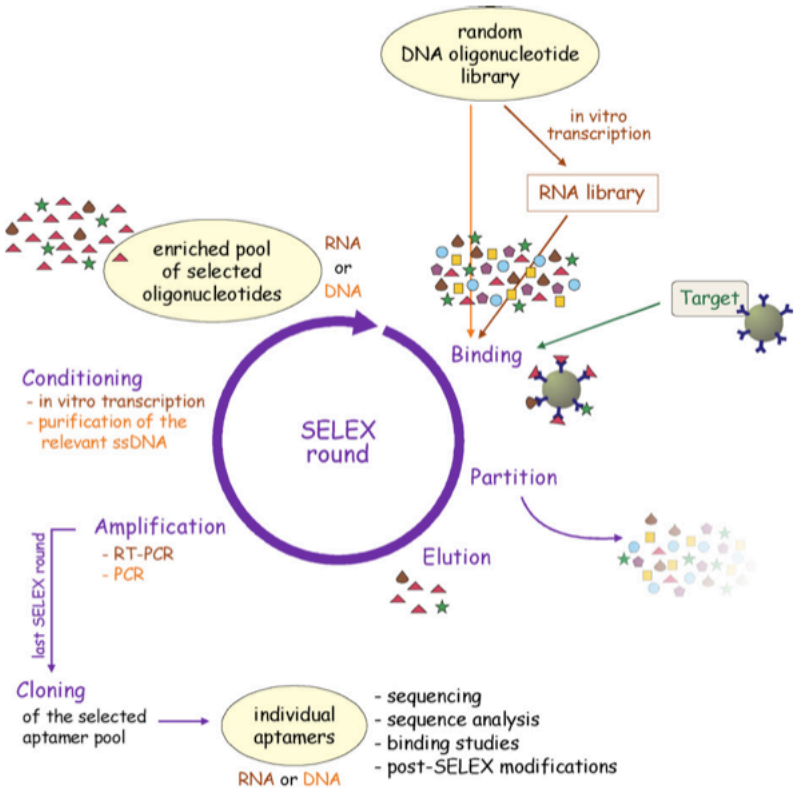

Figure 2.4: The SELEX process. Starting point is a large random DNA or RNA library. The single-stranded oligonucleotides are incubated with the target of choice. Strongly bound complexes are separated and these oligonucleotides are amplified. This enriched pool of sequences can be modified to enhance certain characteristics and is the starting point for the next round. Several cycles produce a small number of oligonucleotides that bind specificly and with great affinity to the target under the conditions chosen for the binding and partition step (adapted from [43]).

[45]. Tuerk and Gold developed a new method named SELEX - systematic evolution of ligands by exponential enrichment - to select RNA oligonucleotides from a large library with the property to bind a certain ligand tightly and with high specificity. Andrew D. Ellington and Jack W. Szostak used a similar technique to find RNA molecules that bind specifically to a variety of organic dyes and termed these oligonucleotides aptamers after the Latin expression "aptus" meaning "fitting" [44]. Shortly after, single-stranded DNA aptamers were discovered [46]. The SELEX technique is an iterative process to find aptamers for all kinds of ligands under different conditions (see Figure 2.4) . The selection process starts with a large, random DNA library (about 10^{15} different sequences) that can either be directly used or transferred via *in vitro* transcription into an RNA library. The oligonucleotides are incubated with the target molecule of choice and the ligand-aptamer complexes are separated from unbound or weakly bound molecules. This step and the methods used for it, e.g. immobilization of the target on a matrix or on magnetic beads or ultrafiltration, is decisive for the binding characteristics of the aptamer to be selected. The so-found oligonucleotides are eluted and amplified and are the basis of a new, enriched pool of DNA or RNA sequences that is used for the next cycle. After 6 to 20 rounds of SELEX, the initially large oligonucleotide library is greatly reduced to relatively few sequences that bind to the ligand with strong selectivity and affinity under the conditions chosen for the incubation and separation step. These sequences can now be further analyzed, for example by sequencing or in binding studies [43]. Aptamers greatly resemble antibody-antigen complexes in their binding properties, but differ in their composition and, most importantly, in their fabrication. While antibodies are expressed in cells and differ from species to species, aptamers are produced completely *in vitro*. Nevertheless, oligonucleotides are present in all cells so that aptamers are non-toxic and do not provoke immune reactions. Furthermore, the *in vitro* fabrication enables the selection of aptamers against all kind of natural or non-natural compounds including toxins. In this work, aptamers are used in a force-based assay for the detection and characterization of analytes (see Chapter 4.1) and as docking station for an RNA ligand that selectively inhibits the protein Dicer (see Chapter 4.2).

2.3 Transcriptional Regulation by Proteins in Eukaryotes

Transcription describes the process, in which a DNA sequence is copied into an RNA molecule by the enzyme RNA polymerase. In eukaryotes, three kinds of RNA polymerase can be discerned that produce different kinds of RNA, mostly messengerRNA, transferRNA and ribosomalRNA. Transcription is the first step in gene expression and, thus, the first possibility for the cell to regulate protein levels. It comprises the three steps initiation, elongation and termination. Initation denotes the binding procedure of the protein RNA polymerase to the promoter sequence next to the gene. Elongation is the process in which the DNA sequence is read and the RNA copy is extended according to the bases of the DNA code. Last, the RNA polymerase is stopped and leaves the DNA strand. Every step as well as the rate of transcription is controlled by different proteins. The very first possibility in eukaryotes for gene regulation is to modify the accessibility of the DNA strand for transcription initiation. The DNA is wrapped around histone proteins and forms nucleosomes. The chain of DNA-nucleosomes constitutes the chromatin. Histone modifications influence how the DNA is wrapped around the histone proteins and alters chromatin structure. Thereby some parts of the DNA are exposed while others are concealed. DNA methylation converts cytosine to 5-methylcytosine that behaves like regular cytosine except that highly methylated areas show reduced transcriptional activity. Histone modifications and DNA methylation belong to the epigenetic regulational mechanisms and can be preserved in cell division. Thus, daugther cells of a differentiated cell remain differentiated and do not change back into stem cells (for details see [47]). In eukaryotes, RNA polymerase has only very low affinity for the promoter sequences, but needs general transcription factors that bind to the DNA and the RNA polymerase. Additionally, several other proteins bind to the DNA and build together with the RNA polymerase the transcription initiation complex. These other proteins can bind in close proximity to the gene to be transcribed but also to regions thousands of base pairs away from the gene. Looping of the DNA enables proteins bound to a distant DNA sequence to interact with the protein complex at the promoter region and to activate or to repress the initiation of transcription. This highly elaborate network of protein-protein and protein-DNA interactions regulates in its entirety if and when a gene is transcribed. Nevertheless, a single protein in this network can make a difference and can stop or start transcription. In elongation, RNA polymerase unwinds the DNA double helix at its active site and moves stepwise along the DNA molecule adding

ribonucleotides to the RNA strand that are complementary to the DNA template strand. Elongation factors prevent the RNA polymerase from dissociation before the end of the gene and assist in unwinding of the DNA. Beside producing the RNA molecule, RNA polymerase assembles proteins on its tail that can process the RNA into the functional mRNA. Examples are capping, which means the modification of the 5' end of the RNA molecule for the discriminaton of mRNA from other RNAs, and splicing that removes the introns, non-coding sequences, from the pre-mRNA. Transcription termination is encoded in the DNA so that the transcribed RNA can recruit proteins that end transcription and modify the RNA 3' end if necessary (for details see [48]). Summing up, every step in transcription is regulated by proteins that can activate, accelerate or terminate transcription and thus enable the cell to react very flexibly and rapidly to its needs. In this work, a force-assay is presented that characterizes protein-DNA specificity via the binding strength (see Chapter 4.3). This assay has the potential to contribute to the understanding of the complex network of protein- DNA interactions that govern transcriptional regulation.

2.4 The role of the protein Dicer in the regulation of gene expression

The enzyme Dicer is a multidomain RNAse III-related endonuclease of about $250kDA$ and is responsible for cleaving double-stranded RNA into pieces of 19-22 base pairs. Dicer has been found in the cytoplasm of all eukaryotes studied to date [49], sometimes in several variants with different tasks. The L-shape of the protein seems to be well-conserved for all variants. Recognition of dsRNA by a PAZ-domain occurs in the head of Dicer, which is separated from the two RNAse III-domains by a ruler domain (see Figure 2.5). The base of the L is formed by a helicase, whose function is not totally understood [49]. Dicer cleaves long and short (more than 30 nucleotides) dsRNA strands with equal efficiency, whereas duplexes of 21 nucleotides or less are not processed *in vitro*. A 3' 2-nucleotide long overhang increases Dicers efficiency compared to blunt ends [50].

In the last decade, Dicer has increasingly been attracting attention due to its crucial role in the RNA interference (RNAi) pathway. The term RNAi describes the process how pieces of short RNA strands control gene activity in a homology-dependent manner. Dicer cuts the long double-stranded RNA precursors into pieces of 19-22 base pairs. These short RNA strands are unwound and a single strand is loaded into a protein complex generally termed RNA-induced silencing complex (RISC) which varies according to species

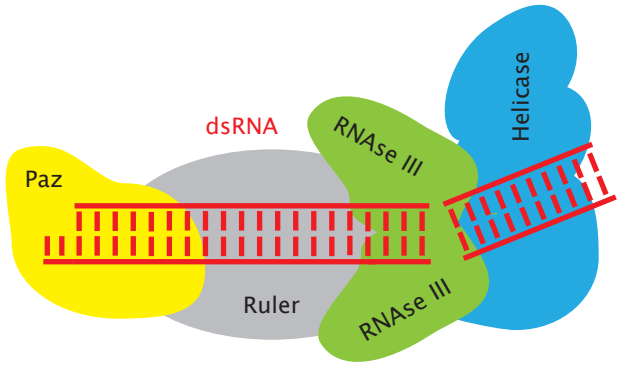

Figure 2.5: Schematics of the protein Dicer. The L-shape of the protein seems to be well-conserved for all variants. The PAZ-domain in the head part recognizes dsRNA. The two RNAse III domains are separated from the PAZ head by a ruler domain and cut the two RNA strands. A helicase, whose function is not totally understood, forms the base of the L.

and function. The short RNA in the RISC complex binds via Watson-Crick base pairs to the mRNA and inhibits translation. Various classes of small, regulatory RNA have been identified. Two main categories of single-stranded RNA involved in metazoan RNA interference can be distinguished that differ in their origin and function but share processing by Dicer: short-interfering RNA (siRNA) and microRNA (miRNA) (see Figure 2.6). siRNA precursors are long, fully complementary double-stranded RNA molecules that are either introduced directly into the cytoplasm or taken up from the environment, but may also originate from endogenous sources like transposons [52]. Hence, the main task of the siRNA-processing machinery seems to be the defense of genome integrity in response to foreign or invasive nucleic acids [53]. In most cases, siRNA binds to a fully complementary target mRNA which is subsequently degraded. miRNAs are transcribed and pre-processed in the nucleus into incomplete base-paired stem-loop structures, known as pre-microRNAs. They are then transferred to the cytoplasm, where Dicer matures the pre-miRNA by cleaving the stem loop structure. The mature miRNA strand binds to the mRNA and inhibits translation in combination with the RISC [54], although gene upregulation by the RISC complex has also been reported [55][56]. In contrast to siRNA, which usually requires total complementarity to its target sequence, miRNAs and their target mRNA do not need to base-pair perfectly. However, a seed region between residues 2 to 8 seems to dominate the mRNA recognition process. Consequently, a certain miRNA can bind and regulate a variety of mRNA sequences. Several miRNAs may also play a role in the regulation of a

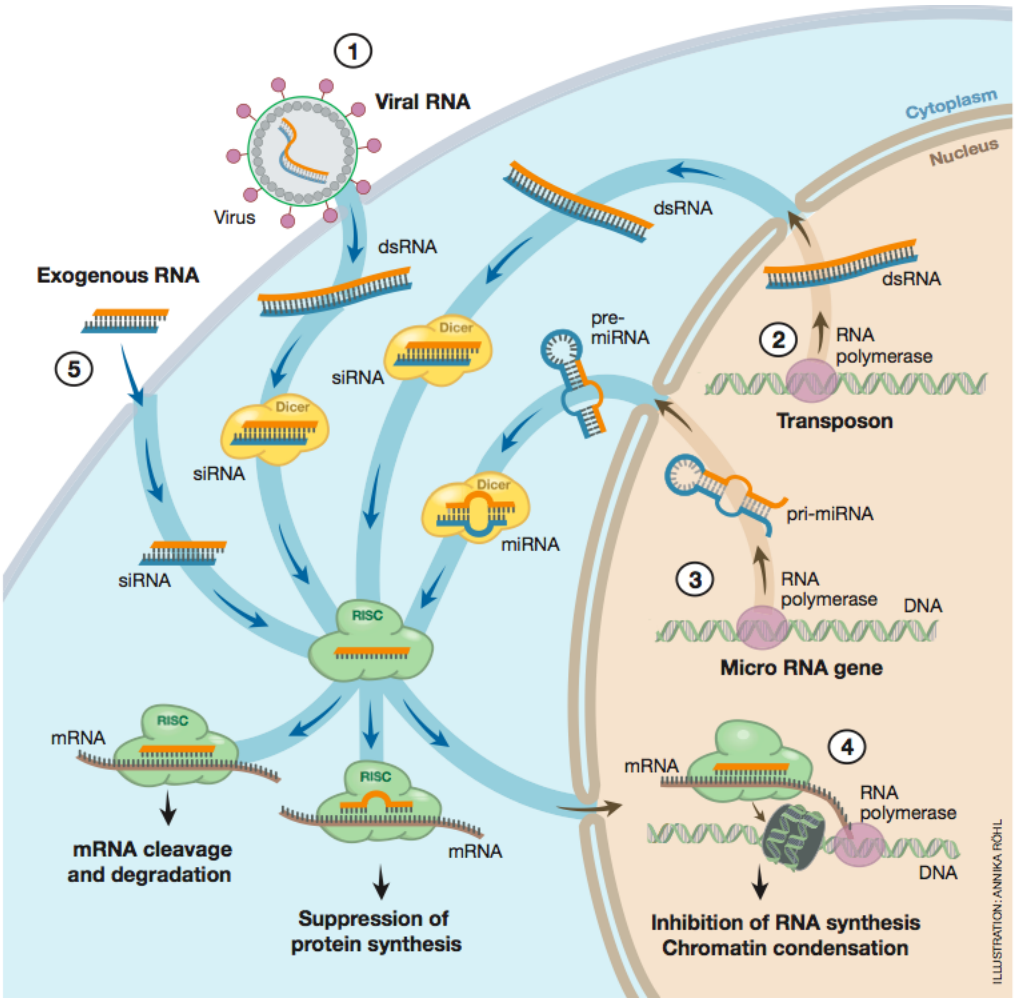

Figure 2.6: Small RNA biogenesis. siRNA precursors are long double-stranded RNA sequences that are either taken up from the enviroment (1 and 5) or orginate from endogeneous sources like transposons (2). miRNA precursors are transcribed from genetic DNA and form pre-microRNA hairpins that are transported into the cytoplasma (3). Dicer processes siRNA and miRNA precursors into pieces of 19-22 base pairs. One of the two strands is loaded into the RISC (RNA-induced-silencing-complex) and in most cases inhibits protein expression by different mechanisms like mRNA degradation. Additionally, gene expression is influenced by the inhibition of RNA synthesis and chromatin condensation (4) (taken from [51]).

single mRNA transcript. Thus, miRNA seems to fine-tune protein expression. Nevertheless, binding of a miRNA to a perfect complementary target leads to direct degradation of the mRNA as would be the case for siRNA. Incomplete base pairing of a siRNA and a mRNA only hinders translation without direct degradation of the mRNA. Thus, the inhibitory function of miRNA and siRNA seems to be interchangeable [53]. The variability and diversity make small RNAs very adaptable to the current situation and contribute to their importance for gene regulation. Malfunction of the RNAi machinery has a severe impact on the cell and can lead to illnesses like cancer. One possiblity to influence RNAi at the Dicer step is demonstrated in Chapter 4.2.

Chapter 3

The Molecular Force Assay

This chapter describes the technique of the Molecular Force Assay (MFA) that enables the parallelization of force measurements by comparing the mechanical stability of two molecular bonds.

3.1 Basic principle

Two molecular bonds, a sample and a reference bond, are connected in series via a thymine-linker to which a fluorophore is conjugated. The lower complex is covalently bound to a functionalized glass slide, while the upper complex is attached to a soft PDMS surface. The two surfaces are separated by a constant velocity so that the two molecular bonds are loaded with a force until the weaker one ruptures. An alternative view is that the force greatly enhances the off-rate of the bonds under investigation and reduces the otherwise extremely long spontaneous dissociation times towards seconds [57]. The fluorophore conjugated to the linker sequence indicates the intact bond. Hence, the ratio of the fluorescence intensity before and after the force probe allows to determine the mechanical stability of the sample bond in comparison to the reference bond. Every molecular complex under load corresponds to a single molecule force experiment since the stability of every sample bond is measured against its own reference bond. This enables about 10^4 parallel force measurements per μm^2 so that a single MFA experiment already provides a valid result supported with very good statistics.

For most applications of the MFA, sample and reference bond are composed of DNA or RNA duplexes. Three oligonucleotide strands are successively hybridized to form the two bonds. The lowermost oligonucleotide strand is attached via an amino-modification to

an aldehyde functionlized glass slide. Five HEGL (hexaethylene glycol) polymer units and a poly-T stretch act as spacer between the surface and the molecular complex. Sample and reference bond are also separated by a poly-thymine sequence to which a fluorophore is conjugated. The uppermost strand is functionalized with a biotin that binds to the streptavidin-coated PDMS stamp during the contact process. Figure 3.1 displays the details of the molecular setup for two DNA duplexes.

3.2 Contact and separation process

Macroscopically, the contact and separation process is performed as described in the following. The functionalized stamp adheres upside-down to a glass block glued to a closed-loop piezoelectric actuator and a DC motorized translation stage (see Figure 3.2) . The slide with the molecular constructs is fixed beneath the stamp on a stainless steel stage with permanent magnets so that every stamp pillar meets a spot of $1mm$ diameter of molecular complexes on the glass slide. The whole contact device is mounted on an inverted microscope with an xy-DC motorized high-accuracy translation stage. Contact is made by means of the piezo and care is taken that each individual pillar is not compressed more than $3\mu m$. The planar adjustment of stamp and slide as well as the contact process are controlled by reflection interference contrast microscopy [58]. The contact between stamp and slide is maintained for 10 minutes to ensure that the molecular complexes are coupled to the surfaces. If DNA or RNA duplexes form sample and reference bond, the molecular complex is completely built up on the glass slide before the contact and separation process and the biotin modification of the uppermost strand binds to the streptavidin-coated PDMS surface during the contact time. The piezo retracts the stamp with a constant velocity of $1\mu m/s$, and a force builds up in the molecular complexes until the weaker one breaks with higher probability. In order to quantify the number of intact lower bonds in relation to the total number of molecular constructs, images of the fluorescence intensity on the glass slide are taken before and after the contact process.

3.3 Analysis

Calculating the ratio of intact lower bonds to the total number of molecular complexes, the fluorescence intensities of the images are analyzed by subtracting the background signal and subsequently determining the mean fluorescence intensity of the images measured before

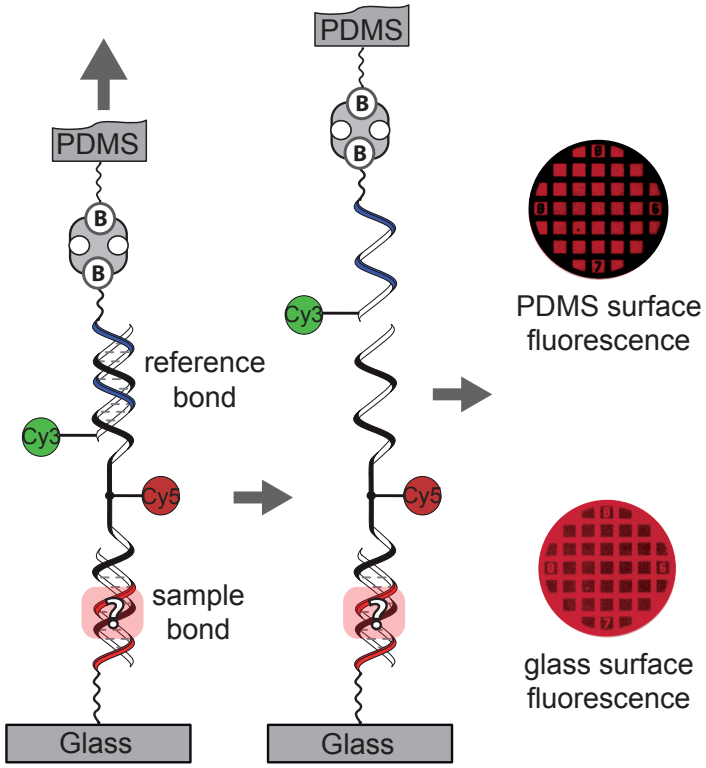

Figure 3.1: Molecular setup of the MFA for DNA duplexes. Sample and reference bond are connected in series between two surfaces. The lowest strand is covalently bound to an aldehyde-functionlized glass slide via an amino-modification. Five HEGL (hexaethylene glycol) polymer units and a poly-T stretch act as spacer between the surface and the molecular construct. Sample and reference bond are also separated by a poly-thymine sequence to which a fluorophore is conjugated. The uppermost strand is modified at its 5' end with a biotin that connects the whole construct with the streptavidin-functionalized upper surface. Upon surface separation, one of the molecular complexes ruptures and the fluorophor in the middle stays with the intact bond. This leads to a distribution of the fluorescence signal between the two surfaces. The outcome of an example measurement is shown on the right. As it cannot be assumed that all molecular complexes bound to the PDMS surface, the uncoupled constructs have to be subtracted. Their number is either determined by labeling the free biotins at the upper end (not shown) or by introducing a FRET-pair into the molecular complexes. Thus, the fluorescence FRET signal is a measure for the number of intact molecular constructs.

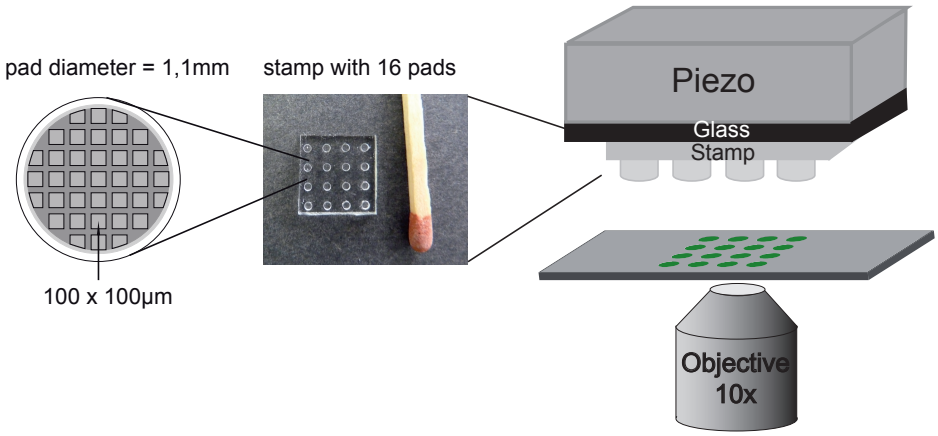

Figure 3.2: Macroscopic setup of the MFA. The contact and separation unit consists of a closed-loop piezo to which the PDMS stamp is attached via a glass block. Current technical implementation allows the measurement of 16 molecular constructs in parallel corresponding to 16 pillars of the stamp and the 4x4 pattern on the glass slide. Every stamp pillar is microstructured with pads of $100\mu m \times 100\mu m$ separated by $41\mu m$ wide and $5\mu m$ deep rectangular trenches enabling the drainage of liquid during the contact and separation process. The contact unit is mounted on an inverted microscope.

$\langle I^{Start} \rangle$ and after the separation process $\langle I^{Final} \rangle$. The quotient is given by

$$F_{intact\ lower\ bonds} = \frac{\langle I^{Final} \rangle}{\langle I^{Start} \rangle}. \tag{3.1}$$

In order to accurately determine the number of intact lower bonds, however, two additional outcomes of the force probe have to be considered. First, it cannot be assumed that every molecular construct couples via the biotin-streptavidin bond to the PDMS surface. Second, instead of sample or reference bond a rupture of the biotin-streptavidin bond is also possible, though not probable due to the high rupture force of the biotin-streptavidin complex that lies around $250pN$ [10]. Both cases are taken into account by determining the number of molecular complexes with intact sample as well as reference bond after the separation process. This can be done in two ways. One possibility is to mark the biotin modification of the molecular complexes on the glass slide with a streptavidin that is labeled with a spectrally distinct second fluorophore. The fluorescence signal of the labeled streptavidin is a measure for the number of molecular complexes that were not tested. As the streptavidin can only be labeled after the force probe measurement, the mean

fluorescence intensities are calculated from a single image. Due to the microstructure of the PDMS stamp, every fluorescence image taken after the contact and separation process will always show both contacted and non-contacted areas. Thus, the ratio of molecular complexes that did not couple to the total number of molecular constructs is determined by dividing the mean fluorescence intensity values of contacted to non-contacted areas

$$F_{non-coupled} = \frac{\langle I^{contacted} \rangle}{\langle I^{non-contacted} \rangle}. \tag{3.2}$$

This number is subtracted from $F_{intact\ lower\ bonds}$ and the result is normalized to the total number of molecules that have been under load, yielding the Normalized Fluorescence NF

$$NF = \frac{F_{intact\ lower\ bonds} - F_{non-coupled}}{1 - F_{non-coupled}}. \tag{3.3}$$

Thus, the Normalized Fluorescence is the mean number of intact lower bonds to the total number of molecular complexes that have been tested. The data of the publications P1 (see Chapter 4.1) and P3 were analyzed according to this method.

An alternative method for the determination of molecular constructs that have not coupled to the PDMS surface is the labeling of the uppermost strand with a fluorophore at the lower end that constitutes a FRET-pair (Förster-Resonance-Energy-Transfer [59]) with the fluorophore attached to the middle strand (see Figure 3.1) . For this thesis, the cyanine dyes Cy3 and Cy5 were chosen as FRET-pair. Cy5 is conjugated to the middle strand and indicates the number of intact lower bonds on the glass slide, while Cy3 is attached to the uppermost strand so that a FRET-signal is only measured for molecular constructs of intact sample and reference bond. This configuration enables the calculation of the Normalized Fluorescence by analyzing the images pixel-by-pixel. In addition to the images of the Cy5 fluorescence intensity that indicate the intact lower bonds, the FRET signal is also detected before and after the contact and separation process. After background subtraction, the fluorescence images of the Cy5 signal as well as of the FRET signal are divided and corrected for bleaching, yielding

$$F_{Cy5} = \frac{I_{Cy5}^{Final}}{I_{Cy5}^{Start}}. \tag{3.4}$$

and

$$F_{FRET} = \frac{I_{FRET}^{Final}}{I_{FRET}^{Start}}. \tag{3.5}$$

An image of the Normalized Fluorescence is calculated according to equation 3.3 in the form of

$$NF = \frac{F_{Cy5} - F_{FRET}}{1 - F_{FRET}}. \tag{3.6}$$

The mean of the pixel intensities of the NF image is calculated and defined as NF value that describes the fraction of intact lower bonds to the total number of molecules under load. A huge advantage of the pixel-by-pixel analysis for the determination of the NF is that it cancels out inhomogeneities due to the Gaussian illumination profile and surface defects, rendering the MFA very robust. The data of publication P2 (see Chapter 4.2) were analyzed according to this method. As manuscript M1 describes an application of the MFA that does not compare DNA or RNA bonds with each other but a DNA-protein complex to a DNA duplex, a different analysis is required and described in Chapter 4.3.

Chapter 4

Results

The objective of this thesis was to adapt the MFA for new forms of application that contribute to the solution of current biological problems. The main results are shortly presented in the following. Additional information can be found in publications P1 and P2 and manuscript M1. The utilization of aptamers in a force-based biochip for the capture of small molecules is described in Chapter 4.1 and enables the detection of a broad range of ligands that include toxins and low affinity binders. Due to the label-free detection, complex fluids do not cause problems. The protein Dicer is one of the major protagonists in the RNA interference pathway so that a selective inhibition of Dicer activity has a great potential for the development of future medical therapeutics. Chapter 4.2 describes the application of the MFA for the screening of small molecules that selectively bind a RNA sequence and hinder Dicer from processing. Furthermore, the MFA can directly quantify the binding strength of DNA-protein interactions. Chapter 4.3 describes the necessary changes in the molecular setup as well as in the analysis and demonstrates in a proof-of-principle experiment the potential of this application of the MFA.

4.1 DNA as a force sensor in an aptamer-based biochip for adenosine

Bioanalytical methods that probe multiple interactions simultaneously in massively parallel assays with label-free detection are of great importance for the development of new analytical tools [60]. The MFA offers the possibility to provide a label-free detection in a highly parallel format by the implementation of aptamers. Aptamers are oligonucleotides

that are selected to specifically bind their ligand with high affinity and specificity (see Chapter 2.1.4). They are similar to antibodies but surpass them in terms of small molecular weight, ease of modification and ability to detect toxins [61]. As a proof-of principle, a split aptamer selective for adenosine [62][63][64] was introduced into the upper, sample bond. Ligand binding stabilized the sample bond and led to a higher rupture probability for the reference bond compared to a molecular complex without ligand. This resulted in a decrease of the NF for increasing concentrations of ATP (adenosine triphosphate) and is clearly visble in Figure 4.1 A. In order to determine the dissociation constant, every spot of molecular complexes bound to the surface was incubated with a different concentration of ATP ranging from $0\mu M$ to $2000\mu M$. Fitting the ATP titration data to the Hill equation [65]

$$\theta = \frac{L^n}{L^n + K_D} \tag{4.1}$$

with θ the fraction of occupied binding sites to all possible binding sites, $[L]$ the ligand concentration, K_D the dissociation constant and $n = 2$, yielded a half maximal effective concentration of $EC50 = 124.8\mu M$ with a 95% confidence interval of $[102.8\mu M, 151.4\mu M]$. This agrees well with previously published values of the dissociation constant [62][63]. A negative control measurement with GTP showed no stabilization of the sample bond (see Figure 4.1 A). In order to prove the validity of the method, the geometry of sample and reference bond was inverted so that the sample bond was attached to the glass slide. As expected, an increase in ligand concentration now led to higher values for the NF (see Figure 4.1 B). The same results were obtained for measurements in fetal bovine serum, demonstrating the applicability of the assay in complex ambients. Although the outcome of the MFA experiment is indicated by a fluorophore, the measurement itself, the comparison of unbinding forces, is label-free. Hence, minor changes in the mechanical stability induced by small molecules or low affinity binders can be detected without stringent washing requirements or sophisticated signal amplification, which often makes it difficult for other techniques to charaterize small molecules or low affinity binders. As aptamers can be selected against virtually any target, this force-based aptamer sensor can easily be adapted for the capture and analysis of any ligand. Further details are described in publication P1.

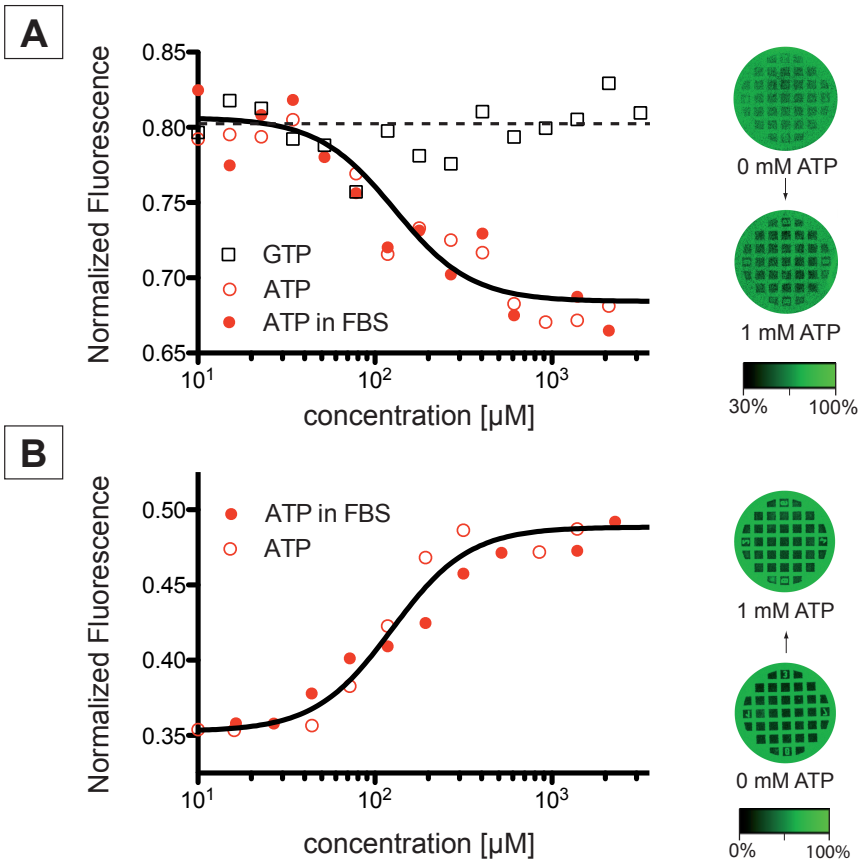

Figure 4.1: Detection of the dissociation constant of ATP to its aptamer. (A) The aptamer was implemented in the upper, sample bond. Addition of ATP resulted in the stabilization of the sample bond and a higher rupture probability of the lower reference duplex. Thus, the NF decreased. Fitting the ATP titration data to the Hill equation with $n = 2$ yielded a half maximal effective concentration of $EC50 = 124.8\mu M$. The same result was obtained for measurements in bovine fetal serum (FBS). Adding GTP as a ligand, no stabilization effect was determined. (B) Inverting the geometry of sample and reference bond, the outcome of the experiment was unchanged with an increase in mechanical stability of the sample bond upon binding of ATP.

4.2 Sequence specific inhibition of Dicer measured with a force-based microarray for RNA ligands

RNA interference describes a mechanism for the regulation of gene expression at the level of translation by small RNAs. The essential role of the protein Dicer is based on its task to mature precursor molecules like hairpin structures or long RNA duplexes into functional small RNAs. Dicer cleaves the precursors into pieces of 19-22 base pairs so that the matured small RNAs can subsequently influence translation in combination with other proteins. microRNAs (miRNA) are one class of small RNAs and an endogenous means in eukaryotic cells to fine-tune gene expression. They are critical for many cellular processes like developmental timing or cell proliferation. Many severe diseases are accompanied by miRNA dysregulation. Thus, a selective inhibition of single miRNAs precursors might be a good approach for the development of a new generation of medical therapeutics. Therefore, parallel screening formats for RNA binders that, in addition, assess their potential for the hindrance of Dicer activity are highly desirable. As part of this thesis, it was demonstrated that the MFA can be utilized for both the screening of RNA ligands that inhibit Dicer cleavage and the characterization of the ligand by the determination of the dissociation constant. The results are published in publication P2.

As a proof-of-principle, a RNA duplex of 35 base pairs incorporating an aptamer against the aminoglycoside paromomycin [66][67] in zipper geometry was used as sample bond and compared against a DNA duplex. Again, measurements were performed in both configurations with the RNA duplex constituting either the lower (RNA down) or upper bond (RNA up). Dicer cleavage should be easily detectable by the MFA since Dicer cuts off around 20 base pairs from the sample bond, thus greatly destabilizing the RNA duplex. This is clearly visible in Figure 4.2 A. Dicer activity caused a destabilization of the lower RNA duplex so that the values of the Normalized Fluorescence decreased compared to the initial value at $t = 0min$. Dicer processes the RNA duplex in multiple enzymatic turnovers. Consequently, the Normalized Fluorescence declined further with increasing incubation time. The experimental design provided Dicer with an excess of substrate, dsRNA, so that the substrate concentration could be assumed constant and the reaction rate of Dicer was solely limited by the amount of Dicer present. Thus, a linear relation of the Normalized Fluorescence to Dicer processing time was expected and verified. The slope of the fit was used to quantify the rate of Dicer processing.

Incubation of every spot of immobilized molecular constructs with a different concen-

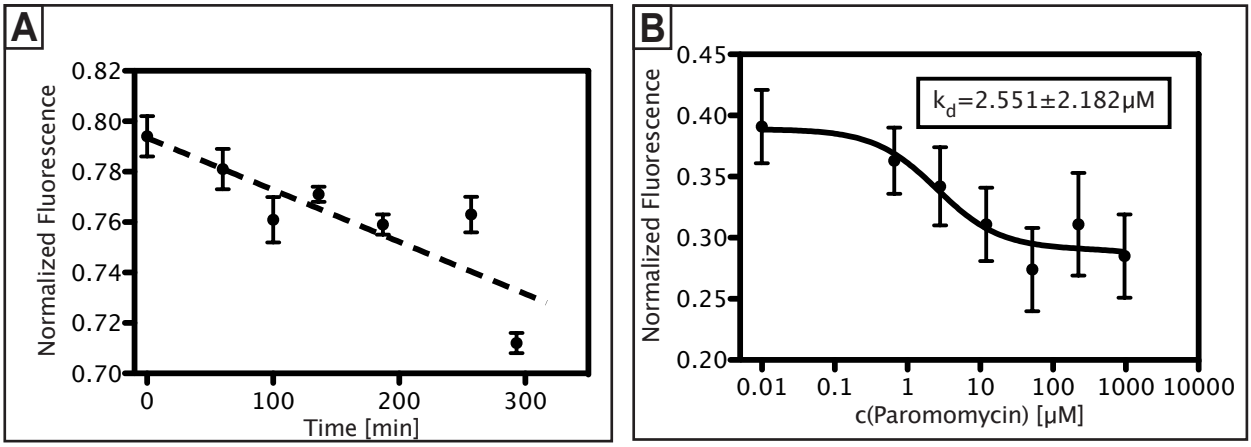

Figure 4.2: Determination of Dicer activity and of the dissociation constant of paromomycin to its aptamer. (A) Dicer processing destabilizes the lower RNA duplex by cutting off around 20 base pairs so that the Normalized Fluorescence decreased with incubation time. Since Dicer was presented with an excess of substrate (dsRNA), its reaction rate was only limited by its own concentration. Thus, a linear decline of the Normalized Fluorescence with time was expected and verified in the presented measurement. (B) Incubation of every spot of immobilized molecular constructs with a different concentration of the aptamer ligand paromomycin allowed to determine the dissociation constant by fitting the data with the Hill equation. For the RNA duplex constituting the upper bond, a dissociation constant of $2.55 \pm 2.18 mM$ was measured in agreement with literature values.

tration of the aptamer ligand paromomycin allowed to determine the dissociation constant by fitting the data with the Hill equation as described in chapter 4.1. Measurements in the RNA up configuration yielded a dissociation constant of $2.55 \pm 2.18 mM$. Literature reports values of $0.2mM - 1mM$ depending on the technique [67][68], in agreement with the results presented in this thesis (see Figure 4.2 B). Measurements with the RNA duplex attached to the glass slide resulted in dissociation constants of about $100 \pm 70 mM$ (data not shown), which deviated by a factor of 50 from the other measurements with the inverted geometry. As non-specific binding of the ligand to the surfaces or molecular complexes would affect the measurements in both configurations, this increase in dissociation constant might be attributed to the proximity of the RNA construct to the glass slide. Notwithstanding the passivation of the glass slide, the RNA duplex as lower bond in zipper geometry presumably stretches across the surface. This might reduce the accessibility of the RNA aptamer binding pocket for the ligand, resulting in an apparent increase of the dissociation constant. Consequently, this configuration with the ligand-binding part integrated in the lower complex in the zipper geometry does not seem suited for the characterization of a RNA-binding ligand. In contrast, providing the ligand-binding sequence with a spacer and removing it from the surface by implementing it in the upper RNA duplex yielded reliable values for the dissociation constant.

In the next step, the two measurements were combined to demonstrate Dicer inhibition upon ligand binding. Figure 4.3 shows the single steps of the experiment. First, the initial value of the Normalized Fluorescence was measured without the addition of Dicer nor ligand. Next, the sample was incubated for a specified amount of time (1h) with $2.5 \mu l$ Dicer solution in $1ml$ buffer before the contact and separation process. Dicer processing led to the destabilization of the RNA duplex and was thus detected. $1mM$ paromomycin was added to another sample and strengthened the RNA duplex upon binding so that the reference bond ruptured with higher probability. A fourth sample was incubated with both, first with paromomycin, then with Dicer for one hour. Binding of the ligand to its aptamer inhibited Dicer to process the RNA duplex and yielded a Normalized Fluorescence close to the ligand-only case. The experiment was performed for both configurations, the RNA duplex as upper bond as well as lower bond. The results are displayed in Figure 4.4. Clearly, Dicer activity weakened the RNA duplex and shifted the Normalized Fluorescence towards the reference bond. Binding of paromomycin strengthened the RNA duplex so that the Normalized Fluorescence decreased in the RNA up configuration and increased in the RNA down configuration, respectively. Dicer was blocked by paromomycin bound to

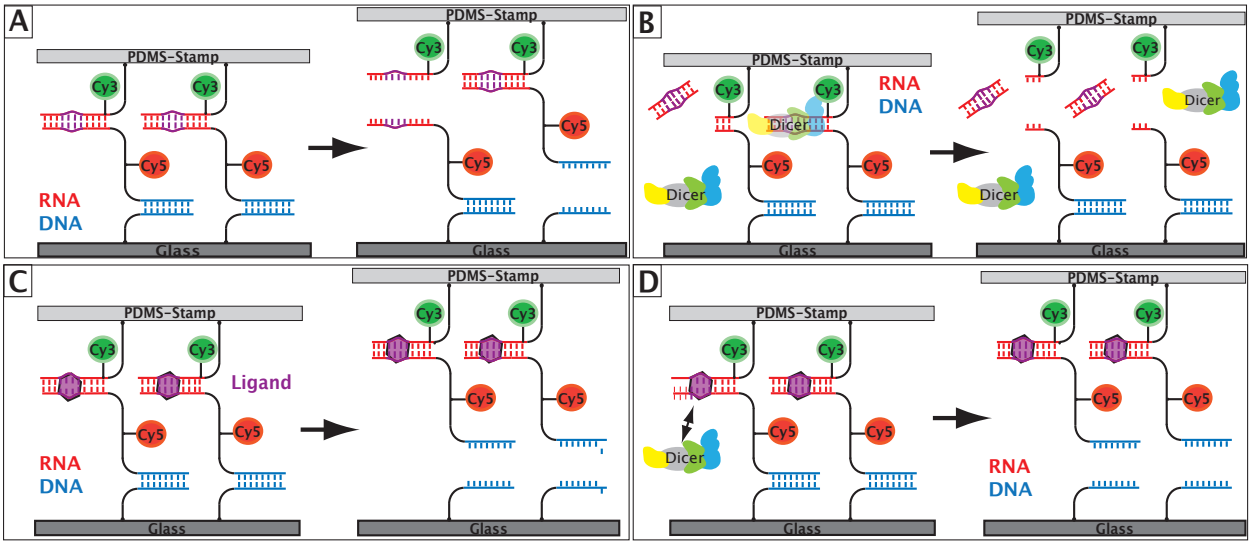

Figure 4.3: The molecular setup for the detection of the selective inhibition of Dicer activity. (A) The initial value of the Normalized Fluorescence is measured without the addition of Dicer and ligand. (B) The sample is incubated for a specified amount of time (1h) with Dicer before the force probe. Dicer processing leads to the destabilization of the RNA duplex and is thus detected. (C) Paromomycin is added and strengthens the RNA duplex upon binding so that the reference bond ruptures with higher probability. (D) The sample is incubated with both, first with paromomycin, then with Dicer for one hour. Binding of the ligand to its aptamer inhibits Dicer to process the RNA duplex and yields a Normalized Fluorescence close to the ligand-only case.

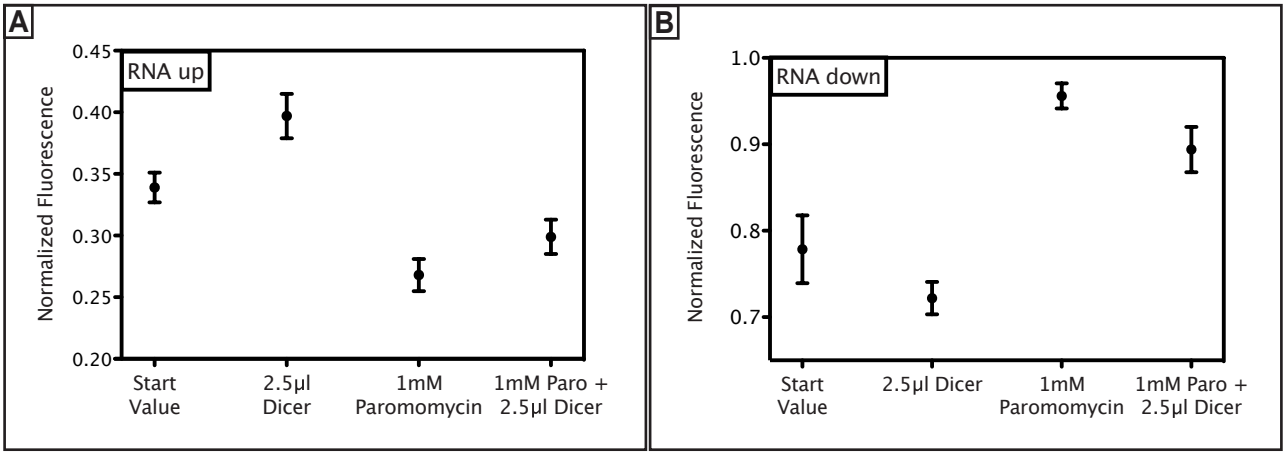

Figure 4.4: Dicer hindrance upon paromomycin binding. (A) In the RNA up configuration, the initial value of $NF = 0.34 \pm 0.01$ increased to $NF = 0.40 \pm 0.02$ due to the destabilization of the RNA duplex by Dicer cleavage. Paromomycin binding strengthened the RNA duplex and decreased the Normalized Fluorescence to 0.27 ± 0.01. If the paromomycin binding blocks Dicer, a NF value close to 0.27 ± 0.01 was expected for the last data point. The measured value 0.30 ± 0.01 confirmed the capability of the assay to inhibit Dicer by ligand binding. (B) The experiment in the RNA down configuration yielded the same results and demonstrates the consistency of the assay.

the RNA aptamer but not completely which led to values of the Normalized Fluorescence close to the ligand-only case. Furthermore, a minimum concentration of paromomycin for Dicer inhibtion was determined. For $2.5\mu l$ Dicer solution in $1ml$ buffer, a partial hindrance was observed at a concentration of $2.82\mu M$ paromomycin, whereas $52\mu M$ paromomycin blocked most of Dicer activity. This result agrees nicely with the measured dissociation constant of $2.55 \pm 2.18mM$.

This proof-of principle experiment demonstrates the applicability of the MFA to screen for RNA ligands that specifically inhibit the protein Dicer from processing RNA duplexes and to characterize those ligands. The MFA reliably detected Dicer processing of the RNA duplex as well as the binding of a small ligand to RNA, which resulted in an inhibition of Dicer. In contrast to other techniques [69], the MFA requires neither labeling of the target sequence, nor the ligand or protein. It only needs fluorophores well-separated from the area of interest so that the interaction of the molecules in question is not disrupted and can be analysed undisturbed. The multiplexing capabilities of the MFA in the currrent setup enable the analysis of 16 different systems, ligands or ligand concentrations, in one measurement. Further standardization and miniaturization offers the possibility to extent

this application of the MFA towards high throughput.

4.3 A force-based, parallel assay for the quantification of protein-DNA interactions

Characterization of protein interactions with genomic DNA is essential to understand the intricate system of the regulation of gene expression, especially transcription. Most techniques can either measure protein-DNA interaction in detail but are very time consuming and not suited to analyze great numbers of proteins or DNA sequences or can determine a large amount of protein-DNA binding events but have difficulties to accurately quantify those interactions. Furthermore, affinity or thermodynamic constants might not be the best quantities to characterize protein-DNA interaction in a nuclear environment, where a DNA-binding protein will probably always be attached to some DNA sequence due to the high concentration of DNA inside the nucleus. Specificity that comprises the discrimination between high and low or no binding sequences is better suited to characterize the binding properties of a protein. This quantitiy can be measured in force measurements by determining the binding strength between two molecules. An adaptation of the MFA that enables the parallel quantification of protein-DNA interactions is described in the following and in manuscript M1.

The standard MFA setup consists of two oligonucleotide duplexes that are compared with each other. Ligand-oligonucleotide interaction is not directly probed, but the ligand stabilizes the molecular bond and is thus detected. The new variant of the MFA probes the protein-DNA interaction directly and compares it to different reference bonds in order to quantify the interaction. As a proof-of-principle, the binding strength of a six zinc finger construct with three different DNA motifs, a high affinity sequence, a low affinity sequence and a no binding sequence, was determined by comparing the protein-DNA interaction to two reference DNA duplexes of different strength (20 and 40 base pairs). Zinc finger motifs are one of the most abundant DNA binding domains in eukaryotic transcription factors [70]. The protein in our experiment Zif268/NRE is an artificial fusion protein of two zinc fingers of the Cys2-His2 class [71]. Zif268 is a transcription factor in mouse and a popular model system due to the existence of structural data of the protein-DNA complex [70][72]. NRE is an engineered variant of Zif268 that binds specifically and with high affinity to a nuclear receptor element [73]. The six zinc finger construct ZIF268/NRE is modified at the N-terminus with a ybbR-tag [74] followed by a superfolderGFP [75] variant and is

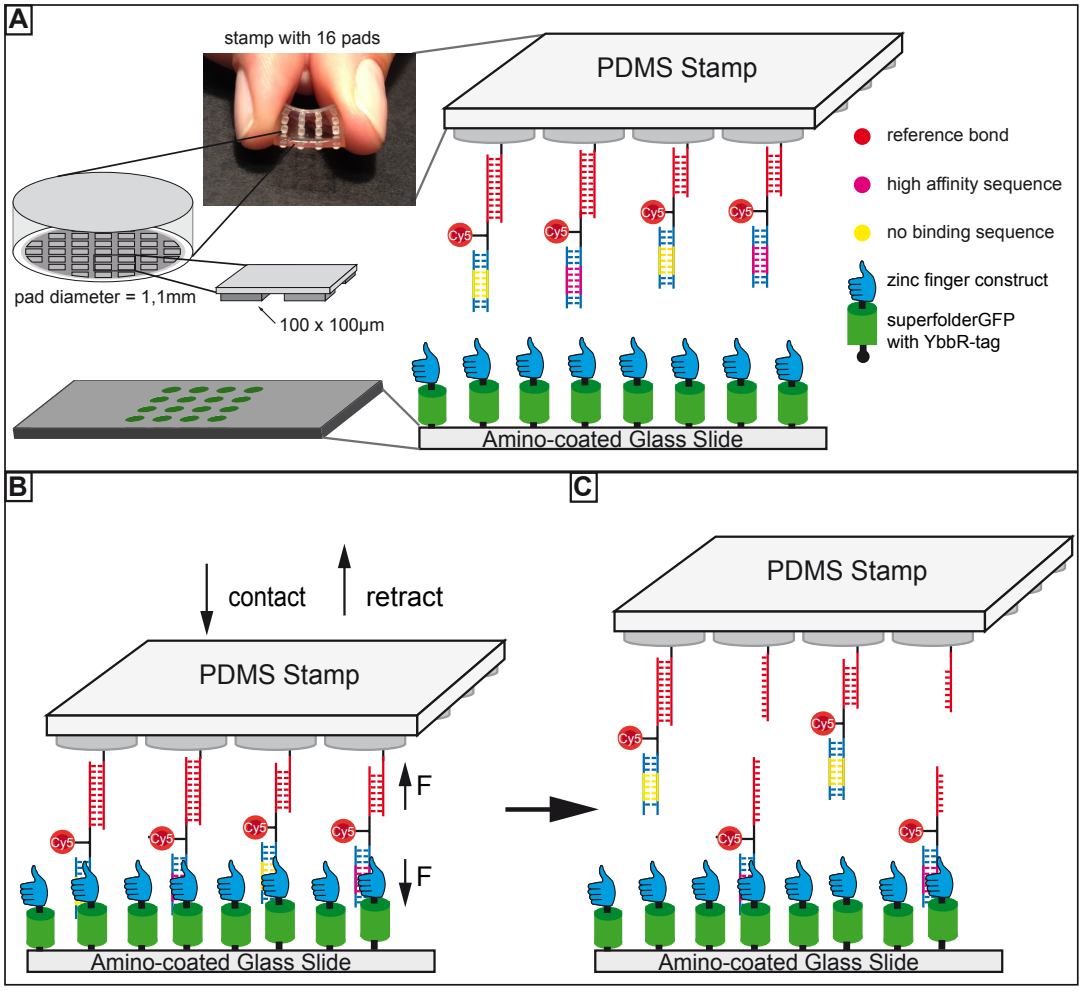

Figure 4.5: The molecular setup for the quantification of protein-DNA binding strength. (A) The geometries of the PDMS stamp and the 4x4 pattern of protein spots on the glass slide are displayed. The zinc finger protein is covalently bound to an amino-coated glass slide functionalized with Coenzyme A via a ybbR-tag. A superfolderGFP acts as an additional spacer and helps to adjust the glass slide beneath the pads of the stamp. Different combinations of reference sequences and DNA binding motifs are attached to each pillar. (B) The PDMS stamp is carefully brought into contact with the glass slide and the DNA sample bonds are allowed to bind to the protein. Subsequently, the PDMS stamp is retracted with constant velocity so that a force builds up in the DNA-protein complexes and the reference bonds until the weaker construct ruptures. (C) After the force probe, the Cy5 fluorescence signal on the glass slide is a measure for the number of intact protein-DNA bonds.

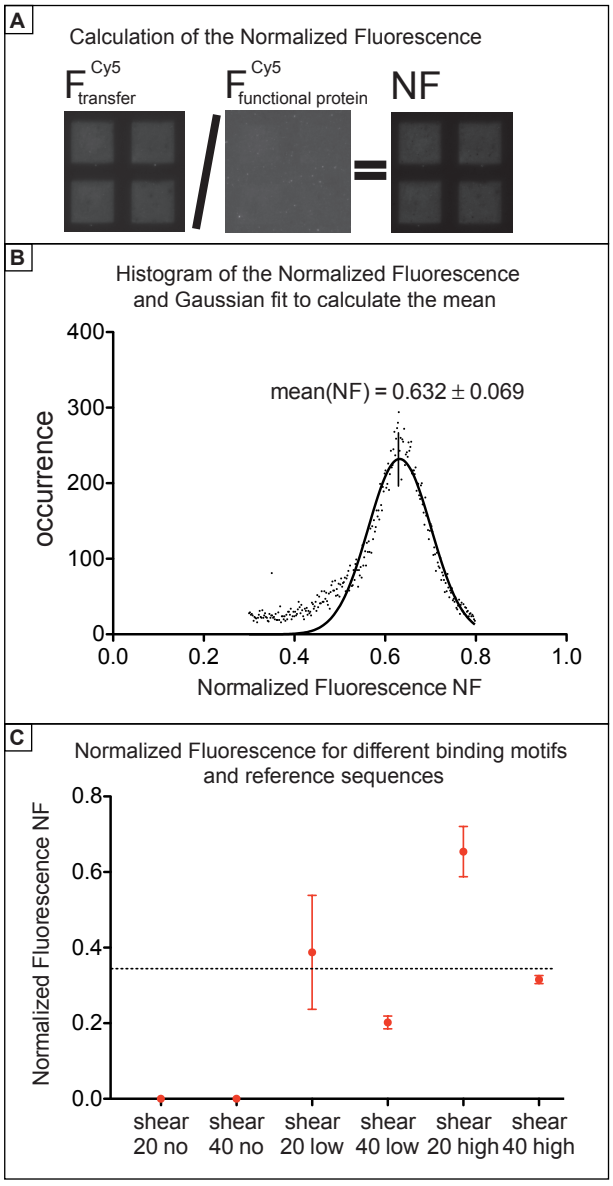

Figure 4.6: Quantification of the binding strength of a six zinc finger construct to different DNA sequences. (A) In order to quantify the binding strength, the fluorescence signal representing the DNA transfer has to be normalized to the number of available protein binding sites. For this purpose, protein binding sites are saturated by adding a Cy5-labeled 40 base pair DNA duplex harboring a high affinity binding motif subsequently to the force measurement. The fluorescence intensity of transferred DNA $F_{transfer}$ is divided by the fluorescence signal corresponding to the saturated protein binding sites $F_{intact\,protein}$, yielding the Normalized Fluorescence NF. (B) Histograms of every pad on the PDMS stamp sum up the huge number of single-molecule experiments and are fitted by a Gaussian distribution in order to calculate an average NF and the standard deviation. Here, the histogram of the NF displayed in A is shown in detail. (C) Two experiments are summarized to validate our approach as a proof-of-principle. Differences between low and high affinity as well as the no binding motif are very pronounced.

covalently attached via the ybbR-tag to a glass slide coated with Coenzyme A in a 4x4 pattern. The two double-stranded DNA complexes in series are covalently bound to the 16 pillars of a soft PDMS surface with the upper one as reference bond and the lower one as sample bond (see Figure 4.5 A). The DNA sequences in shear geometry are separated by a linker sequence to which a Cy5 fluorophore is conjugated. Due to the macrostructure of the PDMS stamp a maximum of 16 combinations of different reference sequences as well as sample sequences can be tested within one experiment. The GFP signal of the fusion protein is used to place the protein spots below the stamp pillars functionalized with the different DNA sequences. The PDMS surface is carefully brought into contact with the glass slide so that the sample sequence is able to bind to the protein on the glass slide (Figure 4.5 B). After 10 minutes, the PDMS surface is retracted with constant velocity by the Piezo actuator. Thereby, a force is applied to the protein-sample complex as well as to the reference bond until the weaker one ruptures (Figure 4.5 C). The fluorescence Cy5 signal on the glass slide is measured by an inverted epi-fluorescence microscope and indicates the number of intact protein-DNA complexes. Thus, the protein-DNA interaction is directly probed and compared to a well-characterized DNA double-strand. In order to approximate the environment in a eukaryotic nucleus, the experiment was designed as a competition assay and the zinc finger protein was pre-incubated with low-molecular weight DNA from salmon sperm before the contact process.

As a first test of the assay, it was demonstrated that specific and unspecific interactions can be discriminated. For that purpose, the zinc finger protein was presented with a no binding sequence and a high affinity sequence implemented into the sample bond. The interactions were compared to two reference DNA duplexes of 20 and 40 base pairs. For both references, hardly any fluorescence intensity above the background signal was detected for the no binding sequence. In contrast, the interaction of the protein with the high affinity motif was very strong compared so that the reference bonds ruptured with higher probability than the protein-DNA bond. Additionally, the 20 base pair reference duplex ruptured more often than the 40 base pair reference bond, demonstrating the ability to discriminate between specific and unspecific binding and to quantify the strength of the protein-DNA bond. In order to calculate a single, comparable number for the binding strength, environmental differences like the binding density of protein and oligonucleotide constructs on the surfaces have to be taken into account. Correcting for differences in protein density on the glass slide, $0.5\mu M$ of a Cy5-labeled 40 base pair DNA duplex carrying a high affinity binding site for the protein in question was added subsequent

to the force probe experiment to saturate all functional proteins bound to the surface. Calibration measurements confirmed a complete saturation after 30 minutes incubation time. After removing unbound fluorophores by a washing step, the fluorescence on the glass slide was determined again. It is a measure for the maximum number of functional proteins on the slide. Since the binding density of the DNA complexes on the PDMS always exceeds the number of functional proteins on the glass slide, further corrections are not necessary. The ratio of fluorescence signal on the glass slide directly after the rupture event $F_{transfer}$ to the maximal number of functional proteins $F_{intact\,protein}$ is defined as the Normalized Fluorescence, NF. The NF was calculated by dividing the pictures after background subtraction pixel-by-pixel (see Figure 4.6 A). Histograms of the NF picture were generated and fitted by a Gaussian to yield the NF mean and standard deviation (Figure 4.6 B). This number can be interpreted as the binding strength of the protein-DNA interaction in comparison to a certain reference bond. A variation of the reference bond will result in a different NF and refines the information about the DNA-protein interaction. The zinc finger protein-DNA interaction was tested with three DNA double-strands incorporating either a high affinity sequence, a low affinity sequence or a no binding sequence against two reference bonds, a 20 base pair and a 40 base pair DNA duplex. The data were analyzed in the way just described with the results depicted in Figure 4.6 C. Due to the low DNA transfer for the no binding sequence, a calculation of the NF was not possible, so these values were approximated with zero. Differences were clearly visible for the NF values for the low and high affinity sequences as well as for the variations of the reference bond. As expected, the highest value of 0.65 ± 0.07 was measured for the high affinity sequence against the 20 base pair reference bond compared to 0.39 ± 0.15 for the low affinity sequence against the same reference bond. The stronger reference bond lowered the values to 0.32 ± 0.01 and 0.20 ± 0.02 for high and low affinity DNA motifs, respectively. For both DNA binding motifs, the mean NF was reduced by half if the number of reference base pairs was doubled: 0.65 (20 base pairs) to 0.32 (40 base pairs) for the high affinity motif and 0.39 (20 base pairs) to 0.20 (40 base pairs) for the low affinity motif. Hence, a linear relationship between the number of reference base pair and the mean NF can be assumed in this range of reference bond length. Interestingly, the NF values for the low affinity sequence against the 20 base pair reference bond, 0.39, and for the high affinity sequence against the 40 base pair reference bond, 0.32, were equal within errors (see Figure 3C) . This allows the interpretation of a difference in binding strength of the zinc finger protein with these two DNA motifs that corresponds to the average binding strength of a

20 base pair DNA double strand.

Thus, it was demonstrated that the specificity of DNA-protein interactions can be quantified via the binding strength in a force-based assay in a single measurement. Furthermore, the binding strength can be characterized with a simple picture by correlating it to the average binding strength of a certain number of DNA base pairs. The parallel format of the current assay allows the measurement of several proteins against multiple DNA duplexes in a single experiment. Further development will extend the technique towards high throughput by increasing the number of DNA duplexes on the stamp by means of a microplotter and decreasing the protein spot size.

Chapter 5

Outlook

This thesis demonstrates various applications for the Molecular Force Assay that have a great potential to contribute to the solution of current biological problems. Especially its parallel format distinguishes the MFA from other force-based techniques and enables its use for investigations that were so far unsuited for force measurements. The force-based aptamer sensor (chapter 4.1) characterizes even small molecules and weak binders in buffer solution as well as complex fluids within a single measurement. Additionally, labeling of the molecules in question is unnecessary. Hence, its principle could be utilized in diagnostic tools that analyze medical samples like blood for properties indicating a certain malfunction or disease. Furthermore, the MFA can assist in the development of new medical therapeutics that aim at the RNA interference pathway. Chapter 4.2 describes the use of the MFA for the screening and characterization of RNA ligands that selectively inhibit the protein Dicer. The third part of this thesis illustrates an application of the MFA that directly quantifies the binding strength between proteins and DNA sequences. The specificity of a protein to all kinds of genomic DNA is of utmost importance in order to understand transcriptional regulation. The specificity correlates with the binding strength and is, thus accessible in force measurements. Chapter 4.3 describes the quantification of the binding strength of a zinc finger protein with several DNA motifs within one measurement. This clearly proves that the binding strength of multiple interactions can be determined in a single experiment.

All three applications will increase their potential with further standardization and miniaturization. Particularly, some progress has already been made in the miniaturization of the MFA. For the measurements in this thesis, the spots of molecular complexes on the glass slide had an average diameter of $1mm$. Severin et al. [24] could prove that a spot size

of $25\mu m^2$ is sufficient to get valid results. Furthermore, the fabrication of DNA microarrays is a standard procedure so that a further parallelization of the MFA seems feasible. Additionally, the possibility to incubate every of these miniature spot with a different ligand or protein concentration would greatly enhance the multiplexing capabilities of the MFA. This was realized only recently by implementing the MFA in a microfluidic device [76]. Another possible development is the combination of *in vitro* protein expression on a microfluidic chip with the MFA. Proteins could be directly expressed on the chip without the need to store them and could be immediately attached to the surface via the ybbR-Coenzyme A technology. A button valve functionlized with the DNA sample and reference bond could come down and quantify the protein-DNA interaction similar as described by Otten et al. [76]. The current microfluidic chip format would, thus, allow the measurement of hundreds of interactions in a single experiment and could extend the potential of this application of the MFA towards high throughput.

Thus, the Molecular Force Assay is a great tool for the quantification of biomolecular interactions. Further developments, as are partly already realized, will greatly enhance its potential to contribute to the solution of current biological problems.

Appendix A

Publications

A.1 Publication 1: DNA as a Force Sensor in an Aptamer-Based Biochip for Adenosine

Dominik Ho, Katja Falter, Philip Severin and Hermann E. Gaub;
Anal. Chem. 2009, 81,3159-3164

Anal. Chem. **2009,** *81,* 3159–3164

DNA as a Force Sensor in an Aptamer-Based Biochip for Adenosine

Dominik Ho, Katja Falter, Philip Severin, and Hermann E. Gaub*

Lehrstuhl für Angewandte Physik and Center for Nanoscience (CeNS), Ludwig-Maximilians-Universität, Amalienstrasse 54, 80799 Munich, Germany, and Munich Center For Integrated Protein Science (CIPSM), Ludwig-Maximilians-Universität, Butenandtstrasse 5-13, 81377 Munich, Germany

Without prior signal amplification, small molecules are difficult to detect by current label-free biochip approaches. In the present study, we developed a label-free capture biochip based on the comparative measurement of unbinding forces allowing for direct detection of small-molecule−aptamer interactions. The principle of this assay relies on increased unbinding forces of bipartite aptamers due to complex formation with their cognate ligands. The bipartite aptamers are immobilized on glass support via short DNA duplexes that serve as references to which unbinding forces can be compared. In a simple model system, adenosine is captured from solution by an adenosine-selective aptamer. Linking the molecular chains, each consisting of a short DNA reference duplex and a bipartite aptamer, between glass and a poly(dimethylsiloxane) (PDMS) surface and subsequently separating the surfaces compares the unbinding forces of the two bonds directly. Fluorescence readout allows for quantification of the fractions of broken aptamer and broken reference bonds. The presence of micromolar adenosine concentrations reliably resulted in a shift toward larger fractions of broken reference bonds. Because of the force-based design, the interactions between the bipartite aptamer and the target, rather than the presence of the target, are detected and no washing step disturbing the equilibrium state prior to probing and no reporter aptamer or antibody is required. The assay exhibits excellent selectivity against other nucleotides and detects adenosine in the presence of a complex molecular background. Multiplexing was demonstrated by performing whole titration experiments on a single chip revealing an effective half-maximal concentration of 124.8 μM agreeing well with literature values.

A current goal within the field of bioanalytical methods is the development of label-free detection formats, which probe multiple interactions simultaneously employing massively parallel assays.[1] High impact of DNA biochips on the field of biology provides motivation to develop arrays for other classes of molecules, including peptides, proteins, and small molecules.[2] DNA or RNA aptamers are promising candidates for fabrication of microarray surfaces, which simply and effectively capture above-mentioned analytes from solution. Numerous reports confirm that aptamers specifically respond to all kinds of molecules[3] such that they are increasingly recognized as rivals for antibodies in in vitro diagnostics[4] and molecular sensor applications,[5−7] surpassing them in terms of small molecular weight, ease of modification, and ability to detect toxins.[8] In contrast to proteins, which are difficult to immobilize on surfaces due to their tendency to adsorb unspecifically and thus lose activity,[9] standard protocols for oligonucleotide microarrays are used for aptamer biochips.

The development of such arrays has proven to be more difficult than expected. Small molecules in particular are rarely detected due to several reasons: First, their small size induces only small signals using current biochip-compatible, label-free detection techniques (e.g., surface plasmon resonance,[10] electrochemical,[11] or cantilever bending[12] based sensors). Second, background signals are generally large in biochip assays due to the tendency of molecules to adsorb to basically all man-made surfaces.[13−15] Third, aptamers developed against small molecules are generally of low affinity,[16] prohibiting washing steps that would increase the signal-to-background ratio. The combination of small signal, high background, and no option for stringent washes creates an overwhelming technical hurdle for the quantification of small molecules without prior signal amplification. Here, we present a widely applicable strategy for the direct detection of small-

* To whom correspondence should be addressed. Phone: +49 89 2180 3172. Fax: +49 89 21 80 2050. E-mail: gaub@physik.lmu.de.

(1) Gurard-Levin, Z. A.; Mrksich, M. *Annu. Rev. Anal. Chem.* **2008**, *1*, 767–800.
(2) Lockhart, D. J.; Winzeler, E. A. *Nature* **2000**, *405*, 827–836.
(3) Hermann, T.; Patel, D. J. *Science* **2000**, *287*, 820–825.
(4) Rimmele, M. *ChemBioChem* **2003**, *4*, 963–971.
(5) Zhang, S.; Xia, J.; Li, X. *Anal. Chem.* **2008**, *80*, 8382–8388.
(6) Wang, J.; Zhou, H. S. *Anal. Chem.* **2008**, *80*, 7174–7178.
(7) Navani, N. K.; Li, Y. F. *Curr. Opin. Chem. Biol.* **2006**, *10*, 272–281.
(8) Tang, J.; Xie, J.; Shao, N.; Yan, Y. *Electrophoresis* **2006**, *27*, 1303–1311.
(9) Kusnezow, W.; Hoheisel, J. *J. Mol. Recognit.* **2003**, *16*, 165–176.
(10) Boozer, C.; Kim, G.; Cong, S.; Guan, H.; Londergan, T. *Curr. Opin. Biotechnol.* **2006**, *17*, 400–405.
(11) Xu, D.; Xu, D.; Yu, X.; Liu, Z.; He, W.; Ma, Z. *Anal. Chem.* **2005**, *77*, 5107–5113.
(12) Zhang, J.; Lang, H.; Huber, F.; Bietsch, A.; Grange, W.; Certa, U.; Mckendry, R.; Güntherodt, H.; Hegner, M.; Gerber, C. *Nat. Nanotechnol.* **2006**, *1*, 214–220.
(13) Haab, B. B.; Dunham, M. J.; Brown, P. O. *Genome Biol.* **2001**, *2*, 0004.10004.13.
(14) Michaud, G.; Salcius, M.; Zhou, F.; Bangham, R.; Bonin, J.; Guo, H.; Snyder, M.; Predki, P.; Schweitzer, B. *Nat. Biotechnol.* **2003**, *21*, 1509–1512.
(15) Ma, H.; Horiuchi, K. *Drug Discovery Today* **2006**, *11*, 661–668.
(16) Hamula, C.; Guthrie, J.; Zhang, H.; Li, X.; Le, X. *TrAC, Trends Anal. Chem.* **2006**, *25*, 681–691.

10.1021/ac802766j CCC: $40.75
Published on Web 03/19/2009

molecule−aptamer complex formation. Our approach reports interactions between small molecules and aptamers, rather than the mere presence of small molecules close to a sensor surface. Thereby, nonspecific adhesion, the major bottleneck in the development of next-generation biochips, is rendered insignificant.

For detection of the bound analyte we applied the comparative unbinding force assay (CUFA), which operates label-free and is insensitive to nonspecifically adsorbed target molecules. CUFA has already been applied to detect single-nucleotide polymorphisms,[17] to study differences of antibody/antigen interactions,[18] to eliminate cross-reactions on protein microarrays,[19] and to investigate the chiral selectivity of small peptides.[20] Whereas standard single-molecule force spectroscopy experiments measure the unbinding forces of molecular complexes by a microscopic, springlike object, e.g., an atomic force microscopy (AFM) cantilever[21] or a bead in an optical trap,[22] CUFA reduces the force detector to a single DNA reference duplex. Many molecular chains, each consisting of a bipartite aptamer and a DNA reference duplex, are grafted between two surfaces. The linker between the bonds is conjugated to a fluorophore. Upon separation of the surfaces, a force gradually builds up within the molecular chain and the unbinding forces of the bipartite aptamer structure are compared directly against the unbinding forces of the short DNA reference duplex. The result, i.e., the fractions of broken aptamer and broken reference bonds, is stored in a binary fluorophore distribution (fluorophore top or bottom surface). If complex formation between aptamer and ligand results in increased unbinding forces of the aptamer structure, a shift toward larger fractions of broken reference bonds is expected. Thereby, CUFA combines the advantages of fluorescence-based techniques, namely, fast and sensitive detection employing commercially available scanners or fluorescence microscopes, with the advantages of label-free methods, namely, no undesirable label interactions and the option for simultaneous detection of multiple analytes. Importantly, high specificity when investigating molecular interactions is a major strength of CUFA. Current fluorescent[23] and label-free biochip methods do not allow for discrimination between specifically and nonspecifically adhered analytes, which may lead to false-positives. Washing steps are performed to reduce nonspecific adhesion. However, if molecular interactions with equilibrium dissociation constants in the micromolar range need to be characterized, specifically but weakly interacting molecules are also removed resulting in false-negatives. CUFA overcomes these difficulties by detecting the interaction between the capture aptamer and its target and not merely the presence of the target.

In the present study, we investigated the interaction between adenosine and an adenosine-selective aptamer. This model system is instructive for the reasons that the aptamer is well-characterized,[24−26,28] the interaction is very weak, and the analyte is so small that it cannot be detected directly with surface plasmon resonance.[6]

EXPERIMENTAL SECTION

Immobilization of Aptamer−DNA Unbinding Force Complex on Slides (Bottom Surface). DNA oligomers **1**, **2**, and **3** were purchased HPLC grade from IBA GmbH (Göttingen, Germany). Sequences and modifications of all oligonucleotides are the following: **1**, NH_2-(hexaethyleneglycol)$_5$-5′-TTT TTT TTT TCG GTC TGT CGC GTA CTT GCA-3′; **2**, 3′-GCC AGA CAG CGC ATG AAC GTT TTT T-5′-5′-T(Cy3) TTT TTC AAC ATA CCT GGG GGA GTA TAT AAT GAC TGA CCC C-3′; **3**, biotin-5′-TTT TTT TTT TGG GGT CAG TCA TTA TAG CGG AGG AAG GTA TGT TG-3′. For the upside-down experiment the NH_2-(hexaethyleneglycol)$_5$ (HEGL) and biotin modifications are exchanged. The five HEGL linkers are connected via phosphate groups. DNA oligomer **1** is amine-modified, which allows covalent linkage to aldehyde-functionalized glass slides (Schott GmbH, Jena, Germany). We spotted 2 μL drops of 5× SSC (saline sodium citrate; Sigma-Aldrich GmbH, Munich, Germany) containing 25 μM oligomer **1** on the aldehyde slide in a 4 × 4 pattern and incubated the slide in a saturated NaCl ddH_2O atmosphere overnight. After washing the slide with ddH_2O containing 0.2% sodium dodecyl sulfate (SDS; VWR Scientific GmbH, Darmstadt, Germany) and thoroughly rinsing the slide with ddH_2O we reduced the resulting Schiff bases with 1% aqueous $NaBH_4$ (VWR Scientific GmbH, Darmstadt, Germany) for 20 min. Subsequently, the slide was washed with 1× SSC and thoroughly rinsed with ddH_2O. In order to reduce nonspecific binding, the slides were blocked in 1× SSC containing 4% bovine serum albumin (BSA; Sigma-Aldrich GmbH, Munich, Germany) for 30 min. Custom-made 16-well silicone isolators (Grace-Biolabs, OR) were placed on top of the immobilized DNA oligomer **1**. The 0.1 μM Cy3-modified oligomer **2** and 0.2 μM biotin-modified oligomer **3** were hybridized to the latter for 1 h, completing the **1·2·3** complex on the glass slide. The slides were washed with 1× SSC containing 0.05% SDS and thoroughly rinsed with 1× SSC. The silicone isolators stayed on the slide throughout the experiment, and care was taken that after hybridization the slide remained immersed in 1× SSC.

Ligand Incubation. The 16-well silicon isolators allow for incubation with different concentrations of the ligand molecule on one slide. An amount of 100 μL of the respective solutions was circulated through the wells employing a self-made microfluidic system. The latter was driven by two 16-channel peristaltic pumps (Ismatec GmbH, Wertheim-Mondfeld, Germany) pumping the different solutions through tubing and blunt needles leading into and out of the wells in a closed circuit. The tubing was

(17) Albrecht, C.; Blank, K.; Lalic-Multhaler, M.; Hirler, S.; Mai, T.; Gilbert, I.; Schiffmann, S.; Bayer, T.; Clausen-Schaumann, H.; Gaub, H. E. *Science* **2003**, *301*, 367–370.
(18) Blank, K.; Mai, T.; Gilbert, I.; Schiffmann, S.; Rankl, J.; Zivin, R.; Tackney, C.; Nicolaus, T.; Spinnler, K.; Oesterhelt, F.; Benoit, M.; Clausen-Schaumann, H.; Gaub, H. E. *Proc. Natl. Acad. Sci. U.S.A.* **2003**, *100*, 11356–11360.
(19) Blank, K.; Lankenau, A.; Mai, T.; Schiffmann, S.; Gilbert, I.; Hirler, S.; Albrecht, C.; Benoit, M.; Gaub, H. E.; Clausen-Schaumann, H. *Anal. Bioanal. Chem.* **2004**, *379*, 974–981.
(20) Dose, C.; Ho, D.; Gaub, H. E.; Dervan, P. B.; Albrecht, C. *Angew. Chem., Int. Ed.* **2007**, *46*, 8384–8387.
(21) Florin, E. L.; Moy, V. T.; Gaub, H. E. *Science* **1994**, *264*, 415–417.
(22) Svoboda, K.; Schmidt, C. F.; Schnapp, B. J.; Block, S. M. *Nature* **1993**, *365*, 721–727.
(23) Warren, C.; Kratochvil, N.; Hauschild, K.; Foister, S.; Brezinski, M.; Dervan, P.; Phillips, G., Jr.; Ansari, A. *Proc. Natl. Acad. Sci. U.S.A.* **2006**, *103*, 867–872.
(24) Huizenga, D. E.; Szostak, J. W. *Biochemistry* **1995**, *34*, 656–665.
(25) Lin, C. H.; Patel, D. J. *Chem. Biol.* **1997**, *4*, 817–832.
(26) Stojanovic, M. N.; de Prada, P.; Landry, D. W. *J. Am. Chem. Soc.* **2000**, *122*, 11547–11548.
(28) Jhaveri, S. D.; Kirby, R.; Conrad, R.; Maglott, E. J.; Bowser, M.; Kennedy, R. T.; Glick, G.; Ellington, A. D. *J. Am. Chem. Soc.* **2000**, *122*, 2469–2473.

passivated prior to use with 1× SSC containing 4% BSA for 30 min. Adenosine triphosphate (ATP), adenosine monophosphate (AMP), and guanosine triphosphate (GTP) were obtained from Roche (Roche GmbH, Grenzach, Germany).

Immobilization of Streptavidin on Poly(dimethylsiloxane) Stamp (Top Surface). Micro- and macrostructered poly(dimethylsiloxane) (PDMS) stamps were fabricated by casting 1:10 cross-linker/base (Sylgard, Dow Corning, MI) into a custom-made Pyrex/silicon wafer (HSG-IMIT, Villingen-Schwenningen, Germany) according to standard procedures.[29] The resulting PDMS stamp carries pillars of 1 mm diameter and 1 mm height in a square pattern on a 3 mm thick basis. The spacing between two adjacent pillars is 3 mm. The flat pillar surface is microstructured with 100 μm × 100 μm pads separated by 41 μm wide and 5 μm deep rectangular trenches allowing for drainage of liquid during the contact and separation process. Before free polymers were extracted from the device in toluene using a Soxhlet device, the PDMS was cut in 4 × 4 pillar pieces. PDMS was then activated in 12.5% HCl overnight and derivatized with (3-glycidoxypropyl)-trimethoxysilane (ABCR, Karlsruhe, Germany) in order to generate epoxide groups. NH_2−PEG−biotin (3400 g/mol; Rapp Polymere, Tübingen, Germany) was molten at 80 °C, and roughly 1 μL was spotted on each pillar followed by overnight incubation in argon atmosphere at 80 °C. The excess polymers were thoroughly removed with ddH_2O. Shortly before the experiment the PDMS was incubated with 1 μg/mL streptavidin (Thermo Fisher Scientific, Bonn, Germany) in 1× SSC and 0.4% BSA for 30 min, washed with 1× SSC containing 0.05% Tween 20 (VWR Scientific GmbH, Darmstadt, Germany), and gently dried with N_2 gas.

Contact Process and Fluorescence Readout. On an inverted microscope (Carl-Zeiss MicroImaging GmbH, Göttingen, Germany) the slide was fixed on a stainless steel stage with permanent magnets. The PDMS device was placed upside down on a glass block connected to a *xyz* stepper motor system (OWIS GmbH, Staufen, Germany) and a closed-loop piezo (Piezo Systems Jena, Germany). Prior to the contact process, the slide and the PDMS stamp were aligned parallel to each other, employing reflection interference microscopy[30] and a commercially available gimbal adjustment system (OWIS GmbH, Germany) mounted to the piezo. With the use of the latter, contact was established. Care was taken that each individual pillar is compressed not more than 3 μm. The separation of the two surfaces was carried out at constant velocity of 1 μm/s. Fluorescence images were recorded before and after the contact process employing a Tecan microarray scanner (Tecan Austria GmbH, Grödig, Austria).

RESULTS AND DISCUSSION

Detection Principle of the Force-Based Aptamer Sensor. The implementation of this format is shown schematically in Figure 1. Although the instrumentation is almost identical to a microcontact printing setup,[31] the key to the comparable unbinding force assay lies within the molecular setup (Figure 1a). A short DNA duplex in shear geometry serves as a force reference. One strand, oligomer **1**, is connected to glass support (bottom surface) via a $(hexaethyleneglycol)_5$ spacer. The complementary strand, oligomer **2**, which also carries a Cy3 fluorescence label, possesses an overhang containing the sequence of one part of the bipartite ATP aptamer. The complementary aptamer strand, oligomer **3**, is biotin-modified at the end of a polythymine linker and completes the **1·2·3** complex on the glass slide. We chose the reference force duplex and the stem regions flanking the aptamer such that their calculated free energies[32] are similar, assuming that similar free energies also imply similar unbinding forces under an external load. The spontaneous off-rates are sufficiently slow such that the complex is stable for days under physiological conditions.

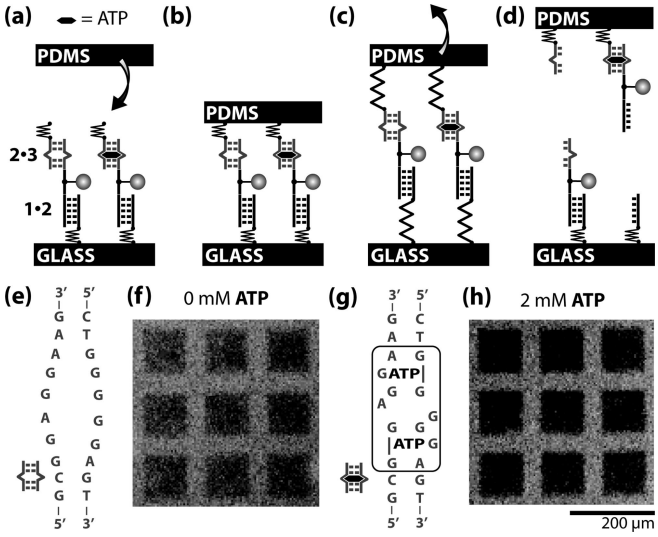

Figure 1. Schematic representation of the comparative unbinding force assay for the detection of small molecules. (a) DNA reference duplexes **1·2** and bipartite aptamers **2·3** are bound in series via PEG spacers to glass support. Depending on the presence of ATP, the aptamer is in its bound or free state. A streptavidin-functionalized PDMS surface is approached to the glass surface. (b) PDMS couples to the **3** oligomers of the bipartite aptamers via biotin·streptavidin complex formation. (c) The two surfaces are separated, and an increasing force builds up until either the reference duplex or the bipartite aptamer breaks. (d) Aptamer−ATP complex formation increases the unbinding forces of the bipartite aptamer. In comparison to the case that no ATP is present, a larger fraction of linking DNA strands conjugated to fluorophores is transferred from the glass to the PDMS. (e) At 0 mM ATP the bipartite aptamer is present as a loose bubble flanked by Watson−Crick base-paired stem regions. (f) Fluorescence on glass after contact without prior incubation with ATP. The squarelike features (100 × 100 μm^2) correspond to the area contacted with microstructured PDMS. (g) At 2 mM ATP the bipartite aptamer bases show enhanced stacking upon binding of two molecules of ATP. (h) Fluorescence on glass after contact with prior incubation with 2 mM ATP. In comparison to the 0 mM ATP case, a larger fraction of fluorescence was transferred from the glass to the PDMS.

In Figure 1b the **1·2·3** complex on the glass surface was brought into contact with a PDMS surface functionalized with streptavidin attached to 3400 g/mol PEG linkers, allowing for biotin·streptavidin complexation. After 10 min, the surfaces were separated at a constant velocity of 1 μm/s (Figure 1c). Thereby, the polymeric anchors were stretched and a force gradually built up until the chain of molecular complexes ruptured either at the

(29) Wilbur, J. L.; Kumar, A.; Kim, E.; Whitesides, G. M. *Adv. Mater.* **1994**, *6*, 600–604.
(30) Wiegand, G.; Neumaier, K. R.; Sackmann, E. *Appl. Opt.* **1998**, *37*, 6892–6905.
(31) Bernard, A.; Renault, J. P.; Michel, B.; Bosshard, H. R. *Adv. Mater.* **2000**, *12*, 1067–1070.
(32) Kibbe, W. A. *Nucleic Acids Res.* **2007**, *35*, 43–46.

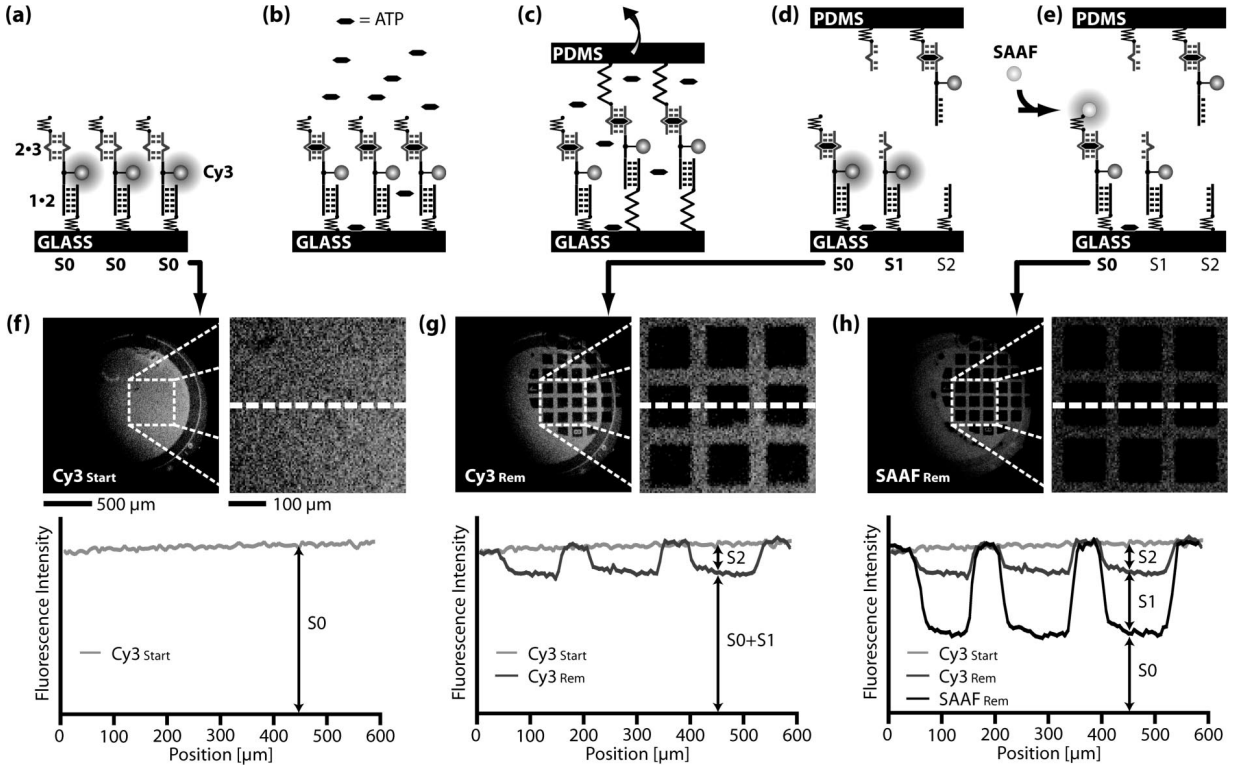

Figure 2. Detailed schematic of data acquisition and processing. (a) Initially all DNA-hybrids are in the state S0. The chip fluorescence is recorded at 550−600 nm ($Cy3_{Start}$). (b) Incubation with ATP. (c) Coupling of the DNA-hybrids to a second surface and separation of the surfaces in the presence of ATP. (d) DNA-hybrids appear in the states S0, S1, and S2. The chip fluorescence is recorded again at 550−600 nm ($Cy3_{Rem}$). (e) Labeling of noncoupled DNA-hybrids with streptavidin Alexa Fluor 647 (SAAF) and recording of fluorescence at 655−695 nm ($SAAF_{Rem}$). (f) $Cy3_{Start}$ chip fluorescence image and corresponding line profile allowing for determination of the initial amount of DNA-hybrids. (g) $Cy3_{Rem}$ chip fluorescence image and corresponding line profile allowing for determination of the fraction S2. (h) $SAAF_{Rem}$ chip fluorescence image and corresponding line profile allowing for determination of the fractions S0 and S1. The fluorescence line profiles are averaged over 40 μm.

1·2 reference or at the **2·3** aptamer. We neither recorded nor analyzed the macroscopic force needed to pull the two surfaces apart. The unbinding forces are compared intrinsically and independently for each molecular chain. Aptamer−ATP complex formation is expected to increase the aptamer unbinding forces and as a result increase the fraction of the broken reference bonds (Figure 1d). Macroscopically, the fractions of broken reference bonds and broken aptamer bonds were determined via the location of the fluorescently labeled oligomers **2**. Parts f and h of Figure 1 show the fluorescence intensity of the DNA-hybrids after contact with and without the presence of 2 mM ATP. The squarelike features correspond to the contacted area. It is qualitatively observed that without the presence of ATP a smaller fraction of fluorophores is transferred from the glass slide to the PDMS compared to the case when the spot is incubated with 2 mM ATP. This is in agreement with ATP stabilizing the aptamer bond and thus an increased probability that the reference bonds fail. Consequently, the fraction of retained oligomers **2** and thus fluorophores on the glass slide is reduced.

The breakage of the biotin·streptavidin bond may be neglected since it unbinds at significantly higher forces than short double-stranded DNA. However, unbinding forces strongly depend on the applied force loading rates. Since in our case the force loading rates were not recorded, they are estimated from single-molecule experiments. For the combination of an applied separation velocity of 1 μm/s, a combined PEG linker of 10 000 g/mol and a 20 bp DNA duplex, a force-loading rate in the order of 10^3 pN/s is typically obtained.[33] Under these conditions a 20 bp DNA duplex unbinds at around 40 pN,[33] whereas biotin·streptavidin unbinds at around 80 pN or even higher forces.[34,35]

Quantitative Fluorescence Analysis. Quantitative determination of the ratio between broken aptamer bonds and broken reference bonds requires a more complex analysis, since it cannot be assumed that all DNA-hybrids physically connect to both surfaces via the biotin·streptavidin bond. Uncoupled DNA-hybrids result in a background signal. In our experiments, we determined and subtracted the latter for each squarelike feature individually in order to calculate the normalized fluorescence (NF). The NF is defined as the ratio between broken **2·3** complexes and total amount of DNA-hybrids, to which a load was applied, and is determined as follows: Initially, when the **1·2·3** DNA-hybrids are immobilized on glass, a fluorescence image is taken (Figure 2, parts a and f). The DNA-hybrids are incubated with ATP (Figure 2b). The PDMS stamp is lowered toward the glass surface allowing the DNA-hybrids to couple to the PDMS via biotin·streptavidin complexation. In the presence of the ATP the PDMS is retracted (Figure 2c), and an increasing force is built up until one of the links breaks. Not all of the DNA-hybrids are coupled via the biotin·streptavidin bond. As illustrated in Figure 1d, the DNA-hybrids appear in three different states **1·2·3** (S0), **1·2** (S1),

(33) Morfill, J.; Kuhner, F.; Blank, K.; Lugmaier, R.; Sedlmair, J.; Gaub, H. E. *Biophys. J.* **2007**, *93*, 2400–2409.
(34) Merkel, R.; Nassoy, P.; Leung, A.; Ritchie, K.; Evans, E. *Nature* **1999**, *397*, 50–53.
(35) Pincet, J. *Biophys. J.* **2005**, *89*, 4374–4381.

and **1** (S2) on the glass slide. For simplicity we refer to the amounts of S0, S1, and S2 as fractions normalized to all DNA-hybrids, i.e., the relation S0 + S1 + S2 = 1 is always true. Only molecules in state S1 and S2 were exposed to an unbinding force. Molecules in the state S0 were not coupled to the PDMS surface and therefore retained the biotinylated oligomer **3**. From the Cy3 fluorescence intensity per unit area the fraction of S2 is determined (Figure 2, parts d and g, eq 3). In order to distinguish S0 and S1, the former is labeled with the spectrally distinct fluorescent marker streptavidin Alexa Fluor 647 (SAAF, Figure 2, parts e and h). The labeling is performed subsequent to the Cy3 readout in order to avoid quenching or fluorescence resonance energy transfer (FRET) effects. This allows us to determine the fractions of S0 and S1 from SAAF fluorescence (eqs 1 and 2).

$$S0 = SAAF_{Ratio} \tag{1}$$

$$S1 = Cy3_{Ratio} - SAAF_{Ratio} \tag{2}$$

$$S2 = 1 - Cy3_{Ratio} \tag{3}$$

$$Cy3_{Ratio} = \frac{Cy3_{Result}}{Cy3_{Start}} \tag{4a}$$

$$SAAF_{Ratio} = \frac{SAAF_{Result}}{SAAF_{Start}} \tag{4b}$$

For the analysis only the $Cy3_{Rem}$ and $SAAF_{Rem}$ fluorescence images are employed. $SAAF_{Start}$ and $Cy3_{Start}$ are determined from the noncontacted regions adjacent to each squarelike feature. The NF is given by the fraction of broken **2·3** bonds (S1) normalized to the fraction of bonds that have been under load (S1 + S2).

$$NF = \frac{S1}{S1 + S2} = \frac{Cy3_{Ratio} - SAAF_{Ratio}}{1 - SAAF_{Ratio}} \tag{5}$$

The NF directly reflects the relative unbinding forces, a physical quantity inherent to a pair of molecular complexes, and is not influenced by the number of molecules under load. The NF should not be confused with $Cy3_{Ratio}$. For a fixed mechanical stability, the latter depends on the fraction of coupled DNA-hybrids, whereas the NF does not. The NFs presented in this work are the averages of all squarelike features contacted properly within an experiment. The NF experimental error is estimated from repeated blank measurements yielding a standard deviation of 0.018.

CUFA Detects the Concentration of Adenosine. Varying concentrations of ATP (0−2000 μM) were applied to the different DNA-hybrid spots on one slide (Figure 3a). This way a whole concentration range was measured within a single experiment. Under physiological buffer conditions (15 mM sodium citrate, 150 mM NaCl, 1 mM $MgCl_2$, pH 7.4), the **1·2·3** sensor reliably reported the presence of its target. At zero concentration the normalized fluorescence was 0.792 ± 0.018. Upon addition of micromolar concentrations of ATP, the normalized fluorescence decreased and reached its minimum of 0.683 ± 0.018 at 0.5 mM as shown in Figure 3b. This is in agreement with a stabilizing effect of ATP on the aptamer structure. Fitting the ATP titration data to the Hill equation with slope $n = 2$ revealed a half-maximal effective concentration EC50 = 124.8 μM with a 95% confidence interval of [102.8 μM, 151.4 μM]. Huizenga and Szostak demonstrated that the equilibrium dissociation constant of the adenosine−aptamer interaction depends upon the specific salt and Mg^{2+} concentrations.[24] For the present buffer conditions, the experimentally obtained EC50 value is in agreement with previously published values of the equilibrium dissociation constant.[24−28]

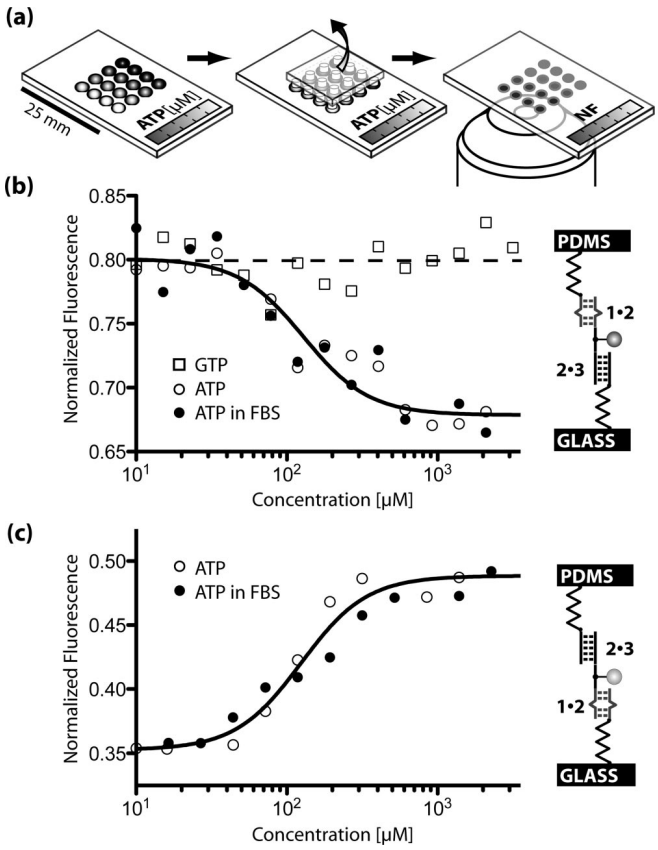

Figure 3. (a) Self-made microfluidic device allows incubation of 16 identical DNA-hybrid spots with different concentrations of ATP on a single chip. In the presence of ATP, the chip is contacted with a 16 pillar PDMS contact device and read out via fluorescence. (b) Normalized fluorescence for increasing concentrations of ATP and GTP in the regular configuration **1·2·3**. The solid line is the corresponding fit to the Hill equation. (c) Upside-down configuration **3·2·1**.

In order to ensure that the molecular setup responds as expected, we investigated, analogously to the regular configuration **1·2·3**, the upside-down configuration **3·2·1**. Here, the position of the target and reference bond is exchanged, and thus the response to the addition of adenosine should be inverted. Indeed, the NF increased from 0.353 ± 0.018 to a maximal NF of 0.489 ± 0.018 upon increasing the ATP concentration from 0 to 0.5 mM (Figure 3c). The aptamer bond is now adjacent to the glass slide. Upon binding of the target molecule, the aptamer is less likely to break and a larger fraction of fluorophores remains on the glass slide.

Sensitivity. The sensitivity of our assay is estimated from the signal-to-noise ratio. For ATP concentrations below 53.5 μM the latter is lower than 1, and thus ATP is not detectable. From 53.5

(27) Stojanovic, M. N.; de Prada, P.; Landry, D. W. *J. Am. Chem. Soc.* **2001**, *123*, 4928–4931.

to 310.3 μM, ATP is quantified via the change in normalized fluorescence. At higher ATP concentrations the change in normalized fluorescence saturates, and thus ATP is detected; however, it cannot be quantified. This is comparable to fluorescent sensors based on aptamer assembly[26] or folding.[27,28] In recent publications, several groups demonstrated the use of structure-switching aptamer sensors in combination with signal amplification techniques using gold nanoparticles. For these assays larger ranges of sensitivity were reported.[5,6]

Selectivity. To demonstrate the selectivity of our force-based assay, separate experiments were conducted on GTP (Roche GmbH, Grenzach, Germany) and AMP (Roche GmbH, Grenzach, Germany). Since the aptamer recognizes adenosine, the addition of AMP resulted in a similar response like ATP (Supporting Information Figure S1). Conversely GTP, where the adenosine base is exchanged with a guanosine base, produced no detectable response (Figure 3c). The results demonstrated that the developed strategy has sufficient selectivity to detect the interaction between adenosine and the antiadenosine aptamers immobilized on the chip surface.

Detection of Adenosine in Molecular Crowded Environment. The experiments presented above were performed in pure 1× SSC buffer. However, because of the force-based design, the experimental result should only be susceptible to molecules interacting directly with the aptamer structure. In order to demonstrate this, we repeated the ATP experiments in 1× SSC buffer and 10% fetal bovine serum (FBS, Sigma-Aldrich, Germany). While the force comparison was carried out in the presence of the ligand and a molecular crowded solution, the readout of the result occurred subsequently and is therefore insensitive to additional washing steps, as long as these do not dissociate the DNA-hybrids. As shown in Figure 3, parts b and c, the same response is observed in the presence of FBS as for the FBS-free measurements.

CONCLUSIONS

In the present study, we employed the CUFA as a label-free aptamer-based capture biochip. The design relies on an increased stability of bipartite aptamers upon binding of its target molecules. The assay reliably reported the presence of adenosine for concentrations above 53.5 μM and allowed quantitative detection of adenosine for concentrations between 53.5 and 310.3 μM. The Hill equation governs the response of the assay with an EC50 = 124.8 μM agreeing well with literature values for the equilibrium dissociation constant of the antiadenosine aptamer.

The limited sensitivity range and the dependence of the equilibrium constant (and thus of the assay response) upon specific salt and Mg^{2+} concentrations renders quantitative detection of adenosine impracticable. Ionic concentrations of real samples are hardly ever known, and adenosine detection assays with superior sensitivity ranges are available. The strength of the assay lies within the fast and reliable characterization of the equilibrium dissociation constant of the interaction between a small molecule and a low-affinity aptamer. This was demonstrated in pure SSC buffer as well as in a molecular crowded solution. Producing reliable equilibrium binding data within the micromolar regime still poses a challenge for existing high-throughput techniques.[36] Conversely, implementing aptamers of higher affinity can yield more sensitive sensors for their cognate molecules. Due to the label-free, microarray-compatible design, it is easily imaginable to test the presence of various analytes in parallel—basically only limited by the number of available aptamer structures. Detection of proteins and peptides, simultaneous detection of multiple analytes, and miniaturization will be reported elsewhere.

ACKNOWLEDGMENT

We thank P. Tinnefeld, F. Weinert, P. Baaske, S. Duhr, U. Steinbach, F. Dehmelt, J. Vogelsang, S. Kufer, and C. Albrecht for helpful discussions. Support was provided by the Nanosystem Initiative Munich and the Deutsche Forschungsgemeinschaft. D.H. and P.S. are grateful to the Elite Network of Bavaria (IDK-NBT) for a doctoral fellowship. K.F. is grateful for a Max-Weber fellowship.

SUPPORTING INFORMATION AVAILABLE

Additional information as noted in text. This material is available free of charge via the Internet at http://pubs.acs.org.

Received for review December 31, 2008. Accepted February 24, 2009.

AC802766J

(36) Titz, B.; Schlesner, M.; Uetz, P. *Expert Rev. Proteomics* **2004**, *1*, 111–121.

Supporting Information

DNA as a force sensor

in an aptamer-based biochip for adenosine

*Dominik Ho, Katja Falter, Philip Severin and Hermann E. Gaub**

Lehrstuhl für Angewandte Physik and Center for Nanoscience (CeNS), Ludwig-Maximilians-Universität, Amalienstrasse 54, 80799 Munich, Germany

Munich Center For Integrated Protein Science (CIPSM), Ludwig-Maximilians-Universität, Butenandtstrasse 5-13, 81377 Munich, Germany

gaub@physik.lmu.de

CONTENTS

Experiments with AMP

Additional to the experiments with ATP, we conducted experiments on the **1•2•3** molecular setup in presence and absence of 2 mM AMP. Within the experimental error, the change in normalized fluorescence was identical compared to the addition of 2 mM ATP. Explicitly, the normalized fluorescence was 0.80±0.018 for the 0 mM case and 0.67±0.018 for the 2 mM case.

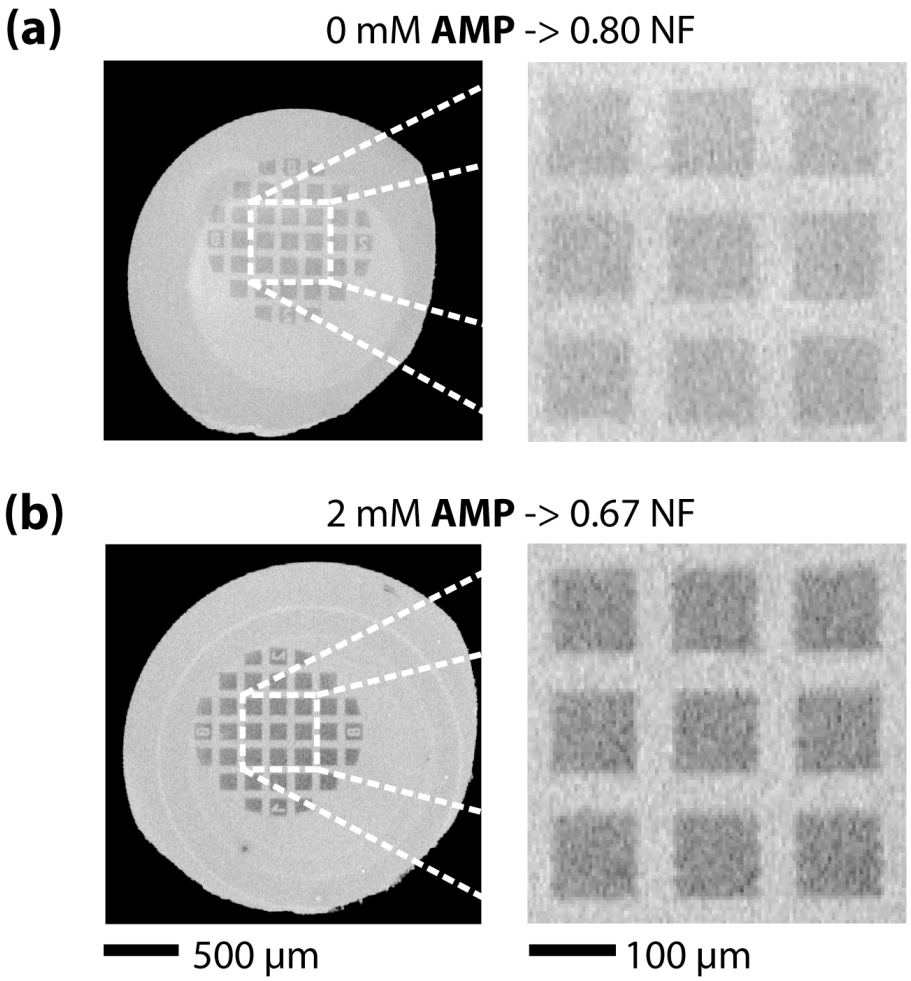

Figure S1. *(a) Fluorescence on glass after contact without prior incubation with AMP. The square-like features (100x100 µm^2) correspond to the area contacted with microstructured PDMS. (b) Fluorescence on glass after contact with prior incubation with 2 mM AMP. Compared to the 0 mM AMP case, a larger fraction of fluorescence was transferred from the glass to the PDMS.*

A.2 Publication 2: Sequence-specific inhibition of Dicer measured with a force-based microarray for RNA ligands

Katja Limmer, Daniela Aschenbrenner and Hermann E. Gaub;
Nucleic Acids Research, 2013, Vol. 41, No. 6, e69

Published online 8 January 2013

Nucleic Acids Research, 2013, Vol. 41, No. 6 ***e69***
doi:10.1093/nar/gks1455

Sequence-specific inhibition of Dicer measured with a force-based microarray for RNA ligands

Katja Limmer, Daniela Aschenbrenner and Hermann E. Gaub*

Lehrstuhl für Angewandte Physik and Center for Nanoscience (CeNS), Ludwig-Maximilians-Universität, Amalienstrasse 54, 80799 Munich, Germany

Received September 17, 2012; Revised December 11, 2012; Accepted December 13, 2012

ABSTRACT

Malfunction of protein translation causes many severe diseases, and suitable correction strategies may become the basis of effective therapies. One major regulatory element of protein translation is the nuclease Dicer that cuts double-stranded RNA independently of the sequence into pieces of 19–22 base pairs starting the RNA interference pathway and activating miRNAs. Inhibiting Dicer is not desirable owing to its multifunctional influence on the cell's gene regulation. Blocking specific RNA sequences by small-molecule binding, however, is a promising approach to affect the cell's condition in a controlled manner. A label-free assay for the screening of site-specific interference of small molecules with Dicer activity is thus needed. We used the Molecular Force Assay (MFA), recently developed in our lab, to measure the activity of Dicer. As a model system, we used an RNA sequence that forms an aptamer-binding site for paromomycin, a 615-dalton aminoglycoside. We show that Dicer activity is modulated as a function of concentration and incubation time: the addition of paromomycin leads to a decrease of Dicer activity according to the amount of ligand. The measured dissociation constant of paromomycin to its aptamer was found to agree well with literature values. The parallel format of the MFA allows a large-scale search and analysis for ligands for any RNA sequence.

INTRODUCTION

The enzyme Dicer has increasingly been attracting attention owing to its crucial role in the RNA interference (RNAi) pathway. RNAi is an endogenous means used by cells to regulate protein translation at the post-transcriptional level (1). Single-stranded RNA sequences of 18–25 nucleotides bind to specific mRNAs and hinder protein translation. Although various classes of small regulatory RNA have been identified, two main categories of single-stranded RNA (ssRNA) involved in metazoan RNA interference can be distinguished that differ in their origin and function but share processing by Dicer: short-interfering RNA (siRNA) and microRNA (miRNA). siRNA precursors are long fully complementary dsRNA that are typically introduced directly into the cytoplasm or taken up from the environment, though recent findings suggest that siRNA may also originate from endogenous sources like transposons (2). Hence, the main task of the siRNA-processing machinery seems to be the defense of genome integrity in response to foreign or invasive nucleic acids (3). miRNAs are transcribed and pre-processed in the nucleus into incomplete base-paired stem-loop structures, known as pre-microRNAs. They are then transferred to the cytoplasm, where Dicer matures the pre-miRNA by cleaving the stem loop structure. The mature miRNA strand binds to the mRNA and usually inhibits translation in combination with a protein complex known as RNA-induced silencing complex (RISC) (4), although gene up-regulation by the RISC complex has also been reported (5,6). In contrast to siRNA, which requires total complementarity to its target sequence, miRNAs and their target mRNA do not need to base-pair perfectly so that a certain miRNA can bind and regulate a variety of mRNA sequences. Several miRNAs may also play a role in the regulation of a single mRNA transcript. Thus, miRNA seems to fine-tune protein expression. The amount of the various miRNA strands differs according to cell age, cell type and health status (7). So miR-1 appears to be tissue specific and was only found in heart tissue and somites of mice embryos (8). Evidence is accumulating that miRNAs are critical for many cellular processes such as developmental timing, cell proliferation or stem cell division (9). Consequently, many disease states occur or are sustained by miRNA dysregulation (10). miR-21, for example, was up-regulated in all tumour samples analysed by (11). Therefore, targeting the RNAi pathway at the step of Dicer cleavage is a promising approach for new therapies against illnesses like cancer or metabolic diseases.

*To whom correspondence should be addressed. Tel: +49 89 2180 3172; Fax: +49 89 2180 2050; Email: gaub@physik.uni-muenchen.de

A relatively small protein of <250 kDA, Dicer has been found in the cytoplasm of all eukaryotes studied to date (12), sometimes in several variants with different tasks. For instance in Drosophila, Dicer-1 cuts pre-miRNA while Dicer-2 generates siRNA from long dsRNA precursors (13). The L-shape of the protein seems to be well-conserved for all variants. Recognition of dsRNA by a PAZ domain occurs in the head of Dicer, which is separated from the two RNAse III domains by a ruler domain (Figure 2A). The base of the L is formed by a helicase, whose function is not totally understood (12). Dicer cleaves long and short (>30 nt) dsRNA strands with equal efficiency, whereas duplexes of ≤21 nt are not processed *in vitro*. A 3′ 2-nucleotide-long overhang, a characteristic of pre-microRNA molecules, increases Dicer's efficiency compared with blunt ends (14).

To interfere with RNAi, knocking out Dicer is not advisable owing to Dicer's crucial role for several cellular processes. On the other hand, a small molecule that binds to the pre-miRNA in question with high specificity and hinders Dicer from maturing the miRNA in question is a great drug candidate. The difficulty, herein, lies in finding potential ligands that bind a certain RNA sequence with high selectivity and also interfere with Dicer cleavage. Krützfeldt *et al.* (15) demonstrated that single-stranded cholesterol-conjugated 2′-O-methyl oligoribonucleotides, complementary to a certain miRNA and termed antagomirs, could specifically reduce the level of that miRNA *in vivo*. Elmen *et al.* (16) could reversibly decrease the level of plasma cholesterol by silencing miRNA-122 with a modified antagomir in non-human primates, thus exemplifying the possible therapeutic value of antagomirs. In both studies, already mature miRNAs are silenced, which might impair the potency of these molecules, as mature miRNA are included in the protein complex RISC and are probably less accessible than pre-miRNA. Cellular uptake of oligonucleotides is another difficulty so that Krützfeldt *et al.* needed high doses to see an effect. Thus, targeting pre-miRNA structures with small molecules has several advantages, but the research of small-molecule RNA binding has encountered several problems [for a review see (17)]. Especially an easy high-throughput technique to screen for and characterize RNA binders could speed up the progress of finding suitable molecules.

Our technique of the Molecular Force Assay (MFA) provides a fast and reliable tool to screen for different RNA binders, to characterize them and to quantify their ability to prevent Dicer from cutting. The MFA is a highly parallel technique, described in detail in (18) and (19), to measure unbinding forces comparatively so that small changes in the structural stability of molecular complexes can be detected. Two molecular bonds, a sample and a reference bond, are linked in series between two surfaces. One surface is retracted and a force gradually builds up in the molecular complexes until one of the bonds breaks. A fluorophor attached to the linking sequence between the two molecular complexes stays with the intact bond (Figure 1A) so that a simple fluorescent measurement by means of a commercially available epi-fluorescent microscope may detect the outcome. Thus, the mechanical stability of two molecular interactions can be probed and compared with each other. In contrast to other force-probe techniques like atomic force microscopy (AFM) or optical traps that measure the unbinding force by a spring-like macroscopic object like a cantilever, the MFA reduces the force detector to the microscopic scale of another molecule, a known reference DNA duplex, so that small differences in structural stability like the binding of a ligand may be resolved. The setup of the MFA is designed such that a large number of molecular complexes are tested simultaneously in one experiment on one chip, and the outcome of this experiment gives statistically significant information on the nature of the molecular interaction in question. Furthermore, as the MFA measures the interaction force between the molecules, unspecific binding events or complex backgrounds like serum do not alter the experimental outcome. Thus, the MFA allows us to detect and characterize the binding of a small molecule to a number of different oligonucleotides or of many small molecules to a certain RNA or DNA sequence in a format, where the analytes are not altered, e.g. by labelling. So far, the MFA has been applied to detect single-nucleotide polymorphism (20), study differences in antibody/antigen interactions (21), investigate the chiral selectivity of small peptides (22), characterize the binding properties of an aptamer to its ligand in a molecularly crowded ambient (23) and to analyse protein–DNA interaction (19).

Here, a 35 bp RNA duplex functions as a substrate for Dicer and is tested against a 22 bp or 27 bp DNA double strand that does not interact with Dicer. The two molecular complexes are linked in a zipper configuration so that a force stretching the bonds unzips the two duplexes (Figure 1A). The construct is covalently attached to the glass slide at the bottom and via a biotin–streptavidin–biotin complex to the upper poly(dimethylsiloxane) (PDMS) stamp surface (Figure 1A). The cyanine dye Cy5 between the RNA and DNA duplex stays with the intact bond after the rupture process, while a second fluorophor Cy3, conjugated to the 3′ end of the uppermost strand, constitutes a Fluorescence Resonance Energy Transfer (FRET) pair with the Cy5 and quantifies the constructs that have not properly coupled to the upper surface and, thus, have not been under force load. If Dicer cuts off about 20 bp of the RNA duplex, this bond is weakened and breaks with higher probability. Thus, Dicer activity can be detected and is quantified for different amounts of Dicer and incubation times. As a proof of principle, the RNA double strand incorporates an RNA aptamer specific for the aminoglycoside paromomycin, which we will characterize by measuring the dissociation constant. It is to be expected that the interaction of paromomycin with its aptamer will hinder Dicer from binding to the RNA duplex and, thus, from cutting.

MATERIALS AND METHODS

DNA/RNA constructs

The molecular complexes consist of three strands that are successively hybridized in our laboratory and are shown in

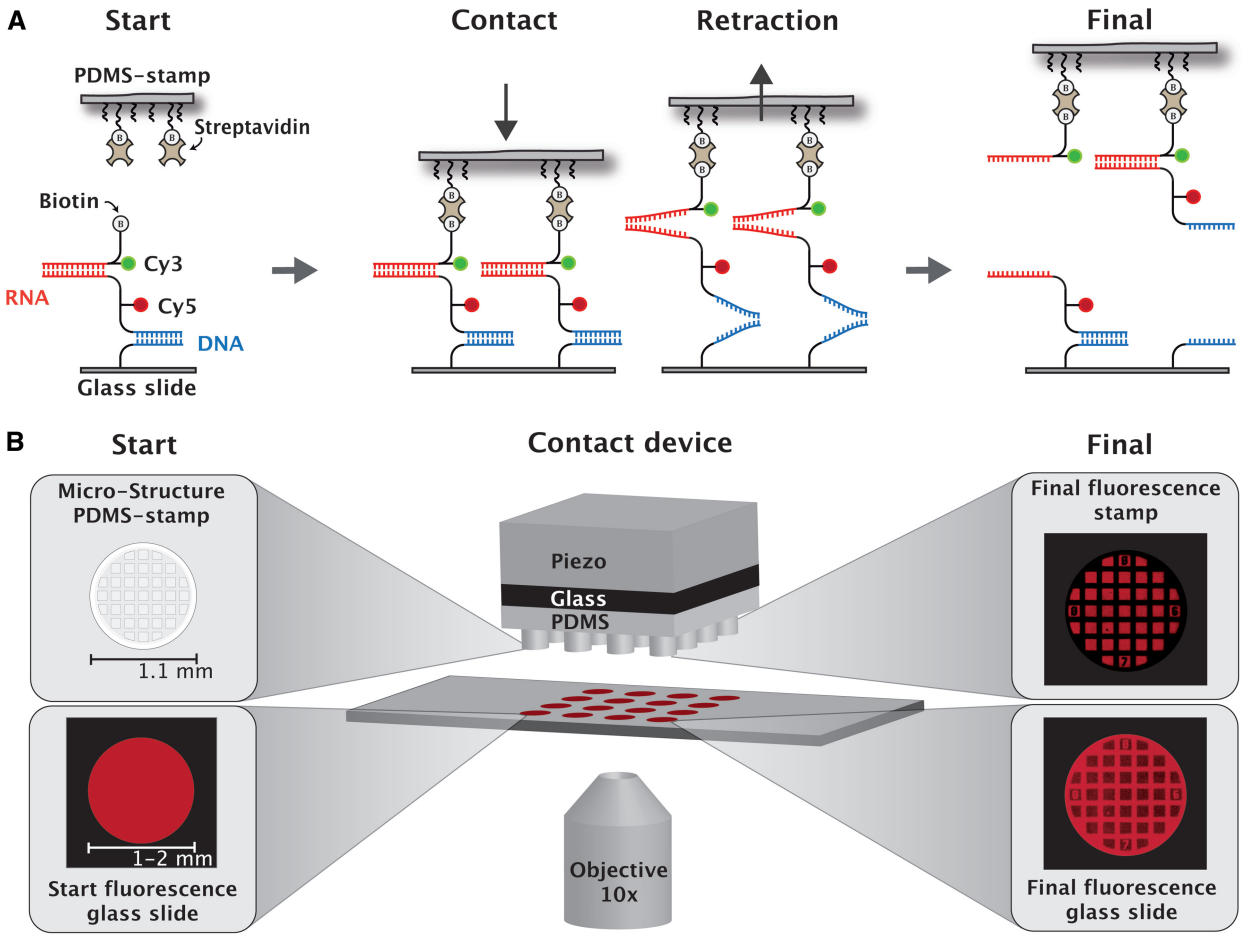

Figure 1. Schematics of the Molecular Force Assay. (**A**) The molecular complex is built up by covalently attaching the lowest strand to a glass slide and, subsequently, binding the pre-hybridized upper duplex to the lowest strand. The fluorophor Cy5 is conjugated to a poly-T sequence connecting the two duplexes. The upper strand is labelled with Cy3 so that a FRET signal provides a measure for a correctly hybridized molecular construct. The 'RNA up' geometry is defined with the DNA complex attached to the glass slide and the RNA duplex constituting the upper part. A biotin–streptavidin–biotin bond links the molecular complex to the upper surface, a soft PDMS stamp. Upon retracting the PDMS stamp, a force builds up in the molecular constructs and unzips the duplexes until the weaker of the two bonds in series ruptures. Note that in this format Cy5 serves as marker for those molecular complexes which remain intact. (**B**) In the setup, the contact device is mounted on an inverted microscope. The PDMS stamp features a micropattern that facilitates leveling and drainage of liquid during the contact and separation process. The oligonucleotide constructs are spotted in a 4×4 pattern, and fluorescence intensities are measured before and after the contact and separation process. After separation the fluorescence intensities of the molecules remaining on the glass and the PDMS surface add up to the total fluorescence intensity measured at the beginning. (**C**) Nucleic acid sequences of the molecular constructs in both configurations.

Figure 1C. The lowermost is modified with an amino group in order to covalenty attach the oligonucleotides to a surface. Avoiding surface effects, 5 HEGL (hexaethyleneglycol) molecules act as an additional spacer between the amino group and the oligonucleotides. Furthermore, poly-T separate the double-stranded sequences from the surfaces and each other. The cyanine dyes Cy5 and Cy3 are attached by a *N*-hydroxysuccinimide ester to the middle and uppermost strand, respectively, at a distance of six nucleobases in the hybridized complex to act as a FRET pair. The medium strand is inverted in the middle by inverse amidites since the force to melt a DNA or RNA double strand depends on the direction of the helix to which the force is applied. The RNA complex features a two nucleotide overhang at the 3′ end in order to maximize Dicer processing (14). Proving the validity of our results, we carried out all experiments in parallel with both possible geometries.

If the RNA target duplex is attached to the glass slide and the DNA complex constitutes the upper part, we call this configuration 'RNA down'. The other geometry with the RNA complex the upper part and the DNA duplex bound to the glass slide we named 'RNA up' (Figure 1C). We bought all oligonucleotides with the modifications from IBA GmbH, Germany.

Slide preparation

All aqueous solutions necessary for the chemical procedures described here were treated with 0.1% Diethyl pyrocarbonate (DEPC) over night and were autoclaved afterwards in order to avoid RNAse contamination. We pipetted 1 µl of the lowermost strand in a concentration of 25 µM in 5× SSC buffer (saline sodium citrate; Sigma-Aldrich GmbH, Germany) on an aldehydesilane-coated glass slide (Nexterion Slide AL, Pequlab, Germany) in a 4×4 pattern and incubated it over night in a humid atmosphere. The slide was rinsed thoroughly with ddH_2O and incubated in a 1% aqueous solution of $NaBH_4$ (VWR Scientific GmbH, Germany) for 90 min in order to reduce the Schiff bases and render the linkage of the oligonucleotide to the slide covalent. Unreacted groups were blocked in 1× SSC containing 4% bovine serum albumin (Sigma-Aldrich GmbH; Germany), minimizing unspecific binding. We placed a custom-made 16-well silicone isolator (Grace-Biolabs; USA) on top of the immobilized lowermost oligomer and transferred to each well 3 µl of 0.2 µM of the upper complex in 5× SSC, which had been heated and cooled down over several hours in a thermocycler beforehand to avoid undesired secondary structures. After an hour hybridization, the molecular complexes as diplayed in Figure 1A were completed. Unbound strands were removed by several washing steps with different salt concentrations (2× SSC, 0.2× SSC, 1× SSC). Care was taken that the samples were kept in an aqueous environment at all times.

Incubation of ligands

For all measurements detecting Dicer activity, the glass slide with the molecular bonds was fastened to a custom-made PMMA well with a silicone lip seal. According to the desired incubation time and quantity, the recombinant human Dicer protein in a concentration of 1 U/µl (Life technologies, UK) was directly pipetted into the PMMA well prior to the contact process. We applied amounts between 0.5 and 5 µl Dicer solution. For measurements with paromomycin and Dicer, the appropriate amount of paromomycin (paromomycin sulphate salt, Sigma, Germany) was directly mixed with the solution of 1× SSC of the last washing step and, thus, added before Dicer. The paromomycin titration experiments were executed on one glass slide within the spotted 4×4 pattern of oligonucleotides. The custom-made 16-well silicone isolator (Grace-Biolabs; USA) allows the incubation of every spot with a different solution by means of a self-made microfluidic system driven by two 16-channel peristaltic pumps (Ismatec GmBH; Germany). Hence, a whole titration curve can be recorded within a single experiment.

Stamp preparation

Micro- and macrostructured PDMS stamps were fabricated by casting 1:10 crosslinker/base (Sylgard, Dow Corning, MI, USA) into a custom-made Pyrex/silicon wafer (HSG-IMIT, Germany) according to standard procedures (24). The resulting PDMS stamps feature pillars of 1 mm diameter and height with a spacing of 3 mm in a square pattern on a 3-mm-thick basis and are cut in pieces of 4×4 pillars. The flat surface of the pillars is microstructured with 100×100 µm pads separated by 41 µm wide and 5 µm deep rectangular trenches enabling the drainage of liquid during the contact and separation process (Figure 1B). For the surface functionalization, the cleaned stamp surface was first activated in 12.5% HCl overnight and derivatized with (3-glycidoxypropyl)-trimethoxysilane (ABCR, Germany) in order to generate epoxide groups. 1:1 methoxy-PEG-NH_2 (MW 2000 Dalton) and Biotin-PEG-NH_2 (MW 3400 Dalton) (Rapp-Polymere, Germany) were melted at 80°C, and ~1 µl was transferred to each pillar followed by overnight incubation at 80°C in an Argon atmosphere. The excess polymers were thoroughly removed by rinsing with ddH_2O. Shortly before the experiment, the stamps were incubated in 0.4% BSA in 1× SSC containing 1 µg/µl Streptavidin (Thermo Fisher Scientific, Germany) for 30 min, washed with 0.05% Tween 20 (VWR Scientific GmbH, Germany) in 0.2× SSC and gently dried with N_2 gas.

Contact process and fluorescence read-out

The functionalized stamp adheres upside-down to the glass block glued to a closed-loop piezoelectric actuator (PZ 400, Piezo Systems Jena, Germany) and a DC motorized translation stage (Physik Instrumente GmbH, Germany), as shown in Figure 1B. The slide with the oligonucleotide constructs is fixed beneath the stamp on a stainless steel stage with permanent magnets so that every stamp pillar meets a 1–2 mm diameter spot of oligonuclotides on the glass slide. The whole contact device is mounted on an inverted microscope (Axio Observer Z1, Carl Zeiss MicroImaging GmbH, Germany) with an xy-DC motorized high-accuracy translation stage (Physik Instrumente GmbH, Germany). Contact is made by means of the piezo, and care is taken that each individual pillar is not compressed more than 3 µm. The planar adjustment of stamp and slide as well as the contact process are controlled by reflection interference contrast microscopy (25). To let the biotin of the oligonucleotides bind to the streptavidin coating of the PDMS stamp, the contact between stamp and slide is maintained for 10 min. The piezo retracts the stamp with a velocity of 1 µm/s in all experiments, and a force builds up in the double strands until the weaker one breaks with higher probability. Quantifying the number of intact bonds in relation to total molecular constructs, fluorescence images of the Cy5 intensity are taken before and after the contact process. As it cannot be assumed that all oligonucleotides have bound to the stamp, their contribution has to be substracted. Therefore, a fluorescence picture of the FRET intensity between the Cy3 of

the upper strand and the Cy5 label of the middle strand, being a measure of the integrity of the upper molecular complex, is taken before and after the contact process as well. Three outcomes are possible: First, the lower bond broke so that no fluorescence, neither Cy5 nor FRET signal, can be detected. Second, the upper bond broke so that the Cy5 intensity can be measured but no FRET signal. Third, the molecular construct did not bind to the stamp, which means that the Cy5 and FRET intensity are unchanged except for bleaching. The quotient of the image taken after the contact process to the image taken before, $F_{Cy5} = I_{Cy5}^{Final}/I_{Cy5}^{Start}$ and $F_{FRET} = I_{FRET}^{Final}/I_{FRET}^{Start}$, cancels out inhomogeneities due to the Gaussian illumination profile and surface defects, rendering the MFA rather robust. The normalized fluorescence is given by $NF = \frac{F_{Cy5} - F_{FRET}}{1 - F_{FRET}}$. A detailed description can be found in (26). The normalized fluorescence is thus the fraction of intact lower bonds of the total number of molecules under load.

RESULTS AND DISCUSSION

Characterization of Dicer activity

Initially, we developed a platform for analysing the protein Dicer. The schematic outline and RNA sequences are shown in Figure 1. We built a molecular complex comprising a 35 bp double-stranded RNA duplex covalently bound to a glass slide at one end, and covalently attached to a 27 bp reference DNA duplex at the other end. Dicer could be titrated in solution to the completed molecular constructs, and the surfaces were separated after incubation times varying between 60 and 300 min. Figure 2B depicts the results of such a measurement upon addition of 1 µl of Dicer to every sample except the first, which acts as a reference value. The normalized fluorescence at time t = 0 provided a value of $NF = 0.79 \pm 0.01$. An initial value at time t = 0 of $NF = 0.5$, corresponding to two complexes nearly identical in their structural stability, would be desirable to resolve small differences in stability induced through binding of a ligand or mismatch. However, our system was designed to quantify enzymatic RNAse activity. Because Dicer cuts off around 20 bp, we designed our sytem such that the RNA complex before Dicer cleavage was stronger than the DNA, while the RNA complex after Dicer cleavage was weaker than the reference DNA duplex. As in our system the RNA construct is 8 bp longer than the DNA complex, in the absence of Dicer, the weaker DNA reference bond ruptures with higher probability. In the 'RNA down' configuration, the RNA complex is attached directly to the glass slide; therefore, the likelihood for the Cy5 label to be found at the lower surface is higher than at the upper surface, and the normalized fluorescence lies around $NF = 0.8$. If Dicer cleaves off about 20 bp of the RNA double strand, the lower molecular complex is weakened and the normalized fluorescence decreases (Figure 2B). Dicer processes the RNA duplex in multiple enzymatic turnovers. Consequently the normalized fluorescence declined further with increasing incubation time (Figure 2B). Our experimental design provides Dicer with an excess of substrate, dsRNA, so that the substrate concentration can be assumed constant and the reaction rate of Dicer is solely limited by the amount of Dicer present. Thus, a linear relation of the normalized fluorescence to Dicer processing time was expected and verified by our measurement. The slope of the fit was used as a measure of the rate of Dicer processing, allowing us to quantify Dicer activity.

Proof of Principle of the microarray test format for RNA ligands

Next, we analysed the binding properties of the aminoglycoside of the neomycin family, paromomycin, to its RNA aptamer by means of the MFA. The structure of this aptamer and its ligand-binding behaviour are well-known and described in detail in (28) and (29). The aptamer sequence was incorporated into our RNA duplex 11 nucleotides from the 3′ end, and was located within the portion of the RNA duplex cleaved by Dicer. We hypothesized that this position could disrupt Dicer interaction with the RNA duplex. Every second spot in the 16-spot pattern of oligonucleotide constructs bound to the glass slide were incubated for at least 1 h with a different concentration of paromomycin in 1× SSC, ranging from 0 to 1995 µM, so that a single experiment resulted in a full titration curve with two values for every concentration paromomycin. The experiment was carried out several times for both the 'RNA up'and 'RNA down' configurations. From the resulting values for the normalized fluorescence, the mean and standard error of the mean were calculated so that every data point represents between two and four experiments. The data were fitted by a hill equation isotherm that accounts for specific and non-specific binding by means of the software package GraphPad Prism 5 (GraphPad Software, San Diego, CA, USA). The result for the 'RNA up' configuration is shown in Figure 2D, which yielded a dissociation constant of 2.55 ± 2.18 µM and negligible unspecific binding. Literature reports values of 0.2–1 µM depending on the technique (29,30), in agreement with our results. The measurements in the 'RNA down' geometry resulted in dissociation constants of about 100 ± 70 µM (data not shown), which deviated by a factor 50 from our other measurements with the inverted geometry. Non-specific binding of the ligand to the surfaces or molecular complexes would be indentical in both configurations, so we attributed the increase in dissociation constant for the 'RNA down' configuration to the proximity of the RNA construct to the glass slide. Notwithstanding the passivation of the glass slide, the RNA duplex in the 'RNA down' configuration presumably stretches across the surface, which might reduce the accessibility of the RNA aptamer binding pocket for the ligand paromomycin, resulting in an apparent increase in the dissociation constant. Consequently, the 'RNA down' configuration with the ligand-binding part integrated in the lower complex does not seem suited for the characterization of a RNA-binding ligand. In contrast, providing the ligand-binding sequence with a spacer and locating away from the surface by implementing it in the upper RNA duplex yielded reliable values for the dissociation constant

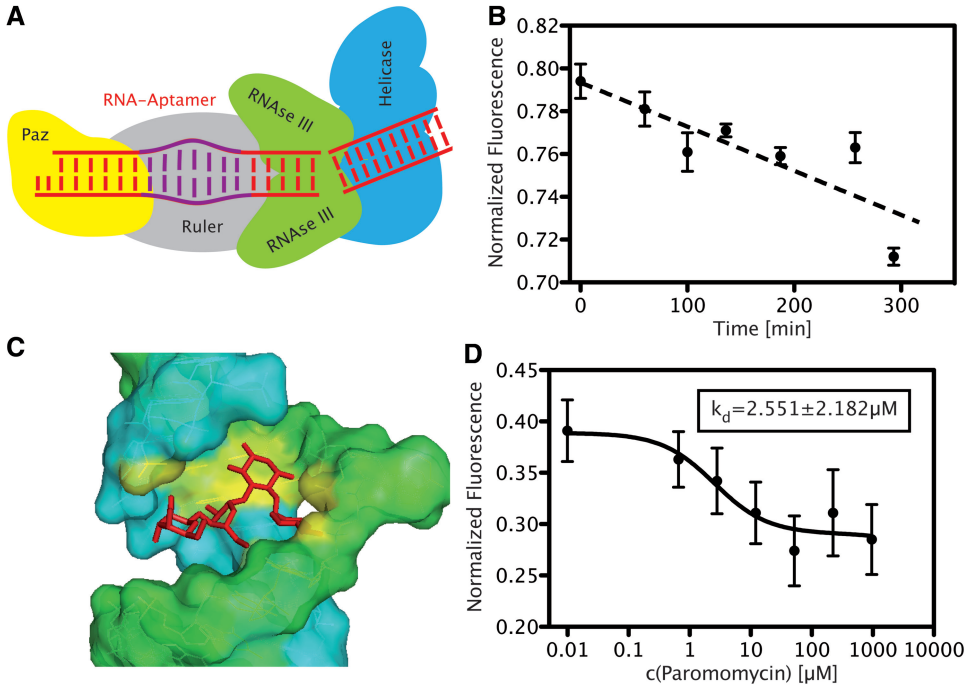

Figure 2. Characterization of molecules in question. (**A**) Schematics of Dicer and its sub-domains. (**B**) The activity of Dicer is measured in an excess of substrate so that the processing rate is constant. Accordingly, the normalized fluorescence decreases linearly with incubation time. The data were measured in the 'RNA down' configuration. (**C**) Schematic picture of paromomycin (red) binding to its RNA aptamer. The two strands of the RNA duplex are displayed in blue and green, while the bases interacting with the ligand are coloured in yellow [PDB: 1J7T by (27)]. (**D**) Titration of the ligand paromomycin to the complexes in the 'RNA up' geometry increasingly stabilizes the upper RNA duplex so that the normalized fluorescence decreases. The fluorescence data were fitted by a Hill equation isotherm.

in agreement with literature values. Although the dissociation constants measured by other more laborious and time-consuming techniques might be more accurate, our assay provides sufficiant accuracy in a parallel screening format for dissociation constants, ranging from the picomolar (26) (chiral polyamides binding to DNA) to the high micromolar scale (23) (DNA-aptamer specific for ATP). Moreover, the current format with 16 spots can be varied to titrate two ligands in parallel (eight spots per ligand) or change the binding sequence in half the spots in order to gain a deeper insight into the ligand-binding sequence interaction in a one-shot experiment.

Hinderance of Dicer processing by ligand binding

In the next step, we prepared four different slides with our oligonulceotide constructs in the 'RNA down' configuration as well as in the 'RNA up' configuration. The initial value for *NF* was determined in pure buffer (Figure 3A). To the second sample, we added 2.5 µl of the Dicer solution and separated the surfaces after 60 min, while we incubated the third sample with 1 mM paromomycin at least 1 h before the measurement (Figure 3B and C). The buffer of the fourth sample contained 1 mM paromomycin, and 2.5 µl Dicer solution was added 60 min before separation of the surfaces (Figure 3D). The first sample acted as reference and gave $NF = 0.34 \pm 0.01$ (standard deviation) in the 'RNA up' configuration. The addition of Dicer weakened the upper RNA double strand by cutting off around 20 basepairs so that the flurophor was found more often on the lower side. Therefore, the *NF* increased to 0.40 ± 0.02, as displayed in Figure 3E. Upon binding of paromomycin, the RNA duplex was stabilized and the *NF* decreased to 0.27 ± 0.01 in the third case. If paromomycin hinders Dicer from cutting the RNA duplex, we expect that the fourth measurement yields *NF* close to the ligand-only case, but at least below the $NF = 0.40$ obtained for measurement with only Dicer in the solution. As shown in Figure 3E, we measured an *NF* of 0.30 ± 0.01, which is close to the result of only paromomycin. From these data, we concluded that Dicer was definitely hindered by binding of paromomycin, but not completely blocked. The 'RNA down' configuration yielded the same outcome (Figure 3F).

Correction of fluorescence data

During the measurments with the 'RNA down' configuration, we found that the quantum yield of the fluorophors, especially of the Cy5, varied slightly owing to the changing local environment. In particular, the fluorescence intensity of Cy5 increased if the upper strand ruptured leaving behind the single-stranded overhang. This leads to the phenomenon that the normalized fluorescence value can adopt values above one in the 'RNA down' configuration (see raw data in the Supplementary Data). Levitus and co-workers reported a change of fluorescence intensity upon interaction of Cy3 with single and double-stranded

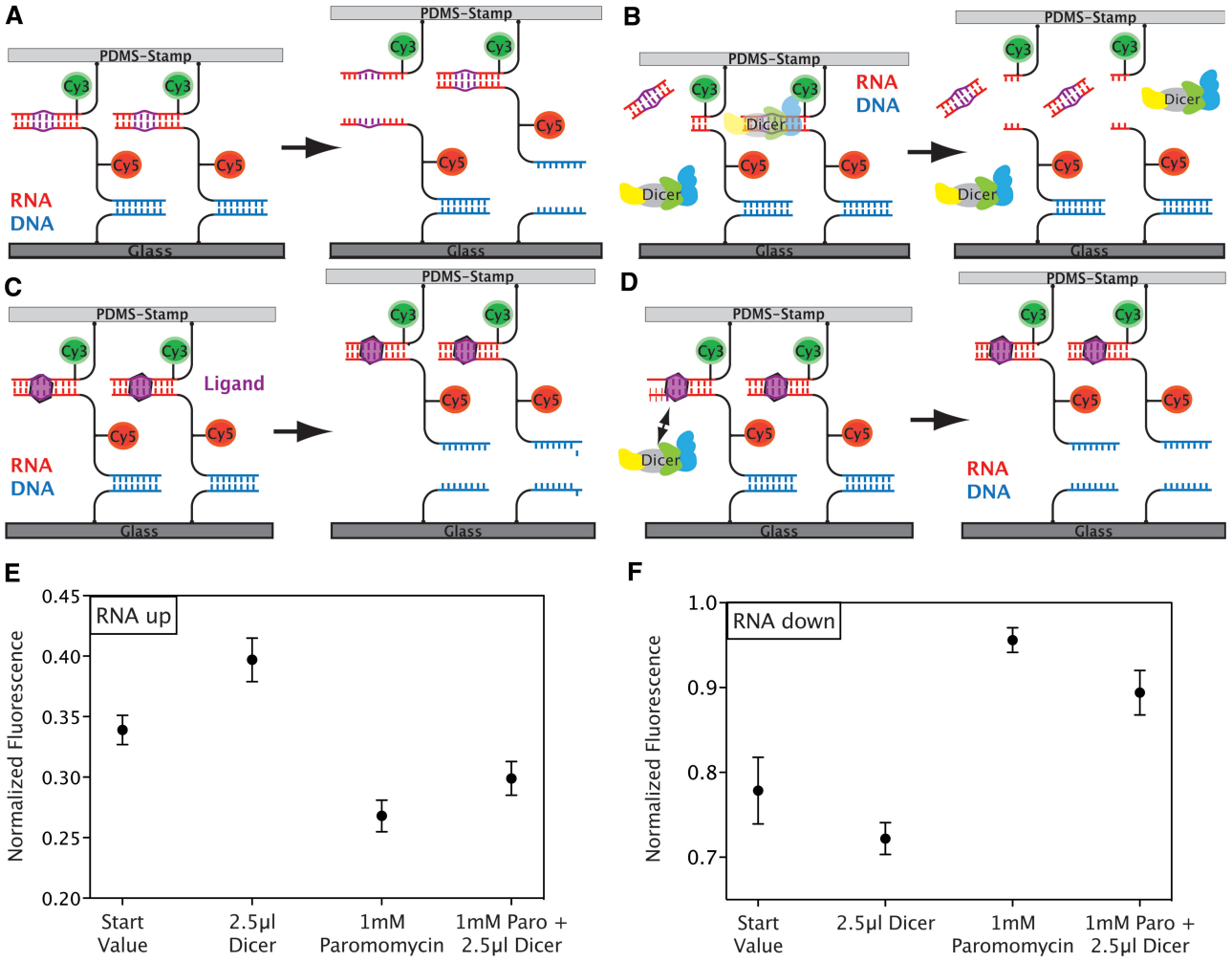

Figure 3. Dicer inhibition. (**A**) Separating the molecular constructs in the absence of Dicer or ligand provides an initial value in the 'RNA up' geometry for the *NF* of 0.34 ± 0.01. (**B**) Upon addition of Dicer, the protein cleaves off around 20 bp of the RNA duplexes and weakens the upper part so that the balance of the fluorophor distribution is shifted towards the lower side and the *NF* increases to 0.40 ± 0.02. (**C**) Binding of the ligand to its aptamer strengthens the RNA complex and the fluorophor distribution after rupture of the molecular complexes is shifted towards the upper surface, decreasing the *NF* to 0.27 ± 0.01. (**D**) Upon addition of Dicer and ligand, binding of the ligand to the RNA duplex blocks Dicer and strengthens the upper complex so that the *NF* yields 0.30 ± 0.01, which is close to the value we measured with ligand only. (**E**) Display of the data measured in the experiment just described. (**F**) Inverting the geometry yields the same result in reverse. From an initial value of 0.78 ± 0.02, the *NF* decreases to 0.72 ± 0.01 through the destabilization by Dicer. Ligand binding strengthens the lower RNA duplex and shifts the *NF* to higher values of 0.96 ± 0.01. If Dicer is hindered from cutting by ligand binding, the *NF* with 0.90 ± 0.01 stays close to the value measured with ligand only.

DNA. They attributed this change to the blocking of non-radiative decay pathways of the excited state fluorophor by steric hindrance (31). In (32), a similar behaviour for Cy5 is described. Although the Cy5 label is, in our case, always conjugated to the middle single strand and six basepairs away from both duplexes, an interaction between the fluorophor and the oligonucleotide duplex seems a plausible explanation for the observed increase in fluorescence intensity. Because the Cy3 is only measured as part of a duplex, any effect due to interactions with the oligonucleotides cancels out in the ratio. To correct the Cy5 fluorescence intensities, we measured the intensity of its emisson spectrum in bulk solution in both cases, the single middle strand and the complete upper duplex, by fluorescence spectroscopy and calculated a quenching factor F (see Supplementary Data). Determining the experimental error for F, we calculated the maximum range of possible factors and re-analysed our data measured by the MFA. Although all measured data points are shifted to smaller *NF* values, the outcome of the experiments and the corresponding conclusions remain unchanged (see Supplementary Figure S1). For further analysis, we therefore chose a medium value for the quenching factor of $F = 1.19$ for the 'RNA down' geometry, and $F = 1.06$ for the 'RNA up' geometry and corrected all measured data accordingly.

Minimum amount of ligand necessary for Dicer inhibition

We investigated what concentration of paromomycin is nessecary to hinder Dicer from cleaving. We incubated samples in the 'RNA down' configuration with

paromomycin, with the concentration ranging from 0.66 to 224 μM, and added 2.5 μl Dicer solution 1 h before the separation. The result is displayed in Figure 4. The lowest concentration of 0.66 μM paromomycin did not affect Dicer processing, but already a concentration of 2.82 μM partially inhibited Dicer, whereas 52 μM paromomycin hindered most of Dicer processing.The dissociation constant, which we had determined in the previous section to be 2.55 ± 2.18 μM, agrees nicely with the finding here, that a paromomycin concentration in this range leads to a partial inhibition of the cleavage process. It points directly towards a close relationship between the dissociation constant of a ligand and its potential to hinder Dicer processing. For ligands that bind thighter to their RNA sequence, we expect a blocking of Dicer at lower concentrations of the ligand.

CONCLUSION

In a proof of principle, we demonstrated that the function of the protein Dicer can be selectively blocked by a ligand that sequence specifically binds to the RNA. Our MFA reliably detected processing of the RNA duplex as well as the binding of a small ligand to RNA, which resulted in an inhibition of Dicer. In contrast to other techniques (33), the MFA requires neither labelling of the target sequence, nor the ligand or protein. It only needs flurophors well-separated from the area of interest so that the interaction of the molecules in question is not disrupted and can be analysed undisturbed. The localization of our molecular constructs between two surfaces is both an advantage and a drawback at the same time. Because we measure interaction forces rather than the mere presence of a ligand, our assay can easily test different ligand–oligonucleotide interactions in parallel without interfering background signals from the bulk or the need for stringent washing procedures. But possible surface effects e.g. non-specific adhesion between ligand or oligonucleotides and surface have to be carefully excluded. Furthermore, our assay allows us to analyse the interaction of Dicer with our RNA construct and the interaction of the ligand to its binding sequence separately without changing the molecular complexes. This ensures that Dicer cleavage is blocked by hindering the protein to bind to its substrate not by any interaction between Dicer and the ligand. In addition, we illustrated the capability of our assay to characterize RNA-binding molecules in a one-shot experiment, enabling examination of the binding behaviour of a large number of molecules with moderate effort. The current setup allows to test 16 different systems in parallel, either one substance against 16 different DNA or RNA sequences or one oligonucleotide construct against 16 different ligands or concentrations of one ligand or a combination of both. To expand the multiplexing capabilities of our setup towards high throughput, the amount of reacting agent has to be reduced to a minimum and the number of RNA sequences have to be increased. Microfluidic devices can drastically diminish the reaction volume, and DNA/RNA spotting techniques allowed us to test eight different systems within $100 \times 100\,\mu m^2$ (19,34). With further standardization and development, our technique of the MFA has the potential to become the first force-based high throughput technique.

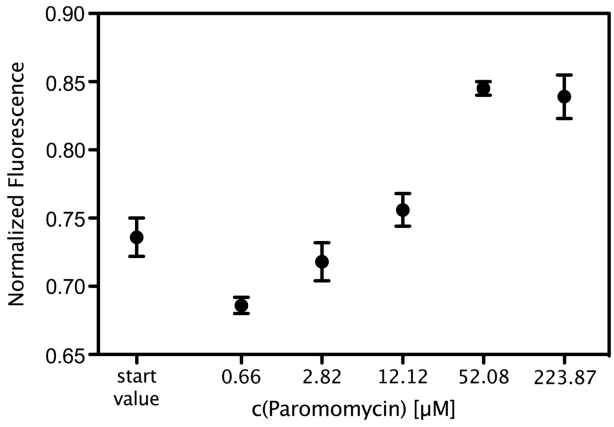

Figure 4. Paromomycin efficiency. To determine the minimum amount of paromomycin necessary to block Dicer, we prepared samples in the 'RNA down' configuration with different amounts of paromomycin and added 2.5 μl Dicer solution 1 h before the measurement. We found that 0.66 μM paromomycin has no effect, but already 2.82 μM paromomycin hinders Dicer processing, while for 52.08 μM paromomycin, all Dicer activity is blocked.

SUPPLEMENTARY DATA

Supplementary Data are available at NAR Online: Supplementary Method and Supplementary Figure 1.

ACKNOWLEDGEMENTS

The authors thank Christoph Arenz from HU Berlin, P. Tinnefeld from TU Braunschweig, Matthias Rief from TU Munich, P. Severin, I. Stein and U. Wienken for helpful discussions. K.L. is grateful to the Elite Network of Bavaria (IDK-NBT) for a doctoral fellowship.

FUNDING

German Science Foundation [SFB 863]; Nanosystems Initiative Munich; European Research Council Advanced Grant. Funding for open access charge: German Science Foundation [SFB 863].

Conflict of interest statement. None declared.

REFERENCES

1. Mello,C.C. and Conte,D. Jr (2004) Revealing the world of RNA interference. *Nature*, **431**, 338–342.
2. Siomi,H. and Siomi,M.C. (2009) On the road to reading the RNA-interference code. *Nature*, **457**, 396–404.
3. Carthew,R.W. and Sontheimer,E.J. (2009) Origins and Mechanisms of miRNAs and siRNAs. *Cell*, **136**, 642–655.
4. Bartel,D.P. (2004) MicroRNAs: genomics, biogenesis, mechanism and function. *Cell*, **116**, 281–297.
5. Vasudevan,S., Tong,Y. and Steitz,J.A. (2007) Switching from repression to activation: microRNAs can up-regulate translation. *Science*, **318**, 1931–1934.

6. Orom,U.A., Nielsen,F.C. and Lund,A.H. (2008) MicroRNA-10a binds the 5'UTR of ribosomal protein mRNAs and enhances their translation. *Mol. Cell*, **30**, 460–471.
7. Ambros,V. (2011) MicroRNAs and developmental timing. *Curr. Opin. Genet. Dev.*, **21**, 511–517.
8. van Rooij,E. (2011) The art of microRNA research. *Cir. Res.*, **108**, 219–234.
9. Shruti,K., Shrey,K. and Vibha,R. (2011) Micro RNAs: tiny sequences with enormous potential. *Biochem. Biophys. Res. Commun.*, **407**, 445–449.
10. Friedman,J.M. and Jones,P.A. (2009) MicroRNAs: critical mediators of differentiation, development and disease. *Swiss Med. Wkly.*, **139**, 466–472.
11. Conti,A., Aguennouz,M., La Torre,D., Tomasello,C., Cardali,S., Angileri,F.F., Maio,F., Cama,A., Germano,A., Vita,G. *et al.* (2009) miR-21 and 221 upregulation and miR-181b downregulation in human grade II-IV astrocytic tumors. *J. Neurooncol.*, **93**, 325–332.
12. Lau,P.W., Guiley,K.Z., De,N., Potter,C.S., Carragher,B. and MacRae,I.J. (2012) The molecular architecture of human Dicer. *Nat. Struct. Mol. Biol.*, **19**, 436–440.
13. Lee,Y.S., Nakahara,K., Pham,J.W., Kim,K., He,Z., Sontheimer,E.J. and Carthew,R.W. (2004) Distinct roles for Drosophila Dicer-1 and Dicer-2 in the siRNA/miRNA silencing pathways. *Cell*, **117**, 69–81.
14. Vermeulen,A., Behlen,L., Reynolds,A., Wolfson,A., Marshall,W.S., Karpilow,J. and Khvorova,A. (2005) The contributions of dsRNA structure to Dicer specificity and efficiency. *RNA*, **11**, 674–682.
15. Krützfeldt,J., Rajewsky,N., Braich,R., Rajeev,K.G., Tuschl,T., Manoharan,M. and Stoffel,M. (2005) Silencing of microRNAs *in vivo* with 'antagomirs'. *Nature*, **438**, 685–689.
16. Elmen,J., Lindow,M., Schutz,S., Lawrence,M., Petri,A., Obad,S., Lindholm,M., Hedtjarn,M., Hansen,H.F., Berger,U. *et al.* (2008) LNA-mediated microRNA silencing in non-human primates. *Nature*, **452**, 896–899.
17. Thomas,J.R. and Hergenrother,P.J. (2008) Targeting RNA with small molecules. *Chem. Rev.*, **108**, 1171–1224.
18. Albrecht,C.H., Clausen-Schaumann,H. and Gaub,H.E. (2006) Differential analysis of biomolecular rupture forces. *J. Phys. Condens. Matter*, **18**, S581–S599.
19. Severin,P.M., Ho,D. and Gaub,H.E. (2011) A high throughput molecular force assay for protein-DNA interactions. *Lab Chip*, **11**, 856–862.
20. Albrecht,C., Blank,K., Lalic-Multhaler,M., Hirler,S., Mai,T., Gilbert,I., Schiffmann,S., Bayer,T., Clausen-Schaumann,H. and Gaub,H.E. (2003) DNA: a programmable force sensor. *Science*, **301**, 367–370.
21. Blank,K., Mai,T., Gilbert,I., Schiffmann,S., Rankl,J., Zivin,R., Tackney,C., Nicolaus,T., Spinnler,K., Oesterhelt,F. *et al.* (2003) A force-based protein biochip. *Proc. Natl Acad. Sci. USA*, **100**, 11356–11360.
22. Dose,C., Ho,D., Gaub,H.E., Dervan,P.B. and Albrecht,C.H. (2007) Recognition of "mirror-image" DNA by small molecules. *Angew. Chem. Int. Ed. Engl.*, **46**, 8384–8387.
23. Ho,D., Falter,K., Severin,P. and Gaub,H.E. (2009) DNA as a force sensor in an aptamer-based biochip for adenosine. *Anal. Chem.*, **81**, 3159–3164.
24. Xia,Y. and Whitesides,G.M. (1998) Soft lithography. *Annu. Rev. Mater. Sci.*, **28**, 153–184.
25. Wiegand,G., Neumaier,K.R. and Sackmann,E. (1998) Microinterferometry: three-dimensional reconstruction of surface microtopography for thin-film and wetting studies by interference contrast microscopy (RICM). *Appl. Opt.*, **37**, 6892–6905.
26. Ho,D., Dose,C., Albrecht,C.H., Severin,P., Falter,K., Dervan,P.B. and Gaub,H.E. (2009) Quantitative detection of small molecule/DNA complexes employing a force-based and label-free DNA-microarray. *Biophys. J.*, **96**, 4661–4671.
27. Vicens,Q. and Westhof,E. (2001) Crystal structure of paromomycin docked into the eubacterial ribosomal decoding a site. *Structure*, **9**, 647–658.
28. Fourmy,D., Recht,M.I., Blanchard,S.C. and Puglisi,J.D. (1996) Structure of the A site of *Escherichia coli* 16 S Ribosomal RNA complexed with an aminoglycoside antibiotic. *Science*, **274**, 1367–1371.
29. Anderson,P.C. and Mecozzi,S. (2007) Minimum sequence requirements for the binding of paromomycin to the rRNA decoding site A. *Biopolymers*, **86**, 95–111.
30. Recht,M.I., Fourmy,D., Blanchard,S.C., Dahlquist,K.D. and Puglisi,J.D. (1996) RNA Sequence determinants for aminoglycoside binding to an A-site rRNA model oligonucleotide. *J. Mol. Biol.*, **262**, 421–436.
31. Sanborn,M.E., Connolly,B.K., Gurunathan,K. and Levitus,M. (2007) Fluorescence properties and photophysics of the sulfoindocyanine Cy3 linked covalently to DNA. *J. Phys. Chem. B*, **111**, 11064–11074.
32. Levitus,M. and Ranjit,S. (2011) Cyanine dyes in biophysical research: the photophysics of polymethine fluorescent dyes in biomolecular environments. *Q. Rev. Biophys.*, **44**, 123–151.
33. Davies,B.P. and Arenz,C. (2006) A homogenous assay for micro RNA maturation. *Angew. Chem. Int. Ed. Engl.*, **45**, 5550–5552.
34. Severin,P.M. and Gaub,H.E. (2012) DNA-Protein Binding Force Chip. *Small*, **8**, 3269–3273.

SUPPLEMENTARY DATA

Characterization of fluorophores

In order to quantify the interaction of the fluorophors with the oligonucleotides to which they are conjugated, the fluorescence intensities of the middle strand and and the upper duplex are measured by means of a Fluorometer (Fluorolog3, Horiba Jobin Yvon). The oligonucleotides are diluted in 1xSSC to 0.5 µM and the duplex in a mixture of 1:1 is heated and cooled down over several hours. The excitation wavelength and emission spectra are set according to the parameters of the MFA setup. The resulting intensity curve is integrated and a quenching factor F is calculated by dividing the integrated intensity of the single strand by the integrated intensity of the duplex. Multiplying I_{Cy5}^{Start} by this factor gives the corrected normalized fluorescence.

Several repetitions yielded slightly different factors. Determining a maximum range of possible factors we could prove that the outcome of the experiment is not changed by correcting the NF with the different quenching factors. This is also visible in the Figure S1. Therefore, a medium factor was calculated and used for all analyses.

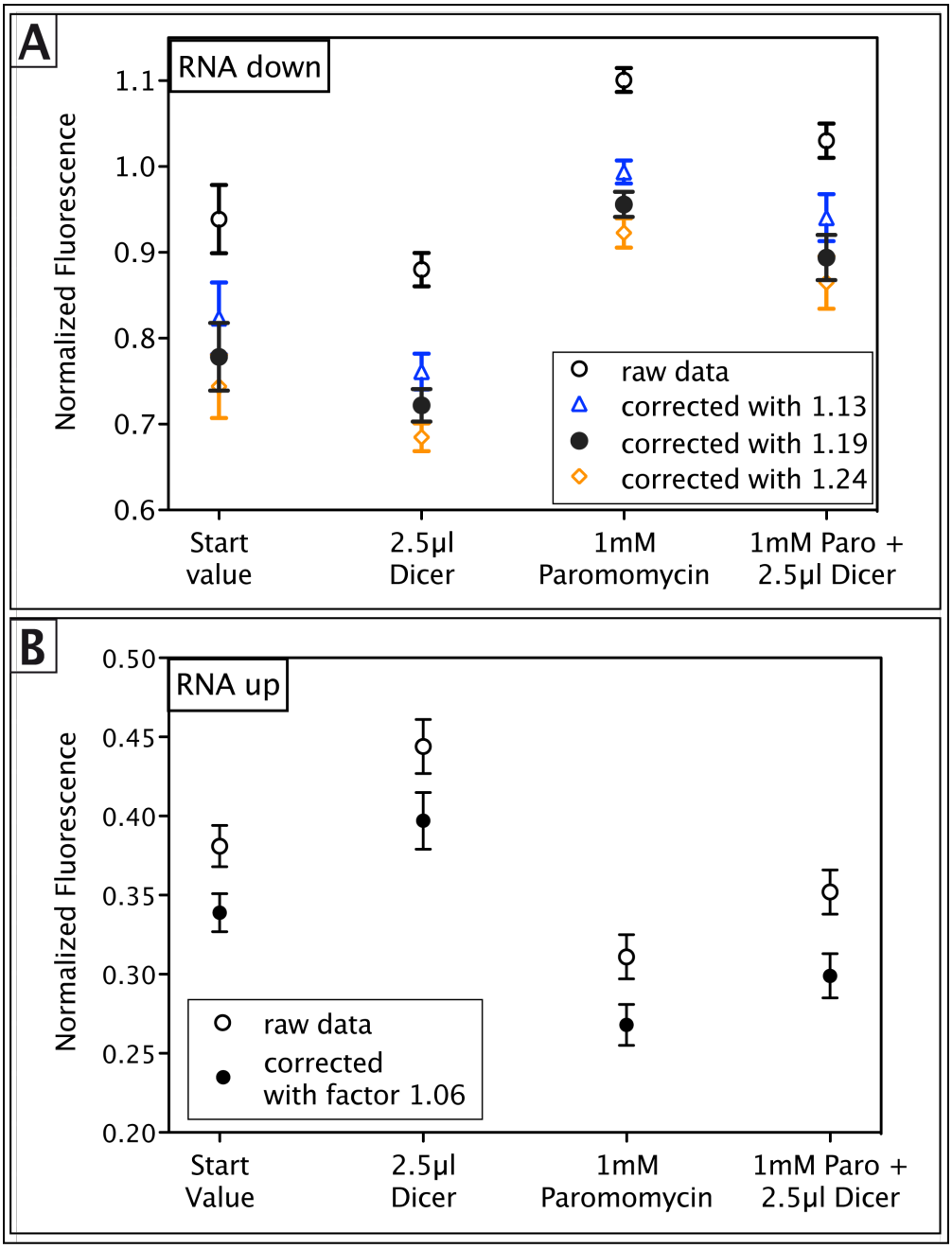

Figure S1: Proximity effects on the fluorescence intensities of Cy5.

The Cy5 with the oligonucleotide bases requires a correction of the measured fluorescence intensity in order to calculate the actual NF. A quenching factor is determined by measuring the fluorescence intensity of Cy5 conjugated to the single, middle strand as well as to the complete upper duplex by means of a fluorometer. Re-analyzing the data with a maximum range of factors does not change the outcome of the experiment. Dicer destabilizes the RNA duplex, while binding of paromomycin strengthens it. Blocking of Dicer leads to NF values close to ones of paromomycin binding. This holds true for both geometries, the RNA complex attached to the glass slide with the DNA duplex constituting the upper part (A) as well as for the inverse (B).

A.3 Publication 3: Quantitative Detection of Small Molecule/DNA Complexes Employing a Force-Based and Label-Free DNA-Microarray

Dominik Ho, Christian Dose, Christian H. Albrecht, Philip Severin, Katja Falter, Peter B. Dervan and Hermann E. Gaub;

Biophysical Journal, 2009, Vol. 96, 4661-4671

Quantitative Detection of Small Molecule/DNA Complexes Employing a Force-Based and Label-Free DNA-Microarray

Dominik Ho,[†‡] Christian Dose,[§] Christian H. Albrecht,[†] Philip Severin,[†] Katja Falter,[†] Peter B. Dervan,[§] and Hermann E. Gaub[†*]

[†]Lehrstuhl für Angewandte Physik and Center for Nanoscience Ludwig-Maximilians-Universität, 80799 Munich, Germany; [‡]Munich Center For Integrated Protein Science (CIPSM) Ludwig-Maximilians-Universität, 81377 Munich, Germany; and [§]Division of Chemistry and Chemical Engineering California Institute of Technology, Pasadena, CA 91125

ABSTRACT Force-based ligand detection is a promising method to characterize molecular complexes label-free at physiological conditions. Because conventional implementations of this technique, e.g., based on atomic force microscopy or optical traps, are low-throughput and require extremely sensitive and sophisticated equipment, this approach has to date found only limited application. We present a low-cost, chip-based assay, which combines high-throughput force-based detection of dsDNA·ligand interactions with the ease of fluorescence detection. Within the comparative unbinding force assay, many duplicates of a target DNA duplex are probed against a defined reference DNA duplex each. The fractions of broken target and reference DNA duplexes are determined via fluorescence. With this assay, we investigated the DNA binding behavior of artificial pyrrole-imidazole polyamides. These small compounds can be programmed to target specific dsDNA sequences and distinguish between D- and L-DNA. We found that titration with polyamides specific for a binding motif, which is present in the target DNA duplex and not in the reference DNA duplex, reliably resulted in a shift toward larger fractions of broken reference bonds. From the concentration dependence nanomolar to picomolar dissociation constants of dsDNA·ligand complexes were determined, agreeing well with prior quantitative DNAase footprinting experiments. This finding corroborates that the forced unbinding of dsDNA in presence of a ligand is a nonequilibrium process that produces a snapshot of the equilibrium distribution between dsDNA and dsDNA·ligand complexes.

INTRODUCTION

Small DNA-binding molecules are in the spotlight of many fields of research. Whether it is genomics, systems biology, or molecular medicine, the knowledge if and how strong a molecule interacts with a specific DNA sequence is of utmost interest. The formation of such complexes is typically linked to changes in the double-helical structure and may even result in the displacement or blocking of other molecules. This enables important functions in e.g., transcription, recombination, and DNA repair (1,2).

Given the importance of understanding the basis of molecular recognition, assays are needed that allow for fast, sensitive, and quantitative detection of dsDNA·ligand complexes. Traditionally, DNase footprinting experiments are employed to identify the binding sites of a ligand on dsDNA and also quantify the respective affinities. Although certainly powerful, DNase footprinting is a complex procedure and requires several days of preparation (3). Very rapid and also label-free quantification of even minuscule amounts of ligand becomes possible with microcantilever arrays (4). They suffer, however, from the costs associated with the fabrication and chemical modification of large numbers of cantilevers.

It is often of importance to identify the full DNA recognition profile of a certain DNA binder to understand what kind of role the binder plays within a living organism. Chip-based methods accommodate the need for massively parallel analysis of dsDNA·ligand interactions: chromatin immunoprecipitation-on-chip (ChIP-on-chip) is a widespread technique allowing for a genome-wide identification of protein-binding sites (5,6). ChIP-on-chip relies on nonspecific cross-linking of DNA with a DNA-binding molecule in vivo. Cross-linking efficiencies vary from molecule to molecule, and some interactions may even be missed (7). In particular, the detection of small molecules interacting with DNA is nontrivial. Today, a growing number of in vitro chip-based assays are available allowing for the analysis of dsDNA·ligand interactions under controlled experimental conditions. In an experiment by Warren et al. (8,9), all permutations of an eight basepair dsDNA sequence were displayed on a single chip. Ligand binding was detected directly by fluorescence and the cognate sites were ranked in the order of increasing affinity. However, fluorescence trades fast and sensitive readout for a labeled ligand, and the label may alter the sequence specificity profile of the ligand in an unbiased manner. A widespread label-free detection method is surface plasmon resonance imaging. Due to the small change in refractive index, the detection of small molecules with surface plasmon resonance imaging is complicated and requires larger features compared to fluorescence-based techniques (10,11). Depending on the application, the background signal caused by unwanted adsorption imposes a substantially challenge to all chip-based methods. The

Submitted November 4, 2008, and accepted for publication February 25, 2009.

*Correspondence: gaub@lmu.de

Editor: Jane Clarke.

0006-3495/09/06/4661/11 $2.00

doi: 10.1016/j.bpj.2009.02.059

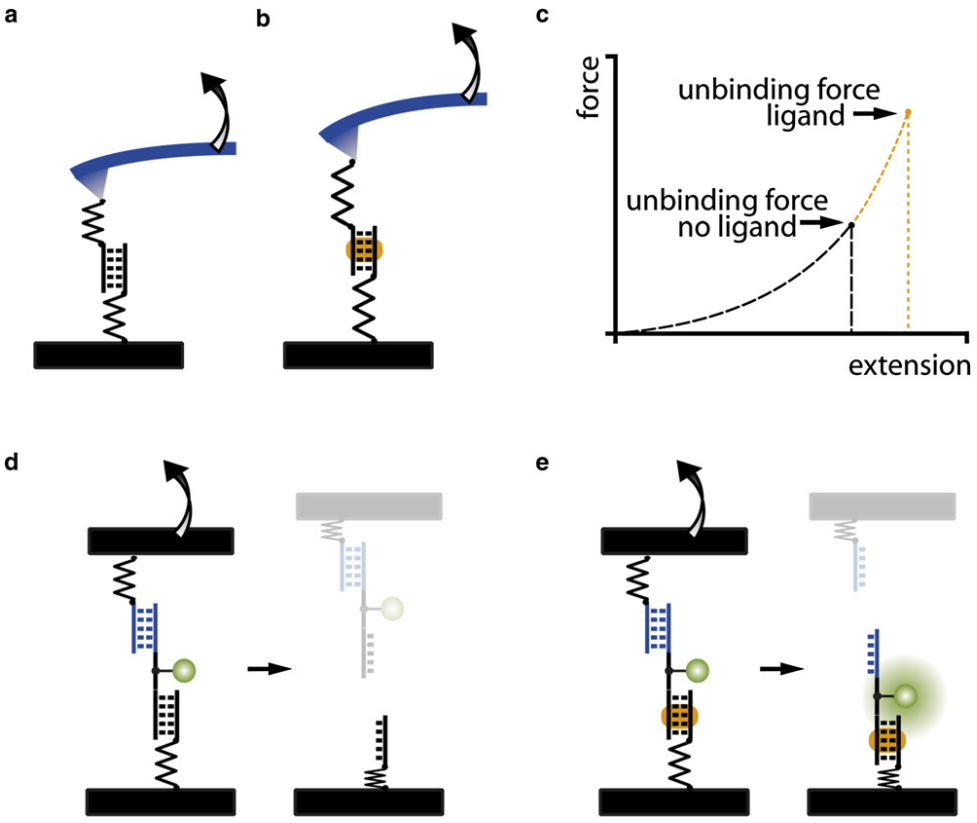

FIGURE 1 (*a*) Conventional, AFM-based single molecule force spectroscopy, in which the force required to unbind a molecular bond, such as a target DNA duplex, is measured with a cantilever spring. (*b*) A ligand bound to the target DNA duplex alters the force required for unbinding. (*c*) Single molecule force spectroscopy data are typically presented as force-extension traces. From two absolute force measurements, the consequences of ligand binding can be investigated. (*d*) The CUFA replaces the cantilever spring by a known reference bond. Upon loading the chain of target DNA duplex and reference DNA duplex, the weaker of the two bonds has a higher probability of unbinding than the stronger one. (*e*) In case a ligand forms a complex with the target DNA duplex and stabilizes it, significantly more fluorophores end up on the side of the target DNA duplex after separation of the two surfaces.

fabrication of inert surfaces is even considered as the main bottleneck for further development of the latter (12).

Here, we present a microarray compatible dsDNA·ligand complex detection format, which is based on the comparative unbinding force assay (CUFA). CUFA has already been applied to detect single nucleotide polymorphisms (13), to study differences of antibody/antigen interactions (14), to eliminate cross-reactions on protein microarrays (15), and to investigate the chiral selectivity of small peptides (16). For dsDNA·ligand interaction detection, CUFA relies on the alteration of the unbinding forces of a target dsDNA as a result of ligand binding (17–19). This effect was demonstrated in single molecule experiments employing atomic force microscopy (AFM) (20) (21,22), optical tweezers (23), and magnetic tweezers (24) (Fig. 1, *a–c*).

Instead of a microscopic, spring-like object, e.g., a cantilever or a trapped bead, CUFA employs a precisely defined molecular bond as force sensor. Thereby, the target DNA duplex is directly compared against a reference DNA duplex and merely fluorescence is required to readout the experiment (Fig. 1, *d* and *e*). In comparison with conventional force-based measurements, many of the experimental uncertainties are removed. With no calibration offsets or instrument drift the comparative unbinding force experiments are more accurate and independent of the experimental apparatus. Naturally, such experiments are primed to be carried out in parallel by using a chip format with many duplicates (in the order of $10^4/\mu m^2$) of the same experiment contributing to the excellent sensitivity of the measurement. The resulting assay is fluorescence based; however, it does not require a labeled ligand. Only the DNA linker between the target and reference DNA duplex is conjugated to a fluorophore at a noninteracting basepair. Rather than detecting the mere presence of the ligand, the change of unbinding forces of the target DNA duplex due to ligand binding is detected. By this means the assay is insensitive to nonspecific adsorption and deals with one of the major bottlenecks of current biochips.

As a model system, we investigated sequence programmable pyrrole-imidazole hairpin polyamides (25). These molecules recognize the minor groove of DNA with affinities and specificities comparable to naturally occurring DNA-binding proteins (26,27). The sequence specificity arises from interactions of pairs of the aromatic amino acids *N*-methylpyrrole (Py), *N*-methylimidazole (Im), and *N*-methylhydroxypyrrole (Hp) with the edges of the Watson-Crick DNA basepairs. A pairing of Im opposite to Py targets a G·C basepair, and Py/Im recognizes a C·G basepair, whereas a Py/Py pair comprises a preference for both A·T and T·A (28). The discrimination of T·A from A·T using Hp/Py pairs completes the four basepair letter code (29). Eight-ring hairpin polyamides provide a good compromise between synthetic ease and molecular recognition properties. In this binding motif, a γ-aminobutyric acid residue connects the carboxylic terminus of one strand to the amino terminus of the other (30). The turn residue also serves as a DNA recognition element for A·T and T·A basepairs. Further,

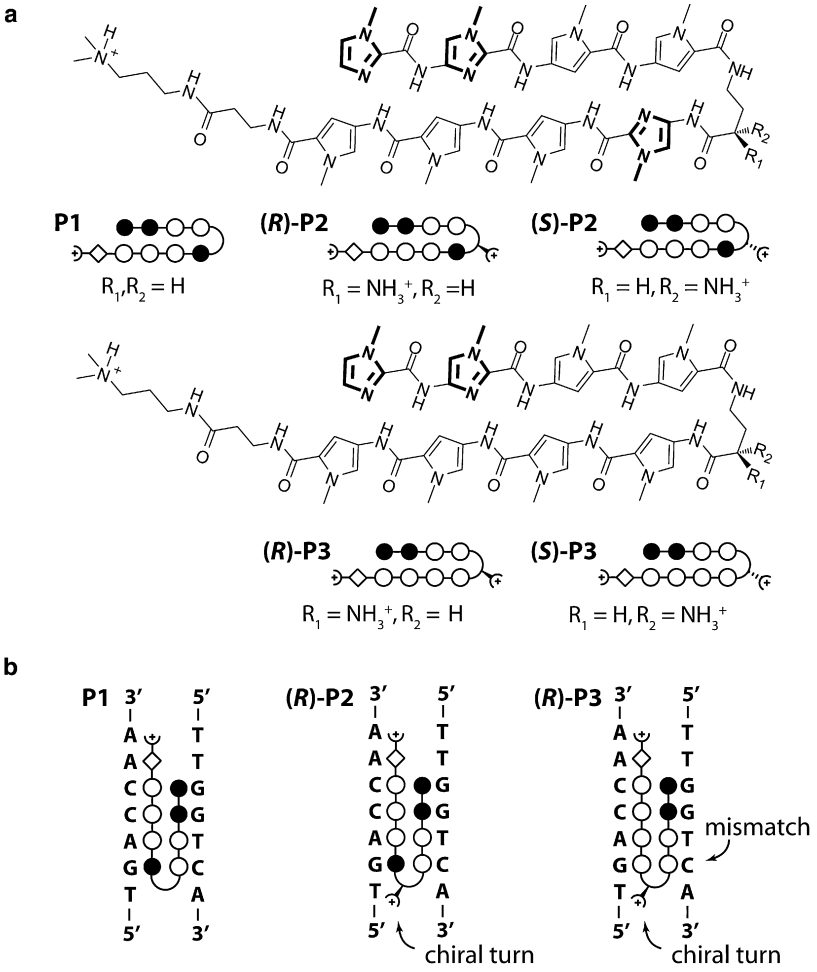

FIGURE 2 (*a*) Chemical structures of matched hairpin polyamides **P1**, **(*R*)-2**, and **(*S*)-2** as well as single basepair mismatched compounds **(*R*)-P3** and **(*S*)-P3**. The ball and stick model represents imidazole and pyrrole as solid and open circles, respectively. The β-alanine residue is shown as a diamond, and the dimethylaminopropylamide tail is shown as a half circle with a plus. The chiral diaminobutyric acid turn residue is represented as a turn, to which a semicircle with a plus is linked. *R* and *S* chirality is indicated by a solid and dashed connection of the semicircle to the turn, respectively. (*b*) Ball and stick representation for the three different hairpin motifs bound to the same target DNA sequence. **P1** binds sequence specific to the target DNA sequence. **(*R*)-2** is modified with a chiral diaminobutyric acid turn, which increases the overall binding affinity. **(*R*)-3** is also modified with a chiral diaminobutyric acid turn, however contains a single basepair mismatch that reduces the overall binding affinity.

a β-alanine residue and a dimethylaminopropylamide tail at the C-terminus each confer a specificity for A·T and T·A basepairs (31). This general addressability of the DNA minor groove is supported by x-ray and NMR structure studies (32,33) and has been utilized in several applications, including, for example, DNA nanostructures (34,35), recruitment of DNA-binding proteins (36,37), and the inhibition of gene expression within living cells (38–40).

Here we report the application of CUFA to accurately determine the thermal dissociation constant K_D of three different dsDNA·polyamide interactions (Fig. 2 *a*). In particular, we investigated the influence of a chiral turn as well as a single mismatch to the overall affinity of an eight-ring hairpin polyamide to the same target DNA sequence (Fig. 2 *b*).

MATERIALS AND METHODS

DNA constructs

DNA oligomers **1**: NH_2-(hexaethyleneglycol)$_5$-5′-TTT TTT TTT TCA GTC GCT GAC CAA CCT CGT-3′, **2**: 3′-GTC AGC GAC TGG TTG GAG CAC TTT T(Cy3)-5′-5′- TTT TTC TGC TCC AAC CAG TCG CTG AC -3′, **3**: Biotin-5′-TTT TTT TTT TGT CAGCGACTGGTTGGAGCA, **4**: 3′-GTC AGC GAC TGG TTG GAG CAC TTT T(Cy3)-5′-5′-*TTT TTC ACG AGG TTG GTC AGC GAC TG*-3′, and **5**: Biotin-5′-*TTT TTT TTT TTT TCA GTC GCT GAC CAA CCT CGT*-3′ were purchased HPLC grade from IBA GmbH (Goettingen, Germany). Italic letters in oligomers **4** and **5** represent L-DNA bases. In upside-down experiments the NH_2-(hexaethyleneglycol)$_5$ (HEGL) and biotin modifications were exchanged.

Molecular setup preparation (DNA slide)

Each individual molecular chain consisting of a reference and a target DNA duplex is referred to as a ''molecular setup''. Oligomer **1** is amine-modified at the 5′ end and allows covalent attachment to an aldehyde-functionalized glass slide (Schott GmbH, Jena, Germany). Two microliter drops of 5× phosphate buffered saline (PBS; Roche GmbH, Grenzach, Germany) containing 25 μM oligomer **1** were spotted on an aldehyde glass slide in a 4 × 4 pattern and were incubated in a saturated NaCl ddH_2O atmosphere overnight. After washing the slide with ddH_2O containing 0.2% sodium dodecyl sulfate (VWR Scientific GmbH, Darmstadt, Germany) and thoroughly rinsing the slide in ddH_2O, the resulting Schiff bases were reduced with 1% aqueous $NaBH_4$ (VWR Scientific GmbH, Darmstadt, Germany) for 20 min. After thoroughly rinsing the slide in ddH_2O, the slides were blocked in 1× PBS containing 4% bovine serum albumin (Sigma-Aldrich GmbH, Munich, Germany) for 30 min. A custom-made 16-well silicone isolator (Grace-Biolabs, OR) was placed on the top of the immobilized DNA oligomer **1** spots. Three microliters of 1× PBS containing 1 μM oligomer **2** and 2 μM oligomer **3** were added to each well and incubated for 1 h, completing the **1**·**2**·**3** molecular setups. Then, the slide was washed with 1× PBS containing 0.05% sodium dodecyl sulfate and thoroughly rinsed with 1× PBS. The

silicon isolator remained on the slide throughout the experiment, and care was taken that after hybridization the slide always remained immersed in 1× PBS. The **1·4·5** and upside-down molecular setups were prepared accordingly.

PDMS stamp

The polydimethylsiloxane (PDMS) stamp was fabricated by casting 10:1 (base/crosslinker) (Sylgard, Dow Corning, MI) into a custom-made micro- and millistructured silicon wafer (HSG-IMIT, Villingen-Schwenningen, Germany) (41). After curing was complete, the PDMS was taken out of the mold and cut into a 4 × 4 pillar arrangement. Each pillar is 1 mm diameter, is 1 mm high, and carries a microstructure on the flat surface: 100 × 100 μm^2 pads are separated by 41 μm wide and 5 μm deep trenches allowing for liquid drainage during the contact and separation process. Free polymers were extracted in toluene for at least 1 day (42). The PDMS was activated overnight in 12.5% hydrochloric acid and subsequently derivatized with (3-glycidoxypropyl)-trimethoxysilane (ABCR, Karlsruhe, Germany) to generate epoxide groups. NH_2-PEG-Biotin (3400 g/mol; Rapp Polymere, Tübingen, Germany) was melted at 80°C, and ~1 μL was spotted on each pillar followed by overnight incubation in argon atmosphere at 80°C. The excess polymers were thoroughly removed with ddH_2O. Shortly before the experiment, the PDMS was incubated with 1 μg/ml streptavidin (Thermo Fisher Scientific, Bonn, Germany) in 1× PBS and 0.4% bovine serum albumin for 30 min, washed with 1× PBS containing 0.05% Tween 20 (VWR Scientific GmbH, Darmstadt, Germany), with 1× PBS and gently dried with N_2 gas.

Ligand incubation

Sixteen-well silicone isolators allowed the addition of up to 16 different concentrations of the dsDNA ligands within a single experiment. Because of technical convenience, we restricted ourselves to the addition of eight different concentrations. Fifty millileters volume of polyamides in 1× PBS was circulated through each well for at least 2 h using a self-made fluidic system driven by a 16-channel peristaltic pump (Ismatec GmbH, Wertheim-Mondfeld, Germany).

Coupling and separation

The streptavidin functionalized PDMS stamp was approached to the DNA slide using high-precision stepper motors (OWIS GmbH, Staufen, Germany) and a piezo actuator (Piezo Systems Jena, Jena, Germany), monitored by reflection interference contrast microscopy (43). The biotinylated molecular complexes and the multivalent streptavidin coated PDMS stamp were allowed to couple via a biotin·streptavidin·biotin complex for 10 min, followed by retraction of the PDMS stamp at a velocity of 5 μm/s. Biotin·streptavidin is an extremely strong molecular interaction and is of significantly greater stability than short dsDNA at the applied separation velocity (44,45). In separate controls, we determined that no noteworthy amount of fluorescently labeled streptavidin was transferred from the PDMS to the DNA array during an experiment.

Analysis

Fluorescence images of the DNA slide were recorded in solution using a confocal scanner with 4 μm resolution (Tecan Austria GmbH, Austria) before and after the contact. The fluorescence per unit area was assumed to be proportional to the fluorescently labeled species per unit area (see Fig. S1 in the Supporting Material). The normalized fluorescence intensity (NF) is defined as the number of broken reference bonds normalized to the total number of individual molecular setups that have been under load. For the **1·2·3** molecular setups, it was determined as follows: initially, all molecular setups are present in the state S0 and were detected via the Cy3 labeled oligomer **2** (Fig. 3 *a*). After separation, the molecular setups on the glass slide exist in three different states, S0 (**1·2·3**), S1 (**1·2**), and S2 (**1**), as shown in Fig. 3 *b*. An unbinding force was applied only to the molecular setups in state S1 and S2. Molecular setups in state S0 did not couple to the PDMS streptavidin surface and therefore retained the biotinylated oligomer **3**. Because S1 and S0 cannot be distinguished, the latter was labeled with the spectrally distinct fluorescent marker streptavidin Alexa Fluor 647 (AF; Fig. 3 *c*). The labeling was performed subsequent to the Cy3 readout to avoid quenching or fluorescence resonance energy transfer effects. The Cy3 and AF fluorescence images allow the quantification of the relative amounts of S0, S1, and S2 (Fig. 3, *d* and *e*). The Cy3 and AF fluorescence images recorded after contact contain square-like features corresponding to the contacted area. From each square-like feature the $Cy3_{Rem}$ and AF_{Rem} were determined individually. $Cy3_{Initial}$ and $AF_{Initial}$ were determined from the noncontacted regions adjacent to each square-like feature.

$$S0 = AF_{Ratio} \tag{1}$$

$$S1 = Cy3_{Ratio} - AF_{Ratio} \tag{2}$$

$$S2 = 1 - Cy3_{Ratio} \tag{3}$$

$$Cy3_{Ratio} = \frac{Cy3_{Rem}}{Cy3_{Initial}}, \tag{4A}$$

$$AF_{Ratio} = \frac{AF_{Rem}}{AF_{Initial}} \tag{4B}$$

S0, S1, and S2 are normalized such that the relation S0 + S1 + S2 = 1 is always true. As defined above, the NF is given by the number of broken **2·3** bonds (S1) normalized to the number of bonds that have been under load (S1 + S2):

$$NF = \frac{S1}{S1 + S2} = \frac{Cy3_{Ratio} - AF_{Ratio}}{1 - AF_{Ratio}}. \tag{5}$$

The NF directly reflects the relative mechanical stability, a physical quantity inherent to a pair of molecular complexes, and is not influenced by the amount of molecules under load. The NF should not be confused with the $Cy3_{Ratio}$. For a fixed mechanical stability, the latter depends on the number of coupled molecular complexes, whereas the NF does not. The NFs presented in this work are the averages of the NFs determined from all square-like features of an experiment. The **1·4·5** and upside-down molecular setups were analyzed accordingly.

Polyamide synthesis

Polyamide conjugates were synthesized on solid-phase using published Boc-based protocols and purified by reverse-phase HPLC (≥95% purity) (46). Ultraviolet-visible spectra were recorded in water on a Hewlett-Packard Model 8452 A diode array spectrophotometer. All polyamide concentrations were determined using an extinction coefficient of 69,200 $M^{-1}cm^{-1}$ at λ_{max} near 310 nm. Matrix-assisted, LASER desorption/ionization time-of-flight mass spectrometry (MALDI-TOF MS) was performed using an Applied Biosystems Voyager DR Pro spectrometer. Polyamide **P1**: MALDI-TOF $[M+H]^+$ calcd for $C_{57}H_{71}N_{22}O_{10}^+$ = 1223.6, observed = 1223.4, **(*R*)-P2**: MALDI-TOF $[M+H]^+$ calcd for $C_{57}H_{72}N_{23}O_{10}^+$ = 1238.6, observed = 1238.6, **(*S*)-P2**: MALDI-TOF $[M+H]^+$ calcd for $C_{57}H_{72}N_{23}O_{10}^+$ = 1238.6, observed = 1238.5, **(*R*)-P3**: MALDI-TOF $[M+H]^+$ calcd for $C_{58}H_{73}N_{22}O_{10}^+$ = 1237.6, observed = 1237.3, **(*S*)-P3**: MALDI-TOF $[M+H]^+$ calcd for $C_{58}H_{73}N_{22}O_{10}^+$ = 1237.6, observed = 1237.5.

Melting temperature analysis

Melting temperatures were monitored on a Beckman ultraviolet-visible spectrometer at 260 nm within 25–90°C by applying a heating rate of

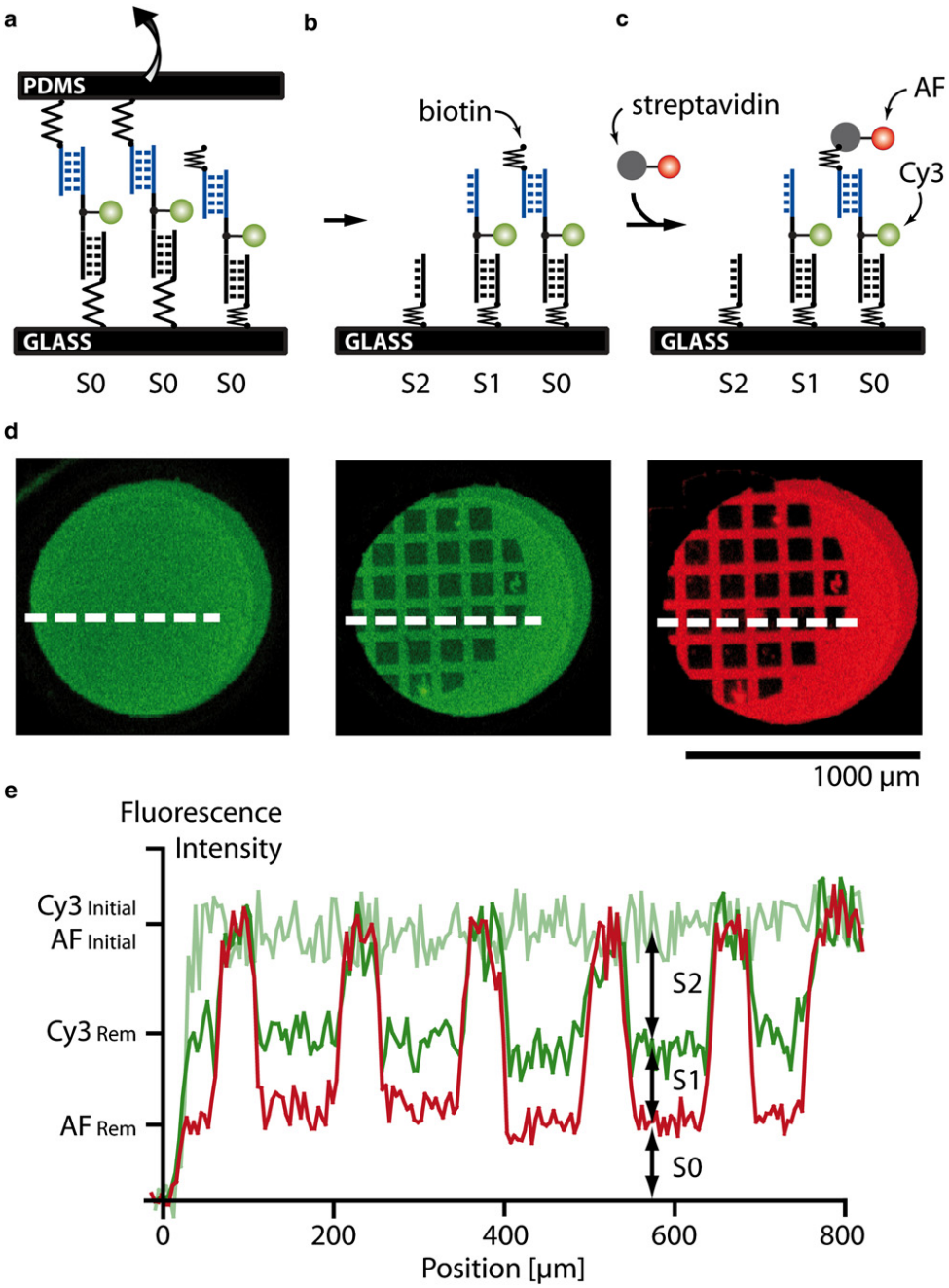

FIGURE 3 Comparative unbinding force experiment on the molecular level. (*a*) Before separation of the two surfaces, all molecular setups are in the state S0. (*b*) After separation, either target (state S2) or reference (state S1) bond is broken or no coupling (state S0) occurred. (*c*) Because states S0 and S1 cannot be distinguished by fluorescence, the free biotin of state S0 is labeled with streptavidin Alexa Fluor 647 (AF). (*d*) Fluorescence images of the glass slide before and after separation as well as after incubation with AF. The dark square-like features correspond to the area contacted with a microstructured PDMS stamp. (*e*) Corresponding line plots. From the fluorescence intensities the relative amounts of the states S0, S1, and S2 can be determined.

0.5°C/min. Measurements were performed in a degassed buffer containing 2 μM DNA duplex/polyamide (1:1), 10 mM NaCl, and 100 mM NaH_2PO_4 at pH 7.0. T_m-values are defined as the maximum of the first derivative of the melting curve.

RESULTS AND DISCUSSION

Force-based ligand detection relies on the alteration of unbinding forces due to dsDNA·ligand complex formation. In the course of conventional single molecule experiments, one strand of a DNA duplex is immobilized to solid support via a polyethyleneglycole (PEG) linker. In the same way, the complementary strand is immobilized to a microscopic force detector such as an AFM cantilever. Upon contacting the AFM cantilever with the solid support, the two complementary DNA strands hybridize. During separation of the support and the detector surface, the PEG linkers act like entropic springs (47,48), and an increasing force builds up until the DNA duplex unbinds (Fig. 1, *a* and *b*). The force extension curve is recorded and the unbinding force determined. Because unbinding is a thermally activated process (49) and the force detector is limited by thermal noise (50), several hundred experiments are typically performed to determine the unbinding forces with sufficient accuracy. As demonstrated by Krautbauer et al. (17) as well as Koch et al. (18), complex formation of a DNA duplex with a small

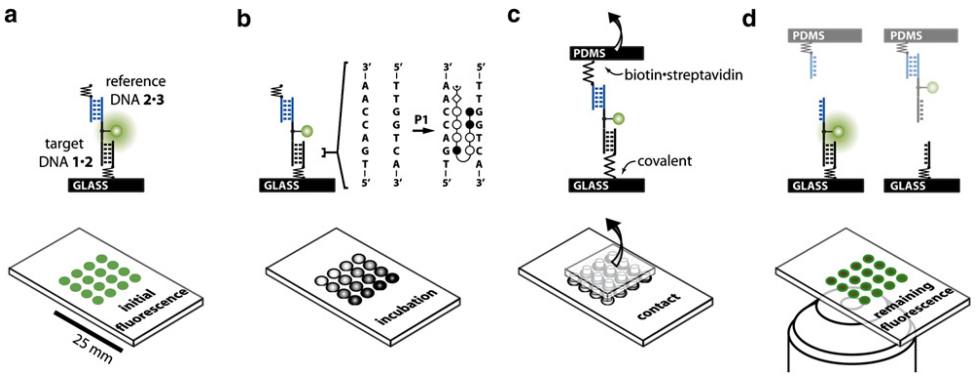

FIGURE 4 Schematics of CUFA experiments. (*a*) The molecular setup consists of two DNA duplexes, i.e., the **1·2** target and the **2·3** reference DNA duplex, linked in series. (*b*) A simple fluidic system allows incubation of 16 identical DNA spots with eight different polyamide **P1** concentrations. (*c*) The molecular setups are linked between glass support and PDMS. Separation of the surfaces applies a load to the chain of duplexes until the weaker fails. (*d*) The fluorescently labeled linking DNA oligomer **2** is more likely to remain on the side of the more stable DNA·ligand complex.

molecule or a protein is accompanied by a shift of the unbinding forces (Fig. 1 *c*). In our comparative unbinding force experiments, a known molecular bond carrying a fluorescent label replaces the microscopic force detector (Fig. 1, *d* and *e*).

Fig. 4 *a* illustrates the molecular setup schematically. Target DNA duplex **1·2** is immobilized to glass support via a $(\text{hexaethyleneglycol})_5$ linker of oligomer **1**. Reference DNA duplex **2·3** is bridged to **1·2** via a 10 basepair single stranded polythymine linker carrying a Cy3 fluorescence label. Oligomer **3** carries a biotin modification at the end of another polythymine linker. Before the force experiment, a fluidic system allows for incubation of the molecular setups with different ligand concentrations (Fig. 4 *b*). In Fig. 4 *c*, a soft PDMS stamp is brought in contact with the **1·2·3** complexes on the glass slide analogously to a microcontact-printing experiment (51,52). **1·2·3** couples to the PDMS stamp via biotin·streptavidin complex formation. Upon retraction of the PDMS stamp at 5 μm/s force is built up gradually acting along the molecular chain consisting of the linkers as well as the **1·2** and **2·3** duplexes until either **1·2** or **2·3** breaks (Fig. 4 *d*).

Approximately 10^4 duplicates of the same experiment are performed per μm^2. The absolute force needed to pull the two surfaces apart is neither recorded nor analyzed. Instead, the unbinding force of each target DNA duplex is compared individually against a separate reference duplex. For each molecular chain, the two possible experimental outcomes are distinguished by determining the location of the fluorescently labeled oligomer **2**. In case the fluorophore remained on the glass slide, the **2·3** DNA duplex is broken, and in case the fluorophore was transferred to the PDMS stamp, the **1·2** DNA duplex is broken.

The target and the reference DNA duplex are comprised of the same basepair composition, and the outcome "**1·2** is broken" should be close to equally likely to the outcome "**2·3** is broken" (53). Experimentally, we determined a NF (see Materials and Methods) of 38.4% with an error of 1.6%, which we estimated from repeated measurements (Fig. 5 *a*). We attribute this deviation from the expected NF of 50% to the symmetry break due to the different surfaces to which the oligomers are attached. DNA duplexes are sensitive to solution conditions such as pH and ionic strength (54), which may differ depending on the proximity of the DNA duplex to the PDMS or the glass surface. This minor imbalance does not affect the quantitative detection of dsDNA·ligand complexes.

Nonchiral hairpin polyamide

To investigate whether the CUFA is applicable to determine the thermal dissociation constant K_D of dsDNA·ligand interactions, we incubated **1·2·3** molecular setups with different concentrations of hairpin polyamide **P1**. Thereby, we make use of a symmetry breaking property, such that **P1** only binds to the target and not the reference DNA duplex: hairpin polyamides bind sequence specific with a preference for N→C orientation with respect to the 5′→3′ direction of the adjacent DNA strand (55,56). The preferred binding motif 5′-TGACCAA-3′ of polyamide **P1** is present in the **1·2** target DNA duplex, whereas the **2·3** reference DNA duplex contains the reverse-binding motif 5′-AACCAGT-3′, to which **P1** binds with significantly decreased affinity.

On a single chip, we incubated 16 identical spots of immobilized **1·2·3** molecular setups with eight different **P1** concentrations ranging from 0 to 2.7 nM and performed a CUFA experiment as described above. The NF increased with increasing polyamide concentration from 38.4% (Fig. 5 *a*) until it saturated at 63.1% (Fig. 5 *b*). This is in agreement with a stabilizing effect of **P1** on the **1·2** duplex. As it is common for quantitative dsDNA·polyamide interaction studies, we fitted the titration data to the Hill equation isotherm (a more detailed discussion follows at the end of this section) (9,58). The apparent thermal dissociation constant K_D was determined to be 105 pM with a 95% confidence interval of [65 pM, 169 pM] agreeing well with previously published quantitative DNase footprinting and microarray data (58). The NF data including the fit are shown in Fig. 5 *c*.

To ensure that the molecular setup responds as expected, we investigated the upside-down molecular setup **3·2·1**.

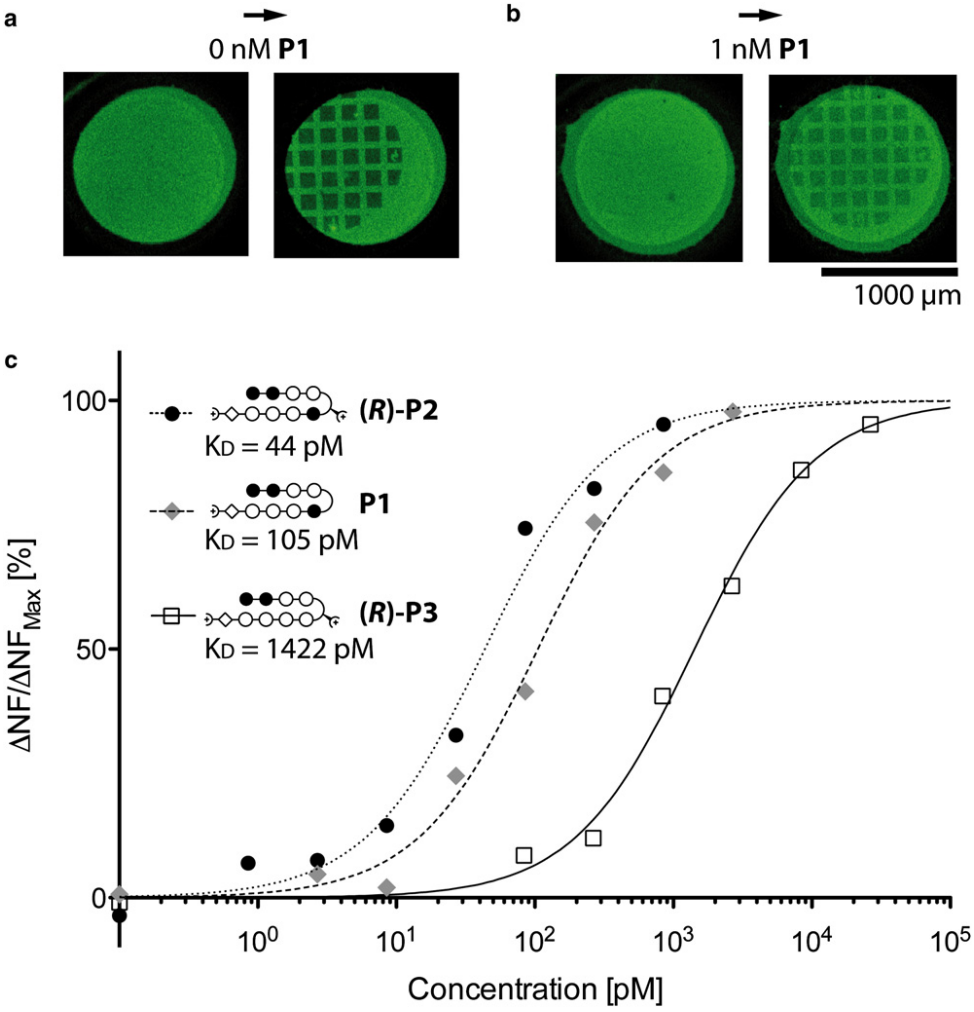

FIGURE 5 (*a*) Cy3 fluorescence image of **1·2·3** molecular setups on a glass slide before and after contact with a PDMS stamp in absence of **P1**. (*b*) Cy3 fluorescence image of **1·2·3** molecular setups on a glass slide before and after contact with a PDMS stamp in presence of 1 nM **P1**. The fluorescence intensity of the contacted area is higher compared to the 0 nM case. (*c*) Relative change in NF due to titration with three different polyamide compounds.

Here, the position of the target and the reference DNA duplex is exchanged, and thus the response to the addition of **P1** should be inverted. Indeed, the NF decreased from 31.9% to 7.7% upon increasing the **P1** concentration from 0 to 10 nM. In this case, the polyamide binds preferentially to the DNA duplex adjacent to the PDMS stamp, and therefore the amount of fluorescently labeled oligomer **2** transferred to the PDMS stamp was increased in presence of **P1**.

Chiral hairpin polyamide

In previous work, we demonstrated that chiral hairpin polyamides distinguish between D- and L-DNA (16). Chiral selectivitiy is introduced by an amine substituent on the γ-turn amino acid of the hairpin polyamide that was also shown to lead to an increase in binding affinity (47). The chiral hairpin polyamide **(*R*)-P2**, which recognizes the same sequence as **P1**, was examined employing the **1·4·5** molecular setup. **1·4** is identical to the **1·2** target DNA duplex, and **4·5** is the mirrored DNA duplex to **1·4**. **(*R*)-P2** binds preferentially to the **1·4** 5′-TGACCAA-3′ binding motif, whereas **4·5** presents less optimal binding sites due to its opposite chirality.

Analogous to the previous experiment, an increase in concentration of **(*R*)-P2** from 0 to 1 nM lead to an increase of the NF from 47.1% to 80.3%, agreeing with a stabilizing effect on the D-DNA duplex **1·4**. Fitting the titration data to a Hill equation isotherm revealed an apparent thermal dissociation constant K_D of 44 pM with a 95% confidence interval of [23 pM, 83 pM]. The K_D for the **(*R*)-P2** hairpin polyamide has not been reported yet. However, a lowered K_D compared to **P1** is consistent with prior experiences with the addition of an amine substituent to the γ-turn amino acid of regular polyamide hairpins (47). The NF data including the fit are shown in Fig. 5 *c*.

For control, the **5·4·1** upside-down molecular setup in combination with **(*R*)-P2** was measured at 0 nM and 10 nM yielding 32.8% and 12.9%, respectively. The regular molecular setup **1·4·5** in combination with mirror imaged polyamide **(*S*)-P2** was also measured at 0 nM and 10 nM resulting in NF of 44.1% and 20.9%. The two controls demonstrated that the response of the assay was as expected: in the **5·4·1** upside-down molecular setup, the target and reference DNA duplex are essentially mirrored (target and reference are of identical sequence but opposite chirality).

In this case, the ligand recognizes the DNA duplex adjacent to the PDMS stamp and the change in NF due to ligand binding was inverted. In case the ligand was mirrored and incubated with the **1·4·5** molecular setup, the ligand recognized the reference bond as its preferential binding motif and the change in NF was also inverted.

Mismatched hairpin polyamide

Introducing the single basepair mismatched polyamide **(*R*)-P3** to the **1·4·5** molecular setup is expected to form a DNA-ligand complex of lower affinity (57). In detail, **1·4** provides a binding motif for **(*R*)-P3** with a single basepair mismatch. The affinity to **4·5** is even further decreased, because the binding motif contains a single basepair mismatch and, in addition, is of opposite chirality. Incubation of the **1·4·5** molecular setup with increasing concentrations of **(*R*)-P3** increased the NF from 47.1% at 0 nM to 71.2% at 27 nM. The apparent K_D, determined from a fit of the NF to the Hill equation isotherm, was 1442 pM with a 95% confidence interval of [932 pM, 2169 pM]. The NF data including the fit are shown in Fig. 5 *c*.

Controls were performed with the **5·4·1** upside-down molecular setup in absence and presence of 10 nM **(*R*)-P3,** yielding NF of 32.8% and 15.4%, respectively. For the regular **1·4·5** molecular setup, the NF fluorescence also decreased from 47.1% in absence to 25.6% in presence of 10 nM mirrored compound **(*S*)-P3**. Both controls, in which either the molecular setup or the ligand was mirrored, produced an inverted change in NF as response to the addition of the ligand.

Melting temperatures

To ensure that the differences in unbinding forces were a result of target DNA duplex stabilization by hairpin polyamides, the melting temperatures of the dsDNA·polyamide complexes were determined. The results clearly showed a larger increase in melting temperature for the target duplexes in presence of the polyamides compared to the reference duplexes (Fig. 6).

Polyamide	Target [°C] **1•2 / 1•4**	Reference [°C] **2•3**	Reference [°C] **4•5**
none	70	70	70
P1	77	73	-
(*R*)-P2	83	-	75
(*R*)-P3	76	-	71

FIGURE 6 Melting temperatures of the target and reference DNA duplex in presence and absence of polyamides. The polyamides and DNA duplexes are mixed at a stoichiometry of 1:1 at 2 μM.

Thermal dissociation constant

The affinity of a hairpin polyamide for its dsDNA binding site is characterized by the thermal dissociation constant K_D. The experimental data suggest that the Hill equation isotherm governs the response of the NF, from which the K_D characteristic for the dsDNA·polyamide complex under investigation is easily determined. In the following, we derive the response of CUFA beginning with the law of mass action.

The law of mass action describes the amounts of dsDNA·ligand complexes, unbound dsDNA, and free ligands at chemical equilibrium with a dsDNA·ligand complex characteristic thermal K_D defined as

$$K_D = \frac{k_{off}}{k_{on}} = \frac{[\text{dsDNA}][\text{ligand}]}{[\text{dsDNA} \cdot \text{ligand}]}. \quad (6)$$

In our experiments, the total amount of added ligand exceeded the available dsDNA binding sites by at least two orders of magnitude. As a result, the probability p of a dsDNA binding site to be occupied by a ligand is given by the Hill equation isotherm and depends on the ligand concentration and K_D only (58):

$$p = \frac{[\text{ligand}]}{[\text{ligand}] + K_D}. \quad (7)$$

For further analysis, it is crucial to compare the timescale of association to a single binding site to the timescale of the force probing. The apparent K_D determined from the CUFA experiment may vary from the initial thermal K_D, if the system is allowed to equilibrate during the application of the external force: at equilibrium and ligand concentrations around the thermal K_D the association rate, given by $[\text{ligand}]\cdot k_{on}$, is of the same order of magnitude as the dissociation rate k_{off}. The lifetime or inverse dissociation rate for a dsDNA·polyamide complex was experimentally determined to be ~500 s (59). At 5 μm/s separation velocity and similar linker lengths, the force needed to rupture a 20 basepair DNA duplex is built up on timescales in the order of $\tau = 0.01$ s (44). The DNA duplex unbinding occurs therefore on a much faster timescale τ than the association or dissociation of the dsDNA·ligand complex at relevant ligand concentrations:

$$\tau << \frac{1}{[\text{ligand}] \cdot k_{on}}. \quad (8)$$

Although the natural off-rate of polyamides is very low, dissociation of the ligand from the DNA duplex during force probing may be nonnegligible. Studies suggest that the B-S transition of DNA under force can be explained by a tilt of the basepairs and a significant reorganization of the helical structure of the DNA (60–62). The B-S transition has not been observed for 20 basepair duplexes yet (44). However, even small deformations of the dsDNA helical structure may lead to the dissociation of the ligand, especially because hairpin polyamides are particularly sensitive to deformations

of the minor groove. This results in a decreased fraction of occupied binding sites at the time of dsDNA unbinding compared to the initial situation before force is applied. Given that the association rate is slow, rebinding of the ligand to the dsDNA is neglected and the fraction of occupied binding sites is reduced by a constant factor f.

$$p' = f \cdot p = f \cdot \frac{[\text{ligand}]}{[\text{ligand}] + K_D}, \quad (9)$$

where f lies within the interval [0,1]. The probability of a binding site to be occupied by a ligand is still governed by the Hill equation isotherm; however with increasing ligand concentration, the probability p' saturates at $f < 1$ instead of 1. Importantly, the apparent K_D is identical with the thermal K_D.

The target DNA sequence was designed such that there is only one preferred polyamide-binding site. Without loss of generality, the no-ligand case is assumed to yield NF_0, whereas the bound-ligand case is assumed to yield NF_1. The fluorescence signals of these two states superimpose each other, and the expected total fluorescence signal as a function of the polyamide concentration is the sum of the NFs of the two states weighted by their relative occurrence:

$$\begin{aligned} NF &= p' \cdot NF_1 + (1 - p') \cdot NF_0 \\ &= NF_0 + f \cdot (NF_1 - NF_0) \cdot \frac{[\text{ligand}]}{[\text{ligand}] + K_D}. \end{aligned} \quad (10)$$

The dissociation of ligands from the DNA duplex results in a decrease of the maximal change in NF, whereas the apparent K_D is not affected. To conclude, in case Eq. 8 holds, the forced unbinding of dsDNA in presence of a ligand is a nonequilibrium process that produces a snapshot of the equilibrium distribution between dsDNA and dsDNA·ligand complexes from which the thermal dissociation constant K_D can be determined.

CONCLUSION

The CUFA was successfully applied to quantify the thermal dissociation constants of three different dsDNA-polyamide complexes. For this purpose, polyamide concentrations as low as 10 pM were detected. This level of sensitivity is comparable to conventional chip methods, which work with fluorescently labeled ligands (9). Labeling, however, may alter the binding behavior compared with the unlabeled ligand and is not always applicable. Label-free high-throughput techniques, such as surface plasmon resonance, are challenged when they are confronted with small molecules like polyamides, which are easily detected employing CUFA. Our approach not only avoids labeling of the interacting molecules (a label is attached to linking DNA strand at a noninteracting basepair), but also permits the combination of different experiments as well as controls on one chip. The current DNA-feature size is hundreds of micrometers but can be reduced to several micrometers using conventional microarray spotters. Miniaturization will allow for a high degree of parallelization and significantly reduced sample volumes.

We foresee CUFA in combination with microarray technology to be used as a tool to rapidly determine and quantify the sequence-recognition profile of small molecules like transcription factors, drugs, or other DNA-binding molecules. In separate experiments, we demonstrated that short-lived molecular interactions are captured in molecular crowded environments, as will be published elsewhere (63). Thus, the sensitivity range covers molecular complexes with micromolar to picomolar thermal dissociation constants and CUFA may prove to be the ideal tool for systems biologists, who have a growing interest in techniques that obtain affinity binder data with sufficient accuracy in a high-throughput fashion (64,65). The experimental procedure is as simple as contacting and separating two surfaces and can be implemented in any laboratory equipped with a quantitative fluorescence microscope.

SUPPORTING MATERIAL

One figure is available at http://www.biophysj.org/biophysj/supplemental/S0006-3495(09)00680-8.

D. Ho and P. Severin are grateful to the Elite Network of Bavaria (IDK-NBT) for a doctoral fellowship. C. Dose is grateful to the Alexander von Humboldt foundation for a postdoctoral fellowship.

Financial support was provided by the Nanosystems Initiative Munich, the Deutsche Forschungsgemeinschaft, the Fonds der Chemischen Industrie, and the National Institutes of Health.

REFERENCES

1. Gottesfeld, J. M., L. Neely, J. W. Trauger, E. E. Baird, and P. B. Dervan. 1997. Regulation of gene expression by small molecules. *Nature*. 387:202–205.
2. Majmudar, C. Y., and A. K. Mapp. 2005. Chemical approaches to transcriptional regulation. *Curr. Opin. Chem. Biol.* 9:467–474.
3. Connaghan-Jones, K., A. Moody, and D. Bain. 2008. Quantitative DNase footprint titration: a tool for analyzing the energetics of protein–DNA interactions. *Nat. Protocols*. 3:900–914.
4. Zhang, J., H. Lang, F. Huber, A. Bietsch, W. Grange, et al. 2006. Rapid and label-free nanomechanical detection of biomarker transcripts in human RNA. *Nat. Nanotechnol.* 1:214–220.
5. Ren, B. 2000. Genome-wide location and function of DNA binding proteins. *Science*. 290:2306–2309.
6. Harbison, C. T., D. B. Gordon, T. I. Lee, N. J. Rinaldi, K. D. Macisaac, et al. 2004. Transcriptional regulatory code of a eukaryotic genome. *Nature*. 431:99–104.
7. Solomon, M. J., and A. Varshavsky. 1985. Formaldehyde-mediated DNA-protein crosslinking: a probe for in vivo chromatin structures. *Proc. Natl. Acad. Sci. USA*. 82:6470–6474.
8. Warren, C., N. Kratochvil, K. Hauschild, S. Foister, M. Brezinski, et al. 2006. Defining the sequence-recognition profile of DNA-binding molecules. *Proc. Natl. Acad. Sci. USA*. 103:867–872.
9. Puckett, J., K. Muzikar, J. Tietjen, C. Warren, A. Ansari, et al. 2007. Quantitative microarray profiling of DNA-binding molecules. *J. Am. Chem. Soc.* 129:12310–12319.

10. Boozer, C., G. Kim, S. Cong, H. Guan, and T. Londergan. 2006. Looking towards label-free biomolecular interaction analysis in a high-throughput format: a review of new surface plasmon resonance technologies. *Curr. Opin. Biotechnol.* 17:400–405.

11. Wang, J., and H. S. Zhou. 2008. Aptamer-based Au nanoparticles-enhanced surface plasmon resonance detection of small molecules. *Anal. Chem.* 80:7174–7178.

12. Gurard-Levin, Z. A., and M. A. Mrksich. 2008. Combining self-assembled monolayers and mass spectrometry for applications in biochips. *Annu. Rev. Anal. Chem.* 1:767–800.

13. Albrecht, C., K. Blank, M. Lalic-Multhaler, S. Hirler, T. Mai, et al. 2003. DNA: a programmable force sensor. *Science.* 301:367–370.

14. Blank, K., T. Mai, I. Gilbert, S. Schiffmann, J. Rankl, et al. 2003. A force-based protein biochip. *Proc. Natl. Acad. Sci. USA.* 100:11356–11360.

15. Blank, K., A. Lankenau, T. Mai, S. Schiffmann, I. Gilbert, et al. 2004. Double-chip protein arrays: force-based multiplex sandwich immunoassays with increased specificity. *Anal. Bioanal. Chem.* 379:974–981.

16. Dose, C., D. Ho, H. E. Gaub, P. B. Dervan, and C. H. Albrecht. 2007. Recognition of ''mirror-image'' DNA by small molecules. *Angew. Chem.* 46:8384–8387.

17. Krautbauer, R., S. Fischerlander, S. Allen, and H. E. Gaub. 2002. Mechanical fingerprints of DNA drug complexes. *Single Mol.* 3:97–103.

18. Koch, S. J., A. Shundrovsky, B. C. Jantzen, and M. D. Wang. 2002. Probing protein-DNA interactions by unzipping a single DNA double helix. *Biophys. J.* 83:1098–1105.

19. Leuba, S. H., M. A. Karymov, M. Tomschik, and R. Ramjit. 2003. Assembly of single chromatin fibers depends on the tension in the DNA molecule: magnetic tweezers study. *Proc. Natl. Acad. Sci. USA.* 100:495–500.

20. Puchner, E. M., A. Alexandrovich, A. L. Kho, U. Hensen, L. V. Schäfer, B. Brandmeier, F. Gräter, H. Grubmüller, H. E. Gaub, and M. Gautel. 2008. Mechanoenzymatics of titin kinase. *Proc. Natl. Acad. Sci. USA.* 105:13385–13390.

21. Schlierf, M., F. Berkemeier, and M. Rief. 2007. Direct observation of active protein folding using lock-in force spectroscopy. *Biophys. J.* 93:3989–3998.

22. Wiita, A., R. Perez-Jimenez, K. Walther, F. Gräter, B. Berne, et al. 2007. Probing the chemistry of thioredoxin catalysis with force. *Nature.* 450:124–127.

23. Clemen, A. E. M., M. Vilfan, J. Jaud, J. S. Zhang, M. Barmann, et al. 2005. Force-dependent stepping kinetics of myosin-V. *Biophys. J.* 88:4402–4410.

24. Gosse, C., and V. Croquette. 2002. Magnetic tweezers: micromanipulation and force measurement at the molecular level. *Biophys. J.* 82:3314–3329.

25. Dervan, P. B., A. T. Poulin-Kerstien, E. J. Fechter, and B. S. Edelson. 2005. Regulation of gene expression by synthetic DNA-binding ligands. *Top. Curr. Chem.* 253:1–31.

26. Dervan, P. B., and B. S. Edelson. 2003. Recognition of the DNA minor groove by pyrrole-imidazole polyamides. *Curr. Opin. Struct. Biol.* 13:284–299.

27. Dervan, P. B. 2001. Molecular recognition of DNA by small molecules. *Bioorg. Med. Chem.* 9:2215–2235.

28. White, S., J. W. Szewczyk, J. M. Turner, E. E. Baird, and P. B. Dervan. 1998. Recognition of the four Watson-Crick base pairs in the DNA minor groove by synthetic ligands. *Nature.* 391:468–471.

29. Kielkopf, C. L., R. E. Bremer, S. White, J. W. Szewczyk, J. M. Turner, et al. 2000. Structural effects of DNA sequence on T.A recognition by hydroxypyrrole/pyrrole pairs in the minor groove. *J. Mol. Biol.* 295:557–567.

30. Mrksich, M., M. E. Parks, and P. B. Dervan. 1994. Hairpin peptide motif - a new class of oligopeptides for sequence-specific recognition in the minor-groove of double-helical DNA. *J. Am. Chem. Soc.* 116:7983–7988.

31. Swalley, S. E., E. E. Baird, and P. B. Dervan. 1999. Effects of γ-turn and β-tail amino acids on sequence-specific recognition of DNA by hairpin polyamides. *J. Am. Chem. Soc.* 121:1113–1120.

32. Kielkopf, C. L., S. White, J. W. Szewczyk, J. M. Turner, E. E. Baird, et al. 1998. A structural basis for recognition of A center dot T and T center dot A base pairs in the minor groove of B-DNA. *Science.* 282:111–115.

33. deClairac, R. P. L., B. H. Geierstanger, M. Mrksich, P. B. Dervan, and D. E. Wemmer. 1997. NMR characterization of hairpin polyamide complexes with the minor groove of DNA. *J. Am. Chem. Soc.* 119:7909–7916.

34. Cohen, J. D., J. P. Sadowski, and P. B. Dervan. 2007. Addressing single molecules on DNA nanostructures. *Angew. Chem.* 46:7956–7959.

35. Schmidt, T. L., C. K. Nandi, G. Rasched, P. P. Parui, B. Brutschy, et al. 2007. Polyamide struts for DNA architectures. *Angew. Chem.* 46:4382–4384.

36. Arndt, H. D., K. E. Hauschild, D. P. Sullivan, K. Lake, P. B. Dervan, et al. 2003. Toward artificial developmental regulators. *J. Am. Chem. Soc.* 125:13322–13323.

37. Stafford, R. L., H. D. Arndt, M. L. Brezinski, A. Z. Ansari, and P. B. Dervan. 2007. Minimization of a protein-DNA dimerizer. *J. Am. Chem. Soc.* 129:2660–2668.

38. Olenyuk, B. Z., G. J. Zhang, J. M. Klco, N. G. Nickols, W. G. Kaelin, Jr., et al. 2004. Inhibition of vascular endothelial growth factor with a sequence-specific hypoxia response element antagonist. *Proc. Natl. Acad. Sci. USA.* 101:16768–16773.

39. Nickols, N. G., and P. B. Dervan. 2007. Suppression of androgen receptor-mediated gene expression by a sequence-specific DNA-binding polyamide. *Proc. Natl. Acad. Sci. USA.* 104:10418–10423.

40. Nickols, N. G., C. S. Jacobs, M. E. Farkas, and P. B. Dervan. 2007. Modulating hypoxia-inducible transcription by disrupting the HIF-1-DNA interface. *ACS Chem. Biol.* 2:561–571.

41. Albrecht, C. H., H. Clausen-Schaumann, and H. E. Gaub. 2006. Differential analysis of biomolecular rupture forces. *J. Phys. Condens. Matter.* 18:S581–S599.

42. Perutz, S., E. J. Kramer, J. Baney, and C. Y. Hui. 1997. Adhesion between hydrolyzed surfaces of poly(dimethylsiloxane) networks. *Macromolecules.* 30:7964–7969.

43. Wiegand, G., K. R. Neumaier, and E. Sackmann. 1998. Microinterferometry: three-dimensional reconstruction of surface microtopography for thin-film and wetting studies by reflection interference contrast microscopy (RICM). *Appl. Opt.* 37:6892–6905.

44. Morfill, J., F. Kuhner, K. Blank, R. Lugmaier, J. Sedlmair, et al. 2007. B-S transition in short oligonucleotides. *Biophys. J.* 93:2400–2409.

45. Merkel, R., P. Nassoy, A. Leung, K. Ritchie, and E. Evans. 1999. Energy landscapes of receptor-ligand bonds explored with dynamic force spectroscopy. *Nature.* 397:50–53.

46. Herman, D. M., E. E. Baird, and P. B. Dervan. 1998. Stereochemical control of the DNA binding affinity, sequence specificity, and orientation preference of chiral hairpin polyamides in the minor groove. *J. Am. Chem. Soc.* 120:1382–1391.

47. Kienberger, F., V. P. Pastushenko, G. Kada, and H. J. Gruber. 2000. Static and dynamical properties of single poly(ethylene glycol) molecules investigated by force spectroscopy. *Single Mol.* 78:123–128.

48. Friedsam, C., A. K. Wehle, F. Kuhner, and H. E. Gaub. 2003. Dynamic single-molecule force spectroscopy: bond rupture analysis with variable spacer length. *J. Phys. Condens. Matter.* 15:S1709–S1723.

49. Evans, E., and K. Ritchie. 1997. Dynamic strength of molecular adhesion bonds. *Biophys. J.* 72:1541–1555.

50. Viani, M., T. Schäffer, A. Chand, M. Rief, H. E. Gaub, and P. Hansma. 1999. Small cantilevers for force spectroscopy of single molecules. *J. Appl. Phys.* 86:2258–2262.

51. Xia, Y., and G. M. Whitesides. 1998. Soft lithography. *Annu. Rev. Mater. Sci.* 28:153–184.

52. Bernard, A., J. P. Renault, B. Michel, and H. R. Bosshard. 2000. Microcontact printing of proteins. *Adv. Mater.* 12:1067–1070.

53. Neuert, G., C. H. Albrecht, and H. E. Gaub. 2007. Predicting the rupture probabilities of molecular bonds in series. *Biophys. J.* 93:1215–1223.

54. Rouzina, I., and V. A. Bloomfield. 2001. Force-induced melting of the DNA double helix. 2. Effect of solution conditions. *Biophys. J.* 80:894–900.

55. White, S., E. E. Baird, and P. B. Dervan. 1997. Orientation preferences of pyrrole-imidazole polyamides in the minor groove of DNA. *J. Am. Chem. Soc.* 119:8756–8765.

56. Hawkins, C. A., R. P. de Clairac, R. N. Dominey, E. E. Baird, S. White, et al. 2001. Controlling binding orientation in hairpin polyamide DNA complexes. *J. Am. Chem. Soc.* 122:5235–5243.

57. Hsu, C. F., J. W. Phillips, J. W. Trauger, M. E. Farkas, J. M. Belitsky, et al. 2007. Completion of a programmable DNA-binding small molecule library. *Tetrahedron.* 63:6146–6151.

58. Halperin, A., A. Buhot, and E. Zhulina. 2006. On the hybridization isotherms of DNA microarrays: the Langmuir model and its extensions. *J. Phys. Condens. Matter.* 18:S463–S490.

59. Baliga, R., E. Baird, D. Herman, C. Melander, P. B. Dervan, et al. 2001. Kinetic consequences of covalent linkage of DNA binding polyamides. *Biochemistry.* 40:3–8.

60. Rief, M., H. Clausen-Schaumann, and H. E. Gaub. 1999. Sequence dependent mechanics of single DNA molecules. *Nat. Struct. Biol.* 6:346–349.

61. Lebrun, A., and R. Lavery. 1996. Modeling extreme stretching of DNA. *Nucleic Acids Res.* 24:2260–2267.

62. Smith, S. B., Y. J. Cui, and C. Bustamante. 1996. Overstretching B-DNA: the elastic response of individual double-stranded and single-stranded DNA molecules. *Science.* 271:795–799.

63. Ho, D., K. Falter, P. Severin, and H. E. Gaub. 2009. DNA as a force sensor in an aptamer-based biochip for ATP. *Anal. Chem.* n press.

64. Titz, B., M. Schlesner, and P. Uetz. 2004. What do we learn from high-throughput protein interaction data? *Expert Rev. Proteomics.* 1:111–121.

65. Kitano, H. 2002. Systems biology: a brief overview. *Science.* 295:1662–1664.

Biophysical Journal, Volume 96

Supporting Material

Quantitative detection of small molecule/DNA complexes employing a force-based and label-free DNA-microarray

Dominik Ho, Christian Dose, Christian H. Albrecht, Philip Severin, Katja Falter, Peter B. Dervan, and Hermann E. Gaub

SUPPLEMENTARY INFORMATION

"Quantitative detection of small molecule/DNA complexes employing a force-based and label-free DNA-microarray"

Dominik Ho[1,2], Christian Dose[3], Christian H. Albrecht[1], Philip Severin[1], Katja Falter[1], Peter B. Dervan[3], Hermann E. Gaub[1]

[1] Lehrstuhl für Angewandte Physik and Center for Nanoscience
Ludwig-Maximilians-Universität
Amalienstrasse 54, 80799 Munich, Germany
Fax: (+49) 89-2180-2050
E-mail: gaub@lmu.de

[2] Munich Center For Integrated Protein Science (CIPSM)
Ludwig-Maximilians-Universität
Butenandtstrasse 5-13, 81377 Munich, Germany
E-mail: dominik.ho@web.de

[3] Division of Chemistry and Chemical Engineering
California Institute of Technology
Pasadena, California 91125, USA
Fax: (+1) 626-683-8753
E-mail: dervan@caltech.edu

DNA surface density. Quantitative analysis of the fluorescence images relies on the assumption that the amount of fluorescently labeled species per unit area is proportional to the obtained fluorescence intensity per unit area. To investigate this relationship, we titrated identically prepared oligomer **1** spots on a glass slide with different amounts of oligomer **2** ranging from 0 to 0.6 pMol. After 2 hours of incubation the slide was washed thoroughly in 1x PBS and read out via fluorescence. The fluorescence intensities were summed over all pixels of each well divided by the fluorescence spot area, which was on average 1.8 mm of diameter. The fluorescence intensity was proportional to the amount of added ligand for amounts of DNA oligomer **2** less than 0.4 pMol. At higher amounts the fluorescence intensity saturated and deviated significantly from a line fit.

The observed saturation can be explained by electrostatic repulsion between the dsDNA. Short dsDNA is a rod like, cylindrical molecule, which is most densely packed in a parallel arrangement. Close packing of short dsDNA on a surface is thus equivalent to the problem of close packing of hard disks. The total hard disk radius is the sum of the dsDNA radius and the length of electrostatic repulsion. The former is known to be 0.95 nm [1] and the latter is best described by the Debye length that is approximately 0.62 nm at 147 mM Na^+ [2]. The total disk radius is therefore 1.57 nm. Randomly packing discs results in a packing efficiency of 82% [2]. The packing efficiency and the total disk radius yield the theoretical maximum in short dsDNA surface density ρ_{Debye} of 0.11 molecules per nm^2 in good agreement with literature values [3].

To compare whether the onset of fluorescence intensity saturation coincides with ρ_{Debye} the densities of **1·2** complexes per unit area were determined from the fluorescence spot size and the assumption that all oligomers **2** hybridized to free oligomers **1** immobilized to the surface. Further, the expected maximal fluorescence intensity was determined by extrapolating the line fit for low densities to ρ_{Debye} yielding I_{Debye}. In Figure S1 the fluorescence intensity ratio I/I_{Debye} was plotted against the corresponding calculated surface density ranging from 0 to 0.13 molecules per nm^2. The observed saturation of fluorescence intensity at around 0.09 molecules per nm^2 is in good agreement with ρ_{Debye}. Remaining free ssDNA strands that also occupy a small fraction of the surface area may explain the slightly lower experimentally determined value.

It is entirely possible that a non-linearity between amount of oligomer **2** per unit area and fluorescence signal at high surface densities contributes to the observed saturation effect. Hence, the molecular setups in the present study were prepared at ρ_0 of 0.06 molecular setups per nm^2. This is a surface density for which we have shown the fluorescence per unit area to

be proportional to the fluorescently labeled species per unit area. Nonetheless, the surface density is rather high: the Flory radius, which is deduced from the radius of gyration, is a good measure of the volume a polymer encompasses [1] [4]. From the actual lengths and the persistence lengths of dsDNA [5], ssDNA [6] and PEG [7] we calculate a Flory radius of 9.38 nm for the **1**·**2**·**3** molecular setups used in our experiments. Assuming again a close packing of disks yields an upper limit of 0.003 molecular setups per nm^2 for the regime wherein the constructs do not interact with each other. The densities used in our experiments are an order of magnitude higher than that. This is a fact that should be kept in mind if the binding of larger and less robust ligands like proteins to dsDNA is going to be investigated. In this case, the surface densities of the molecular setups may have to be decreased further in order to avoid steric hindrance and unwanted interactions.

REFERENCES

[1] Halperin, A., A. Buhot and E. Zhulina. 2006. On the hybridization isotherms of DNA microarrays: the Langmuir model and its extensions. J. Phys.: Condens. Matter, 18:S463-S490.

[2] Berryman, J. G. 1983. Random close packing of hard spheres and disks. Phys. Rev. A. 27:1053-1061.

[3] Ray, S., S. Daube, G. Leitus, Z. Vager and R. Naaman. 2006. Chirality-Induced Spin-Selective Properties of Self-Assembled Monolayers of DNA on Gold. Phys. Rev. Lett. 96: 036101.

[4] Israelachvili, J. N. 1991. Intermolecular and Surface Forces. Academic Press, New York.

[5] Marko, J. F. and E. D. Siggia. 1995. Stretching DNA. Macromolecules. 28:8759-8770.

[6] Rief, M., H. Clausen-Schaumann and H. E. Gaub. 1999. Sequence dependent mechanics of single DNA molecules. Nat. Struct. Biol. 6:346-349.

[7] Oesterhelt, F., M. Rief and H. E. Gaub. 1999. Single molecule force spectroscopy by AFM indicates helical structure of poly (ethylene-glycol) in water. New J. Phys. 1:6.1-6.11.

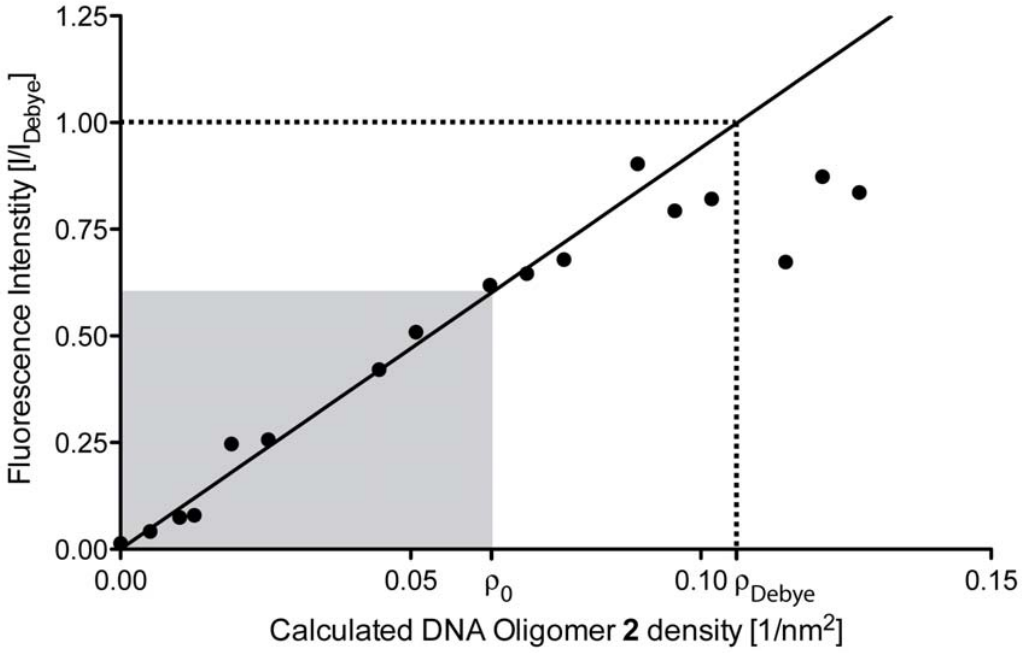

Figure S1. Different amounts of oligomer **2** were incubated with identically prepared oligomer **1** spots. The fluorescence intensities per unit area are plotted against the calculated surface densities. The dashed line indicates the highest possible density of oligomer **2** per unit area based on the electrostatic repulsion argument. The CUFA experiments are performed at densities of oligomer **2** per unit area, wherein the fluorescence intensity per unit area is proportional to the presence of fluorescently labeled oligomer **2** per unit area (highlighted in grey).

A.4 Publication 4: Force-Driven Separation of Short Double-Stranded DNA

Dominik Ho, Julia L. Zimmermann, Florian A. Dehmelt, Uta Steinbach, Matthias Erdmann, Philip Severin, Katja Falter and Hermann E. Gaub;
Biophysical Journal, 2009, Vol. 97, 3158-3167

Force-Driven Separation of Short Double-Stranded DNA

Dominik Ho,[†‡*] Julia L. Zimmermann,[†] Florian A. Dehmelt,[†] Uta Steinbach,[†] Matthias Erdmann,[†] Philip Severin,[†] Katja Falter,[†] and Hermann E. Gaub[†]

[†]Lehrstuhl für Angewandte Physik and Center for Nanoscience, Ludwig-Maximilians-Universität, Munich, Germany; and [‡]Munich Center For Integrated Protein Science (CIPSM), Ludwig-Maximilians-Universität, Munich, Germany

ABSTRACT Short double-stranded DNA is used in a variety of nanotechnological applications, and for many of them, it is important to know for which forces and which force loading rates the DNA duplex remains stable. In this work, we develop a theoretical model that describes the force-dependent dissociation rate for DNA duplexes tens of basepairs long under tension along their axes ("shear geometry"). Explicitly, we set up a three-state equilibrium model and apply the canonical transition state theory to calculate the kinetic rates for strand unpairing and the rupture-force distribution as a function of the separation velocity of the end-to-end distance. Theory is in excellent agreement with actual single-molecule force spectroscopy results and even allows for the prediction of the rupture-force distribution for a given DNA duplex sequence and separation velocity. We further show that for describing double-stranded DNA separation kinetics, our model is a significant refinement of the conventionally used Bell-Evans model.

INTRODUCTION

Double-stranded DNA (dsDNA) is an extensively studied polymer offering a number of striking properties. Among these properties are interstrand recognition according to the Watson-Crick basepairing rules, stability under a broad range of conditions, and ease of synthesis that allows for fast and cost-efficient production of any desired sequence with almost any kind of chemical modification. Within the past several years, various areas of application of DNA have been identified, and nanotechnology, specifically, is increasingly harnessing the potential of this versatile polymer (1). Whereas in earlier published work DNA merely served as simple molecular handles for single-molecule experiments (2,3), today DNA serves as molecular building blocks for complex self-assembled nanostructures (4–7), as well as DNA computing (8). In our laboratory, DNA was even used as a programmable force sensor for detection of single-nucleotide polymorphisms (9), multiplexed antibody sandwich assays (10,11), investigation of chiral preference of small DNA-binding molecules (12), quantitative detection of DNA-binding molecules (13), and aptamer sensors (14). Recently, our laboratory applied this DNA force sensor concept to ''single-molecule cut and paste'' experiments (15) for the bottom-up assembly of nanoparticles (16) and for single-molecule fluorescence applications (17). For many of the abovementioned applications, it is insightful, if not critical, to know what forces a given DNA duplex may withstand. In particular, such knowledge would make it possible not only to predict, tune, and analyze DNA force sensor experiments, but also to design more stable DNA scaffolds.

The elastic response and force-dependent dissociation rate of DNA duplexes has been extensively studied in micromanipulation experiments employing atomic force microscopy (AFM) (18,19), magnetic beads (20), glass microneedles (21), and optical tweezers (22,23). Here, we discuss the stretching of dsDNA along its axis (''shear geometry'') only in contrast to the gradual unzipping of DNA perpendicular to its axis (''unzip geometry''). Stretching a DNA duplex with thousands of basepairs along its axis results in an elastic response with a distinct force plateau at 60–65 pN (18,21,22). During this elongation at almost constant force, the DNA molecule stretches up to a factor of 1.7 of its contour length. This behavior is highly reproducible, independent of the stretching velocity, and commonly attributed to a highly cooperative conversion from regular B-DNA into an overstretched conformation called S-DNA (24–27). On the contrary, Rouzina and Bloomfield (28), as well as Piana (29), argue that S-DNA is not a distinct conformation of the polymer, but simply the melting of the dsDNA into two single strands. However, not only does the B-S transition appear to be too cooperative for a common melting process, but it has been shown also that dsDNA remains stable at forces significantly higher than 65 pN (30), with an elastic response distinct from one single-stranded DNA (ssDNA) polymer or two parallel ssDNA polymers (24). Further support for S-DNA being a distinct conformation is provided by the experimental observation of a second transition in the range 150–200 pN, which is thought to be the final melting transition (18,24) instead of the B-S transition. Based on the assumption that S-DNA is in fact a distinct conformation, several recent theoretical studies have modeled the elongation of DNA duplexes applying three-state (B-DNA, S-DNA, and ssDNA) equilibrium approaches (24,25). These studies concluded that S-DNA is the thermodynamically preferred and stable state for forces between 65 and 130 pN.

Individual basepairing interactions are relatively weak (free energy ~1–3 k_BT), and thermal fluctuations cause opening (''breathing'') of the DNA duplex from its ends,

Submitted July 3, 2009, and accepted for publication September 21, 2009.

*Correspondence: dominik.ho@web.de

Julia L. Zimmermann's present address is Max-Planck-Institut für extraterrestrische Physik, Giessenbachstrasse, 85748 Garching, Germany.

Editor: David P. Millar.

0006-3495/09/12/3158/10 $2.00

doi: 10.1016/j.bpj.2009.09.040

as well as the formation of bubbles, which are regions of ssDNA (opened basepairs) between regions of dsDNA. The shorter the DNA duplex, the more likely it is that all basepairs open up for an instant and the two strands separate even at forces well below 130 pN. For DNA duplexes tens of basepairs long, Strunz and colleagues (31) and Morfill and colleagues (32) observed strand separation at forces as low as 40–70 pN. Repeated measurements resulted in rupture-force distributions that were shifted to higher forces for higher separation velocities. From a theoretical point of view, this can be described as a thermally driven escape process from a free-energy potential and has typically been discussed within the framework of the Bell-Evans model. Herein, the trapping potential is assumed to be a one-dimensional harmonic free-energy potential, and strand separation is treated as the crossing of an energy barrier according to a time dependence similar to that described by the Arrhenius law (31–35). Application of a force tilts the energy landscape, reduces the energy barrier proportional to the applied force, and therefore increases the dissociation rate of the DNA duplex. According to the experimental data, the model predicts higher rupture forces for higher separation velocities (33). Although the experiments are explained quite well by the Bell-Evans model, that model does not allow for the prediction of rupture forces for a given DNA duplex sequence and separation velocity. Apart from the Bell-Evans theory, molecular dynamics simulations, employing force fields and initial molecular structures, provided insight into the DNA separation process. Unfortunately, these simulations cost a significant amount of computation time, such that the timescales accessible for in silico experiments are much shorter than what is experimentally observable (26, 27). Therefore, it is apparent that a theory is needed to fill the gap between the Bell-Evans model, which is too simplistic, and the detailed molecular dynamics simulations, with which mechanics can currently be simulated on very short timescales only.

In this work, we develop a model that describes and predicts the DNA duplex rupture forces for any given sequence and experimentally accessible pulling velocities. To be specific, we derive the dissociation rate as a function of the applied force based on a combination of recent work on DNA equilibrium theory and the canonical transition state theory. On this basis, we calculate the force-extension traces and the rupture-force distribution for a 20- and a 30-basepair-long DNA duplex and compare the obtained results to actual single-molecule experimental data (Fig 1 *a* and *b*). Further, we are able to show that for the description of double stranded DNA separation kinetics, our model is a significant refinement of the conventionally used Bell-Evans model.

RESULTS AND DISCUSSION

The result of this work is a theoretical model that predicts the rupture force of dsDNA tens of basepairs long as it is applied

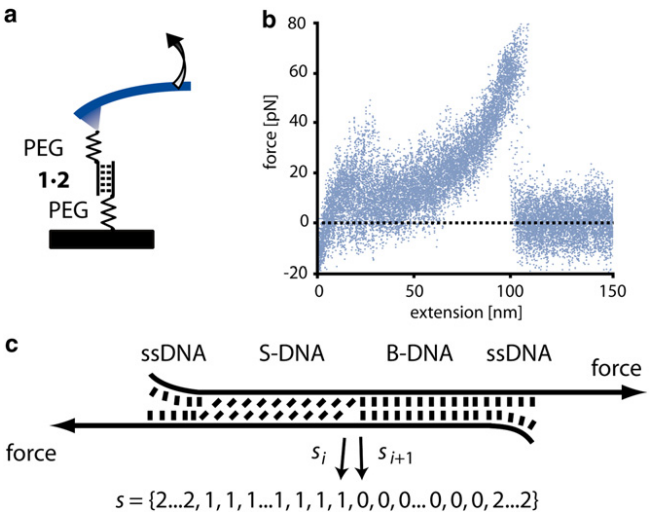

FIGURE 1 (*a*) Schematic of a single-molecule DNA stretching experiment. The 5′ ends of a short, double-stranded DNA duplex are attached to a surface and an atomic force microscope cantilever via elastic poly(ethylene glycol) (PEG) polymers. Separation of the substrate and the cantilever at constant velocity leads to an increasing end-to-end distance and thus to an increasing force. (*b*) Superposition of 20 experimentally obtained force-extension traces obtained from the same 30-basepair 1 × 2 DNA duplex with a separation velocity of 1 μm/s. The duplex dissociates at ~60–65 pN. (*c*) Schematic of the three-state model. Every basepair of the DNA duplex appears in one of three states: B-DNA, S-DNA, or single-stranded DNA. Every state s of an N-basepair-long DNA may thus be represented by a list of length N with entries 0 (B-DNA), 1 (S-DNA), and 2 (ssDNA) for every basepair.

in a DNA force sensor, in DNA nanostructure, and in DNA computing applications. For this purpose, we first set up a three-state equilibrium model similar to a model used previously to describe the force-extension traces of long dsDNA (24). Second, we apply the canonical transition state theory to this equilibrium model, which in turn permits calculation of the rate of duplex dissociation at a given force f. Theoretical results are compared to actual AFM experiments on the 20-basepair (1 × 2) and the 30-basepair (1 × 3) duplex. Details about DNA oligomers 1–3, as well as about the experimental procedures, are provided in the Supporting Material.

Equilibrium theory

Analogous to the Bragg-Zimm theory (36) and a variety of work published recently on the force-induced opening of dsDNA in unzip geometry (37–39,40) and shear geometry (28), as well as the opening of coiled coils (41,42), we calculate the equilibrium free energy of DNA duplexes: The DNA duplex is described as a one-dimensional polymer for which every basepair i is considered to be present in one of three discrete states, namely, regular B-DNA ($s_i = 0$), overstretched S-DNA ($s_i = 1$), and single-stranded DNA ($s_i = 2$) conformations. Thus, any configuration s of an N-basepair DNA duplex is represented by an N-tupel,

$$s = (s_1, s_2, \ldots, s_N), \quad (1)$$

where the ith entry represents the state of the ith basepair, counting from the 5′ to the 3′ end.

Two contributions to the free energy/basepair are taken into account: w, the elastic free energy/basepair at a given force f, and j, the basepairing free energy we derive from a nearest-neighbor model and assume to be independent of the applied force. The free energy of the ith basepair can be determined by

$$g_{s_i,s_{i+1}}(f) = w_{s_i,s_{i+1}}(f) + j_{s_i,s_{i+1}}. \quad (2)$$

These two energy contributions yield the total free energy, $G_{\text{total}}(s,f)$, for any possible configuration s at any force f,

$$G_{\text{total}}(s,f) = \sum_{i=1}^{N-1} g_{s_i,s_{i+1}}(f) + w_{s_N}(f), \quad (3)$$

where the term $w_{s_N}(f)$ corresponds to the Nth basepair, which does not have a next neighbor it can interact with such that $j_{s_N,s_{N+1}} = 0$.

Elastic energy

The free energies due to the elastic deformation of the three different DNA conformations are obtained by simply integrating their extensions with respect to the force:

$$w(f) = -\int_0^f x(f')df'. \quad (4)$$

Phenomenological polymer extension models reproduce the force-extension traces well (see Fig. 2 *a*). In the Supporting Material, we derive the elastic free energy/basepair from such polymer extension models for B-DNA (w_{B}), S-DNA (w_{S}), and ssDNA (w_{ss}) explicitly. Assuming an average basepairing energy of 2.4 $k_{\text{B}}T$, as is the case for the 1 × 2 and 1 × 3 DNA duplexes (Fig. 2 *b*), which DNA configuration is most favorable for forces between 0 and 200 pN? B-DNA remains thermodynamically stable for forces <60 pN. S-DNA is stable between 60 and ~130 pN and ssDNA is the energetically most favorable state at forces >130 pN. Since we employ a nearest-neighbor model to calculate the partition sum of the system, it is convenient to represent the free energy due to the elastic behavior of DNA in a 3 × 3 matrix form,

$$w_{s_i,s_{i+1}}(f) = \begin{bmatrix} w_{\text{B}}(f) & w_{\text{B}}(f) & w_{\text{B}}(f) \\ w_{\text{S}}(f) & w_{\text{S}}(f) & w_{\text{S}}(f) \\ w_{\text{ss}}(f) & w_{\text{ss}}(f) & w_{\text{ss}}(f) \end{bmatrix}, \quad (5)$$

where the rows correspond to the state of basepair i and the columns to the state of basepair $i + 1$. Thus, in our model, the elastic free energy of basepair i is independent of the state of basepair $i + 1$.

Interaction free energy

It has been observed in experiments that the stability of a given basepair depends not only on whether the basepair itself is A·T or G·C, but also on the identity and orientation of adjacent basepairs, presumably due to the differences in free energy for the different possible stacking interactions (43). In our model, we employ the nearest-neighbor model of SantaLucia, which takes these experimental observations into account (44). The stacking free energy between each basepair i and $i + 1$ is given by the constant J_i in case both are either B-DNA or S-DNA. Although the stacking free energies for B-DNA and S-DNA are independent parameters, for simplicity, we assume them to be identical.

In addition, the boundaries between regions of different states are associated with energy penalties. $C_{\text{B-S}}$ is the energy cost associated with a boundary between B-DNA and S-DNA regions. Cluzel and colleagues estimated the B-S boundary energy from the cooperativity of the B-S transition to be close to 3.4 $k_{\text{B}}T$ (21). Unlike the non-nearest-neighbor models for which the latter value was derived, for

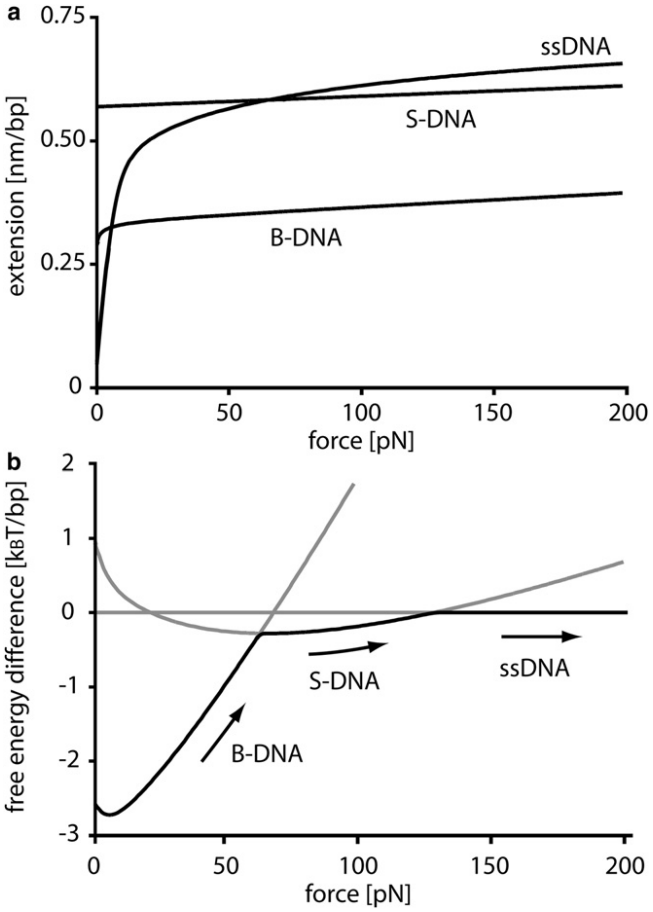

FIGURE 2 (*a*) Force-extension traces obtained from phenomenological models for the three different states of double-stranded DNA. (*b*) Corresponding free-energy difference/basepair between B-DNA and ssDNA as well as between S-DNA and ssDNA. A free-energy penalty of 2.4 $k_{\text{B}}T$, the average basepair free energy of the 1 × 2 and 1 × 3 DNA duplexes, is introduced to the free energy of ssDNA due to the loss of basepairing interactions. Highlighted in black is the state that is thermodynamically most favorable. The most favorable state is B-DNA for forces <60 pN, S-DNA for forces between 60 pN and 130 pN, and ssDNA for forces >130 pN.

our nearest-neighbor model, the total energy penalty is given by C_{B-S} along with the loss of one additional base-stacking interaction. The average energy lost in base-stacking interaction is 2.4 k_BT for the 1 × 2 as well as the 1 × 3 duplex, which is why we set C_{B-S} to 2.2 k_BT (half a base-stacking interaction free energy subtracted from each boundary).

Furthermore, the boundaries between double-stranded and between single-stranded regions of DNA are associated with the free-energy cost, C_{ds-ss}. According to SantaLucia (44) this value is close to 1 k_BT. For any given state s, there are always two boundaries at each side of the dsDNA region and, therefore, the parameter C_{ds-ss} has an impact only on the likelihood of bubbles. Within polymer theory, the latter are commonly referred to as loops. Since bubbles come along with additional degrees of freedom, polymer theory predicts an entropic energy contribution proportional to the logarithm of the bubble size, which favors the creation of bubbles:

$$\Delta G_{loop}(n_{loop}) = k_BT \ln n_{loop}^{-c}, \tag{6}$$

where n_{loop} is the number of opened basepairs within the bubble and c is the loop exponent. The value of the loop exponent is $c = 3/2$ for an ideal loop and $c = 2.1$ for a self-avoiding loop (45). The exact value of c for dsDNA is still under debate. Recent theoretical calculations by Einert and colleagues imply that data for long dsDNA is best fit by setting $c = 0$, which may be explained by the fact that DNA contains a significant numbers of nicks. Such a long-range interaction cannot be implemented into our nearest-neighbor model. Therefore, we simply chose the parameter such that theory agreed best with actual experiments and estimated a value of $-0.25\ k_BT$ for C_{ds-ss}, corresponding to an average bubble size of 4 basepairs. Note that the theoretical predictions (46–48) regarding longer-range entropic contribution to partially melted DNA are in agreement with experimental data obtained by Altan and colleagues (49). Based on Förster energy transfer measurements on tracts of A·T basepairs, they argue that initiating a bubble requires a free energy much larger than k_BT, whereas extending this bubble requires only free energies in the range 0.05–1.0 k_BT/basepair.

In matrix form, the interaction free-energy contributions based on the SantaLucia nearest-neighbor model and the boundary free-energy penalties are

$$j_{s_i,s_{i+1}} = \begin{bmatrix} -J_i & C_{B-S} & C_{ds-ss} \\ C_{B\text{-}S} & -J_i & C_{ds-ss} \\ C_{ds-ss} & C_{ds-ss} & 0 \end{bmatrix}, \tag{7}$$

where the rows correspond to the state of basepair i and the columns to the state of basepair $i + 1$. Thus, if basepair i and basepair $i + 1$ are B-DNA then an energy gain of J_i is introduced to the base-stacking interaction. The same is true for two adjacent S-DNA basepairs. Boundaries between basepairs are associated with an energy penalty C_{B-S} or C_{ds-ss}, where C_{B-S} is 3.4 k_BT and C_{ds-ss} is $-0.25\ k_BT$, as discussed above.

Partition sum

From the total free energy, G_{total} (Eqs. 2 and 3), of each possible state s, we calculate the partition sum, which in turn allows for determination of the force-extension trace and the likelihood of the states s.

$$\begin{aligned} Z(f) &= \sum_s P(s,f) = \sum_s \exp(-G_{total}(s,f)) = \sum_s \prod_{i=1}^{N} \exp\left(-g_{s_i,s_{i+1}}(f)\right) \\ &= \sum_{\substack{\text{all matrix} \\ \text{elements}}} \prod_{i=1}^{N} \begin{bmatrix} \exp(-w_B(f) + J_i) & \exp(-w_B(f) - C_{B-S}) & \exp(-w_B(f) - C_{ds-ss}) \\ \exp(-w_S(f) - C_{B-S}) & \exp(-w_S(f) + J_i) & \exp(-w_S(f) - C_{ds-ss}) \\ \exp(-w_{ss}(f) - C_{ds-ss}) & \exp(-w_{ss}(f) - C_{ds-ss}) & \exp(-w_{ss}(f)) \end{bmatrix}. \end{aligned} \tag{8}$$

Thus, the partition sum may be considered as the sum over all matrix elements of the product of N 3 × 3 matrices (50). Thereby, the ith matrix of the N matrices represents the ith basepair containing nine entries. Each entry represents the Boltzmann factor of one of the nine possible combinations of states that basepair i and basepair $i + 1$ may adopt. We make two corrections to Eq. 8, which we explain in more detail in the Supporting Material. First, we introduce two additional basepairs at $i = 0$ and $i = N + 1$, which are single-stranded. This takes care of the boundary conditions at the end of the DNA duplex. Second, we do not count the states for which two or fewer basepairs remain. These states, as we discuss in more detail in the next section, correspond to already separated strands.

Stretching curves

From the partition sum of our model, we derive the force-extension trace for a given sequence and compare it to experimentally obtained data. The equilibrium force-extension trace follows directly from the derivative of the partition sum with respect to the force (51):

$$x_{DNA\ duplex}(f) = k_BT \frac{\partial \ln Z(f)}{\partial f}. \tag{9}$$

The AFM experiments were prepared according to the Materials and Methods section (see Supporting Material) and are

schematically shown in Fig. 1 *a*. The two complementary single strands 1 and 2 were coupled to the cantilever tip and a substrate via long poly(ethylene glycol) linkers (5 kDa). In a typical experiment, the tip is brought into contact with the glass slide, and the two complementary strands hybridize and form the 1 × 2 duplex. Upon retraction at constant velocity, the PEG spacer and dsDNA elongates, building up an increasing force until the duplex dissociates. Fig. 3 shows an average of 20 force-extension curves. Experimentally, one measures the elasticity of a chain of four elements: the dsDNA duplex, the PEG linker, the ssDNA linker, and the cantilever. The force-extension trace is a superposition of the extension profile of all four of them:

$$x(f) = x_{\text{DNA duplex}}(f) + x_{\text{DNA linker}}(f) + x_{\text{PEG linker}}(f) + x_{\text{cantilever}}(f), \quad (10)$$

where $x_{\text{DNA duplex}}$ is specified by Eq. 9 and $x_{\text{cantilever}}$ is the deflection of the cantilever, which is proportional to the cantilever stiffness, $k_{\text{cantilever}} = 8$ pN/nm . The polymer models from which $x_{\text{DNA linker}}$ and $x_{\text{PEG linker}}$ are derived are described in the Supporting Material. We used the number of monomers within the PEG polymer, N_{PEG}, as a fitting parameter, since PEG polymers are typically synthesized with a rather broad size distribution (32). Fitting of the whole system resulted in a monomer number of 255, which agrees well with the expected monomer number of 227 for a total PEG linker with a molecular mass of 10 kDa.

Fig. 3 shows that the theory fits the experimental data very well for forces >30 pN. However, for lower forces, the theoretical fit underestimates the experimentally obtained forces. The 10- to 15-pN plateau between 10 and 20 nm extension at the beginning of the stretching curve is typical for a DNA desorption process from a surface (52). For higher extensions, we attribute this discrepancy between theory and experiment to nonspecific interactions and entanglement of the strands with each other on the surface. This is entirely possible, since the contour length of the surface-anchored DNA strands is >50 nm and the spacing between two of these strands is typically ~10 nm (12,15,16).

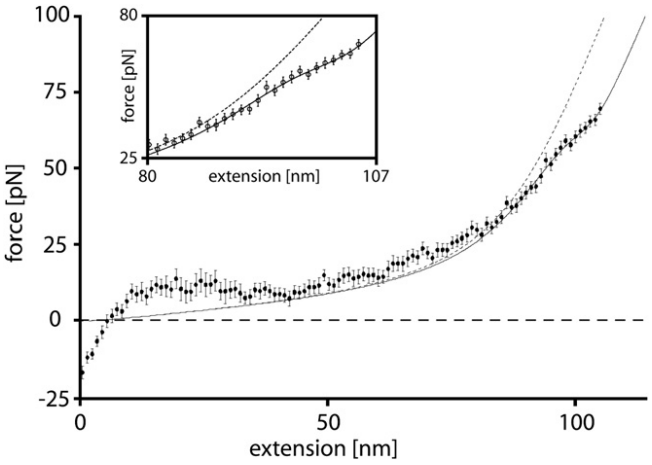

FIGURE 3 Force-extension data of short, double-stranded DNA attached to a surface and an atomic force microscope cantilever via a 5-kDa poly(ethylene glycol) linker for each strand. Data for 20 pulling experiments at a separation velocity of 1 μm/s was binned into 1-pN intervals and averaged (*circles*). The solid line is the corresponding fit of the model presented here. The dashed line represents the fit in the case where the DNA duplex remains in its canonical B-form. At <30 pN, the fit underestimates forces, an observation that we attribute to nonspecific interactions and entanglements with neighboring constructs on the surface. (*Inset*) For forces >30 pN, theory and experimental data agree within the experimental error.

Canonical transition state theory

For an average basepairing free energy of 2.4 k_BT, dsDNA is thermodynamically stable for forces <130 pN (18,24,25). Still, Strunz and colleagues (31) and Morfill and colleagues (32) observed bond breakage at forces between 40 and 70 pN for 20- and 30-basepair dsDNA. They attributed this effect to thermal fluctuations like the opening or ''breathing'' of dsDNA from its ends, and to the formation of bubbles, which are regions of ssDNA between regions of dsDNA. Some of these fluctuations are so large that the whole duplex opens and the two strands separate.

Such a thermally activated escape process can be described by canonical transition state theory (53,54). This theory is purely classical and based on two assumptions: 1), the bond is trapped in a free-energy potential and thermodynamic equilibrium prevails; and 2), once the system has crossed a dividing surface in state space, i.e., the transition state, it will not return to the metastable state. The rate of escape follows directly from the flux through this dividing surface.

In the next paragraphs, we first define the dividing surface, i.e., the transition states, for the dsDNA equilibrium model described in the previous section. We then calculate the equilibrium flux through this dividing surface and thus obtain the rate of escape. We explicitly calculate the rupture-force distributions for the two DNA duplexes 1 × 2 and 1 × 3 and compare them to experimental data. At the end of this section, we discuss why the canonical transition state theory is an appropriate description of our system.

Transition states

In the case of an N-basepair-long DNA duplex, the free-energy potential is N-dimensional and the corresponding coordinate is the state s. A dividing surface between the reactants (dsDNA) and the products (ssDNA) has to be chosen such that once the system has crossed this surface, the chances of recrossing are negligible. In our system, this dividing surface is spanned by the states s_{tst}, for which there is exactly one base-stacking interaction left. One base-stacking interaction corresponds to two adjacent B-DNA or S-DNA basepairs. Therefore, there are $2(N - 1)$ distinct states through which the reaction may occur. For illustrative purposes we can collapse the free-energy landscape onto one coordinate: n, the number of remaining basepairs. Within this picture

(Fig. S1 in the Supporting Material), we identify the transition state as $n_{tst} = 2$. If another basepair opens up, the two DNA strands dissociate, i.e., the polymers will immediately reduce their end-to-end distance and reannealing of the two strands is literally impossible.

Equilibrium flux

The rate of escape is given by the equilibrium flux through the transition states, s_{tst}, in the direction of the product (two separate strands). The flux is essentially twice the basepair opening rate (either one of the two remaining basepairs may open), which, for simplicity, we assume to be the same for all s_{tst}. This allows us to use the collapsed free-energy landscape with only one reaction coordinate, n, the number of remaining basepairs. The equilibrium flux through the transition states, s_{tst}, becomes the probability that the system will be in the collapsed transition state, n_{tst}, multiplied by $.n_+$, twice the basepair opening rate. The result for the rate of escape at a given force f is

$$k(f) = \langle \delta[n - n_{tst}]n^{\cdot}{}_{+} \rangle_{equilibrium} = \frac{1}{Z(f)} \sum_{S_{tsT}} n^{\cdot}{}_{+} \exp(-\Delta G_{totla}(s_{tst}, f)). \quad (11)$$

The calculations are shown explicitly in the Supporting Material. To our knowledge, the basepair opening rate of a single basepair-stacking interaction has never been determined experimentally. From the literature, we estimate the basepair opening rate at the ends of dsDNA to be between 10^3 s^{-1} and 10^9 s^{-1}: Bockelmann and colleagues performed optical tweezers measurements from which we estimate an opening rate of at least 10^3 s^{-1} (55). Fluorescence measurements investigating the end fraying of the dsDNA could not resolve any basepair opening rates on timescales $<10^9$ s^{-1} (56). In their report discussing the unzipping of DNA, Cocco and colleagues assumed a value of 10^8 s^{-1} (24), and nuclear magnetic resonance amino proton exchange studies yielded rates in the order of 10^7 s^{-1} (57). For a basepair opening rate of $.n_+ = 5 \times 10^8$ s^{-1} our theory agrees very well with the experimentally determined rupture forces (32). Note that the rate depends on the applied force, but since the force dependence is rather weak (40), we assume the rate to be constant. In principle, all calculations could also be performed with force- and sequence-dependent rates.

Rupture forces

Based on the canonical transition state theory, we derive the rupture-force distributions obtained for two given sequences, namely, the 1×2 as well as the 1×3 DNA duplex, and different pulling velocities, v. In experiments, we control the separation velocity between cantilever and substrate. Thus, the end-to-end distance, x, of a system composed of dsDNA, ssDNA linker, PEG linker, and AFM cantilever continuously increases in time with constant velocity v. From the end-to-end distance, x, we derive the force acting along this chain of elastic elements. The force in turn allows us to determine the escape rate, k, as a function of time. The resulting differential equation describes the decay from a metastable state, N_{duplex}, with a time-dependent rate (33):

$$dN_{duplex} = N_{duplex} k(t) dt, \quad (12)$$

where $k(t) = k(f(v \times t))$, and $f(x)$ follows from Eq. 10.

For both the 1×2 and the 1×3 DNA duplexes and separation velocities between 10 nm/s and 10 μm/s, we numerically solved this differential equation. The obtained rupture-force distributions are shown in Fig. 4 *a*. A striking finding was that the rupture-force distribution of the 1×2 DNA duplex broadens with increasing force loading rate, whereas the rupture-force distribution of the 1×3 DNA duplex is almost independent of this parameter. We attribute this behavior to the crossing of the B-S transition at ~65 pN, which is only observed for the 1×2 DNA duplex for the experimentally applied force loading rates. For forces >65 pN, and thus above the B-S transition, the slope of the force-extension profile increases significantly, resulting in a wider distribution of the obtained rupture forces. To verify that the broadening of the rupture-force distribution is indeed due to the crossing of the B-S transition, we calculated the 1×3 DNA duplex rupture-force distributions for force loading rates higher than those achievable by experiment. In agreement with this interpretation, the rupture-force distribution of the 1×3 DNA duplex broadens correspondingly for rupture forces above the B-S transition (data not shown). The experimentally obtained rupture-force distributions are further broadened by the thermal and instrumentation noise introduced to the cantilever. According to Morfill and colleagues (32), the total experimental noise was Gaussian, with a width of 4.7 pN. Therefore, to compare theory with experiment, we convolved the theoretically obtained rupture-force distribution with such a Gaussian distribution (Fig. 4 *b*). From these distributions, we determined the most probable rupture force via a Gaussian fit. Fig. 4 *c* shows this fit plotted against the corresponding most probable force loading rate for the theoretical predictions and the experimental data. The theory reproduces the data quite well within the experimental error.

Systematic errors on the experimental side are mainly due to errors of the cantilever calibration, which introduces an error of up to 5–10% (58). The presented AFM force data were obtained with two different AFM cantilever tips, one for all of the 1×2 DNA duplex data and one for all of the 1×3 DNA duplex data. Therefore, the set of most probable rupture forces may be shifted by up to 5–10%. Further, a small error is introduced due to pulling angles that are not perpendicular to the substrate, which is typically in the order of 2% (59).

Systematic errors on the theoretical side include the following: We chose the basepair opening rate for the B-DNA and the S-DNA conformations to be identical,

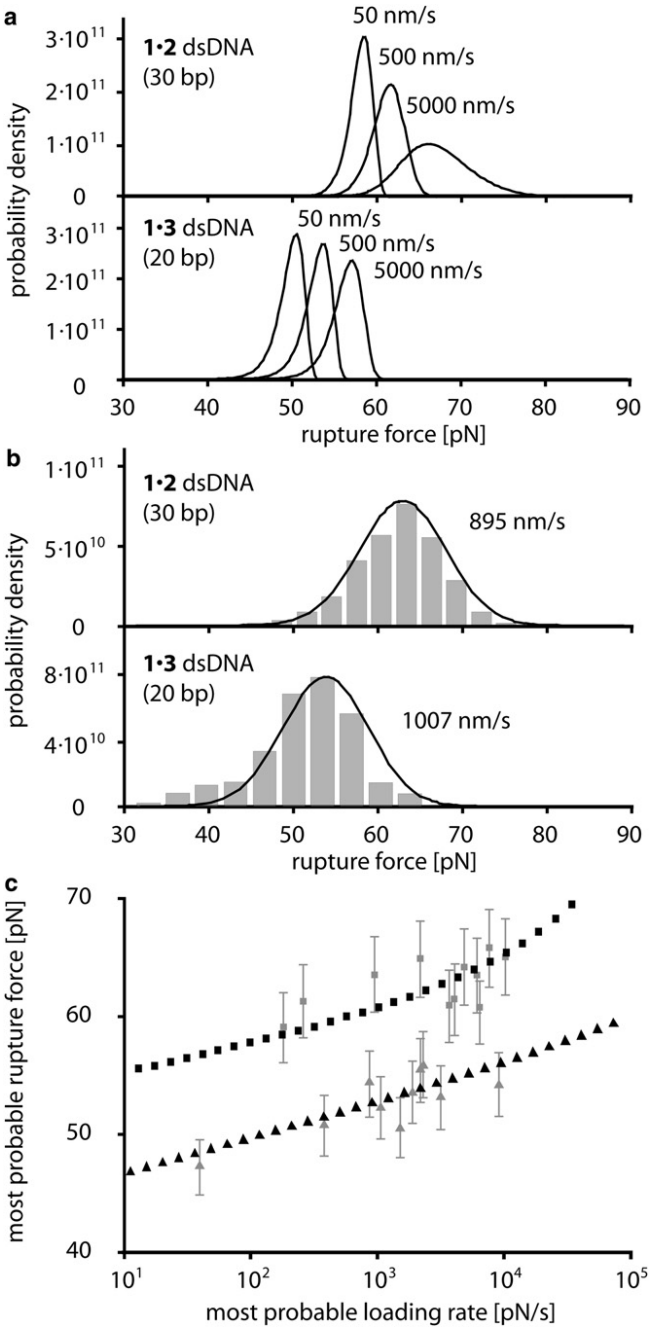

FIGURE 4 (*a*) Calculated rupture-force distribution for the 1 × 2 and the 1 × 3 duplex for 50, 500, and 5000 nm/s pulling velocity. (*b*) Comparison of the experimental (*gray bars*) and calculated (*lines*) rupture-force distribution for the 1 × 2 and 1 × 3 duplex at 895 nm/s and 1007 nm/s, respectively. The calculated rupture-force distributions were convolved with a Gaussian cantilever detection noise of 4.7 pN. (*c*) Comparison of the experimental and calculated most probable rupture forces for different most probable loading rates. The gray data points refer to the experimental data and the black data points to the theory data. Squares refer to the 30-basepair DNA 1 × 2 duplex and triangles to the 20-basepair 1 × 3 duplex.

although they are completely independent parameters. Further, the S-DNA polymer elasticity model is very crude for several other reasons. First, according to the methods of Cocco and colleagues (24), we approximated the force-extension curve of S-DNA to be linear. Second, the basepair free energy was assumed to be identical to the B-DNA interaction. Furthermore, there are most likely two types of S-DNA, depending on whether the force is applied at the 5′ or the 3′ ends of the dsDNA (26,60). Finally, the nearest-neighbor model does not account for long-range interactions, as they are experimentally observed in DNA bubbles, which has a strong influence on the boundary energy, C_{ss-ds}, and thus on how cooperative DNA strand separation occurs. From our calculations, we observed that a more cooperative transition between single-stranded and double-stranded DNA, i.e., a larger value for C_{ss-ds}, leads to a reduced DNA duplex length dependence on the rupture-force distribution. For values of C_{ss-ds} in the range of a few k_BT, the rupture-force distributions of the 1 × 2 and the 1 × 3 DNA duplexes are almost superimposed.

Thermodynamic equilibrium prevails

To appropriately describe the separation of dsDNA employing canonical transition state theory, thermodynamic equilibrium must prevail within the binding potential (54). Two scenarios would contradict such an assumption: Either the changes of state occur on timescales equal to or slower than the rate of escape or, to reach the transition states, an intermediate free-energy barrier needs to be crossed. In the Supporting Material, we discuss these scenarios and conclude that, for the experimentally observed force range between 0 and 100 pN, canonical transition state theory is applicable.

Comparison to the Bell-Evans model

Typically, the rupture of molecular bonds is described employing the Bell-Evans model (34). Like our model, the latter is based on transition state theory assuming a thermally activated escape from a free-energy potential. In this section, we discuss the differences between the Bell-Evans model and our model, how they compare with each other, and why our model is a significant refinement for the description of force-induced separation of short dsDNA.

The main difference between the two models lies within the approximation of the Bell-Evans trapping potential as a harmonic free-energy landscape, which is simply tilted by an external force. As a result of this approximation, the free-energy difference between the equilibrium and the transition state decreases in proportion to the applied force:

$$\Delta G(f) = \Delta G_0 - f \times x_{tst}, \tag{13}$$

where ΔG_0 is the free-energy difference at zero force and x_{tst} is a force-independent distance between the equilibrium state and the transition state. The force-dependent rate is given by

$$k(f) = k_0 \times \exp(-\Delta G(f)), \tag{14}$$

where k_0 is the natural attempt frequency of the molecular bond. In our work, we explicitly model the evolution of

the DNA duplex free-energy landscape with increasing force. To see what differences arise in comparison to the Bell-Evans approach, we calculate an effective barrier height of the transition state from the sum of the Boltzmann probabilities for the states, s_{tst}.

$$\Delta G(f) = -\ln\left(\sum_{s_{tst}} \frac{\exp(-\Delta G_{total}(s_{tst},f))}{Z}\right). \quad (15)$$

As shown in Fig. 5 *a*, the force-dependent evolution of the effective barrier height according to Eq. 15 does exhibit significant differences from the Bell-Evans approach (Eq. 13). Below 10 pN the free-energy difference between the equilibrium state and the transition state increases with applied force. This is in agreement with Fig. 2 *b*, which shows that for increasing applied force the absolute value of the free-energy difference per basepair between B-DNA (equilibrium state for low forces) and ssDNA (transition state) increases for forces <10 pN before it decreases for forces >10 pN. The microscopic origin of this effect is that although the contour length of ssDNA is longer compared to B-DNA, the contour length of ssDNA projected onto the direction of applied force, i.e., the end-to-end distance, is shorter for low forces due to its much shorter persistence length. Thus, low forces stabilize DNA duplexes, a result that was previously shown experimentally (61,62) and discussed theoretically (28,63). Between 10 and 60 pN, the free energy decreases roughly proportionally to the applied force, *f*. Above 65 pN, i.e., above the B-S transition, the energy decreases linearly again, yet with a smaller slope. Taking the negative derivative of the calculated free-energy barrier height with respect to the force yields an effective distance between the equilibrium state and the transition state, x_{tst}:

$$x_{tst} = -\frac{\partial \Delta G(f)}{\partial f}.$$

x_{tst} does exhibit a rather odd force dependency (Fig. 5 *b*), which we explain according to geometrical considerations: Strunz and colleagues estimated an upper limit for x_{tst} assuming that the equilibrium state is B-DNA with a contour length of 0.34 nm/basepair and that the transition state is all ssDNA (apart from two residual basepairs), with a contour length of ~0.7 nm/basepair (31). In the case of the 30-basepair 1 × 2 DNA duplex, this corresponds to a total length difference between these two states of ~10 nm, which is significantly larger than the corresponding values of x_{tst} obtained from our calculations, as well as those from actual experiments (31,32). Two effects contribute to this deviation. First, x_{tst} is the projection of the distance between the equilibrium state and the transition state onto the direction of applied force. Therefore, a more accurate estimate of x_{tst} is the difference in end-to-end distance according to our polymer models for B-DNA and ssDNA (Fig. 5 *b*). Second, within the range 60–65 pN, the equilibrium state switches

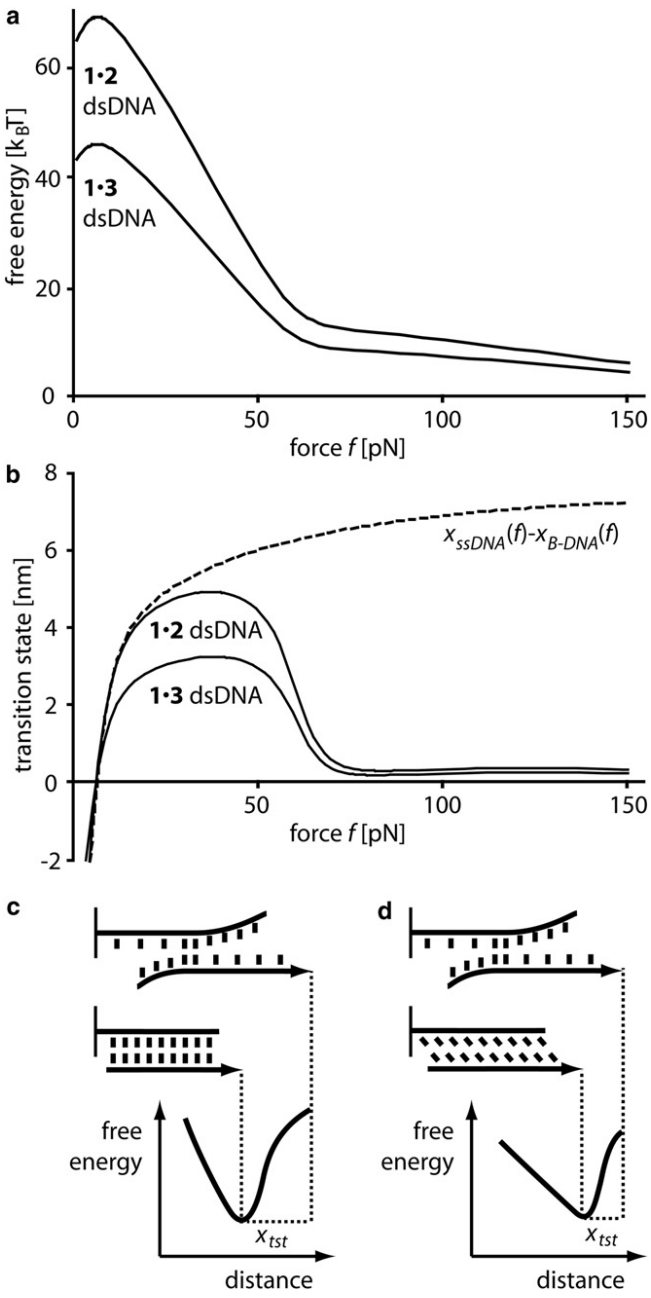

FIGURE 5 (*a*) Calculated effective barrier height, according to the standard Bell-Evans model. At forces between 10 and 50 pN, the free energy decreases proportionally to the applied force *f*. At forces >65 pN, when B-DNA is converted into S-DNA, the energy again decreases linearly, yet with a significantly smaller slope. (*b*) The negative derivative of the force versus free energy profile yields x_{tst}, the effective distance between the equilibrium state and the transition state. The dashed line represents the difference in end-to-end distance for B-DNA and ssDNA for the 1 × 2 DNA duplex as a function of force. (*c*) For forces <60 pN, x_{tst} reflects the increase in end-to-end distance from B-DNA to ssDNA. (*d*) For forces >65 pN, x_{tst} reflects the increase in end-to-end distance from S-DNA to ssDNA.

from a predominantly B-DNA duplex to a predominantly S-DNA duplex. The difference in end-to-end distance between the equilibrium state and the transition states is much smaller for an S-DNA duplex than for a B-DNA

duplex (Fig. 5 *c*). Consequently, x_{tst} decreases to a fraction of a nanometer during the B-S transition.

Due to the force dependence of x_{tst}, we conclude that the standard Bell-Evans model is only a good description of the force-induced separation of DNA duplexes for forces between 10 and 50 pN and between 65 and ~100 pN. However, for both scenarios, a different set of free-energy landscape parameters, i.e., free-energy barrier at zero force and distance between equilibrium and transition state, need to be chosen. Our refined model, on the other hand, provides a reliable description for forces between 0 and ~100 pN. Our results are in agreement with recent literature. Hyeon and Thirumalai (64) argue that x_{tst} changes considerably if the molecular bond is soft or plastic, as is the case for dsDNA. Further, Dudko and colleagues (65) report that the position of the equilibrium state may depend on the applied force leading to a force dependence of the distance between the equilibrium state and the transition state and thus to a nonlinear dependence of the barrier height on the applied force.

CONCLUSION

The result of this work is a theoretical model that employs a combination of a three-state equilibrium model and the canonical transition state theory to describe the force-induced strand separation of dsDNA tens of basepairs long. The three-state equilibrium model serves as a basis for a free-energy trapping landscape. Double-strand separation occurs through transition states, which we identify as the states with two adjacent basepairs remaining, i.e., one remaining stacking interaction. We calculated the rate of escape as a function of force from the total flux through these transition states, assuming a basepair opening rate of 5×10^8 s^{-1}. The rate of escape in turn allowed us to explicitly calculate the rupture-force distribution for two DNA duplexes, 1×2 and 1×3. The theoretically obtained results and actual single-molecule atomic force microscopy experiments are in excellent agreement. We argue that in the case of the force-induced DNA strand separation, our model is a significant refinement of the Bell-Evans model and provides a reliable description for forces between 0 and 100 pN. In the future, we foresee this theory being applied to predict, tune, and analyze the behavior of DNA force sensors.

SUPPORTING MATERIAL

Methods and Materials and one figure are available at http://www.biophysj.org/biophysj/supplemental/S0006-3495(09)01524-0.

Financial support was provided by the Nanosystems Initiative Munich. D.H., P. S., and K. F. are grateful to the Elite Network of Bavaria (IDK-NBT) for a doctoral fellowship.

REFERENCES

1. Seeman, N. 2003. DNA in a material world. *Nature*. 421:427–431.
2. Martin, M. 2000. DNA handles for single molecule experiments. *Single Mol.* 1:139–144.
3. Essevaz-Roulet, B., U. Bockelmann, and F. Heslot. 1997. Mechanical separation of the complementary strands of DNA. *Proc. Natl. Acad. Sci. USA*. 94:11935–11940.
4. Yan, H. 2003. DNA-templated self-assembly of protein arrays and highly conductive nanowires. *Science*. 301:1882–1884.
5. Cohen, J. D., J. P. Sadowski, and P. B. Dervan. 2007. Addressing single molecules on DNA nanostructures. *Angew. Chem. Int. Ed.* 46:7956–7959.
6. Winfree, E., F. Liu, L. A. Wenzler, and N. C. Seeman. 1998. Design and self-assembly of two-dimensional DNA crystals. *Nature*. 394:539–544.
7. Shawn, M. D., H. Dietz, T. Liedl, B. Högberg, F. Graf, et al. 2009. Self-assembly of DNA into nanoscale three-dimensional shapes. *Nature*. 459:414–418.
8. Liu, Q., L. Wang, A. Frutos, A. Condon, R. Corn, et al. 2000. DNA computing on surfaces. *Nature*. 403:175–179.
9. Albrecht, C., K. Blank, M. Lalic-Multhaler, S. Hirler, T. Mai, et al. 2003. DNA: a programmable force sensor. *Science*. 301:367–370.
10. Blank, K., A. Lankenau, T. Mai, S. Schiffmann, I. Gilbert, et al. 2004. Double-chip protein arrays: force-based multiplex sandwich immunoassays with increased specificity. *Anal. Bioanal. Chem.* 379:974–981.
11. Blank, K., T. Mai, I. Gilbert, S. Schiffmann, J. Rankl, et al. 2003. A force-based protein biochip. *Proc. Natl. Acad. Sci. USA*. 100: 11356–11360.
12. Dose, C., D. Ho, H. E. Gaub, P. B. Dervan, and C. H. Albrecht. 2007. Recognition of ''mirror-image'' DNA by small molecules. *Angew. Chem.* 46:8384–8387.
13. Ho, D., C. Dose, C. H. Albrecht, P. Severin, K. Falter, et al. 2009. Quantitative detection of small molecule/DNA complexes employing a force-based and label-free DNA microarray. *Biophys. J.* 96:4661–4671.
14. Ho, D., K. Falter, P. Severin, and H. E. Gaub. 2009. DNA as a force sensor in an aptamer-based biochip for adenosine. *Anal. Chem.* 81:3159–3164.
15. Kufer, S. K., E. M. Puchner, H. Gumpp, T. Liedl, and H. E. Gaub. 2008. Single-molecule cut-and-paste surface assembly. *Science*. 319: 594–596.
16. Puchner, E., S. Kufer, M. Strackharn, S. Stahl, and H. E. Gaub. 2008. Nanoparticle self-assembly on a DNA-scaffold written by single-molecule cut-and-paste. *Nano Lett.* 8:3692–3695.
17. Kufer, S., M. Strackharn, S. Stahl, H. Gumpp, E. M. Puchner, et al. 2009. Optically monitoring the mechanical assembly of single molecules. *Nat. Nanotechnol.* 4:45–49.
18. Rief, M., H. Clausen-Schaumann, and H. E. Gaub. 1999. Sequence dependent mechanics of single DNA molecules. *Nat. Struct. Biol.* 6:346–349.
19. Cao, Y., T. Yoo, and H. Li. 2008. Single molecule force spectroscopy reveals engineered metal chelation is a general approach to enhance mechanical stability of proteins. *Proc. Natl. Acad. Sci. USA*. 105: 11152–11157.
20. Smith, S., L. Finzi, and C. Bustamante. 1992. Direct mechanical measurements of the elasticity of single DNA molecules by using magnetic beads. *Science*. 258:1122–1126.
21. Cluzel, P., A. Lebrun, C. Heller, R. Lavery, J. Viovy, et al. 1996. DNA: an extensible molecule. *Science*. 271:792–794.
22. Smith, S. B., Y. J. Cui, and C. Bustamante. 1996. Overstretching B-DNA: the elastic response of individual double-stranded and single-stranded DNA molecules. *Science*. 271:795–799.
23. Wang, M., H. Yin, R. Landick, J. Gelles, and S. M. Block. 2005. Stretching DNA with optical tweezers. *Biophys. J.* 72:1335–1346.
24. Cocco, S., J. Yan, J. Léger, D. Chatenay, and J. Marko. 2004. Overstretching and force-driven strand separation of double-helix DNA. *Phys. Rev. E Stat. Nonlin. Soft Matter Phys.* 70:011910.
25. Storm, C., and P. C. Nelson. 2003. Theory of high-force DNA stretching and overstretching. *Phys. Rev. E Stat. Nonlin. Soft Matter Phys.* 67:051906.

26. Lebrun, A., and R. Lavery. 1996. Modelling extreme stretching of DNA. *Nucleic Acids Res.* 24:2260–2267.
27. Konrad, M., and J. Bolonick. 1996. Molecular dynamics simulation of DNA stretching is consistent with the tension observed for extension and strand separation and predicts a novel ladder structure. *J. Am. Chem. Soc.* 118:10989–10994.
28. Rouzina, I., and V. A. Bloomfield. 2001. Force-induced melting of the DNA double helix 1. Thermodynamic analysis. *Biophys. J.* 80: 882–893.
29. Piana, S. 2005. Structure and energy of a DNA dodecamer under tensile load. *Nucleic Acids Res.* 33:7029–7038.
30. Clausen-Schaumann, H., M. Rief, C. Tolksdorf, and H. E. Gaub. 2000. Mechanical stability of single DNA molecules. *Biophys. J.* 78: 1997–2007.
31. Strunz, T., K. Oroszlan, R. Schäfer, and H. Güntherodt. 1999. Dynamic force spectroscopy of single DNA molecules. *Proc. Natl. Acad. Sci. USA.* 96:11277–11282.
32. Morfill, J., F. Kuhner, K. Blank, R. Lugmaier, J. Sedlmair, et al. 2007. B-S transition in short oligonucleotides. *Biophys. J.* 93:2400–2409.
33. Friedsam, C., A. K. Wehle, F. Kuhner, and H. E. Gaub. 2003. Dynamic single-molecule force spectroscopy: bond rupture analysis with variable spacer length. *J. Phys. Condens. Matter.* 15:S1709–S1723.
34. Evans, E., and K. Ritchie. 1997. Dynamic strength of molecular adhesion bonds. *Biophys. J.* 72:1541–1555.
35. Merkel, R., P. Nassoy, A. Leung, K. Ritchie, and E. Evans. 1999. Energy landscapes of receptor-ligand bonds explored with dynamic force spectroscopy. *Nature.* 397:50–53.
36. Oesterhelt, F., M. Rief, and H. E. Gaub. 1999. Single molecule force spectroscopy by AFM indicates helical structure of poly(ethyleneglycol) in water. *N.J. Phys.* 1:1–11.
37. Zimm, B. H., and J. K. Bragg. 1959. Theory of the phase transition between helix and random coil in polypeptide chains. *J. Chem. Phys.* 31:526–535.
38. Bockelmann, U., B. Essevaz-Roulet, and F. Heslot. 1997. Molecular stick-slip motion revealed by opening DNA with piconewton forces. *Phys. Rev. Lett.* 79:4489–4492.
39. Bockelmann, U., B. Essevaz-Roulet, and F. Heslot. 1998. DNA strand separation studied by single molecule force measurements. *Phys. Rev. E Stat. Phys. Plasmas Fluids Relat. Interdiscip. Topics.* 58:2386–2394.
40. Cocco, S., R. Monasson, and J. F. Marko. 2001. Force and kinetic barriers to unzipping of the DNA double helix. *Proc. Natl. Acad. Sci. USA.* 98:8608–8613.
41. Bornschloegl, T., and M. Rief. 2006. Single molecule unzipping of coiled coils: sequence resolved stability profiles. *Phys. Rev. Lett.* 96:118102.
42. Bornschloegl, T., and M. Rief. 2008. Single-molecule dynamics of mechanical coiled-coil unzipping. *Langmuir.* 24:1338–1342.
43. Gotoh, O., and Y. Tagashira. 1981. Stabilities of nearest-neighbor doublets in double-helical DNA determined by fitting calculated melting profiles to observed profiles. *Biopolymers.* 20:1033–1042.
44. SantaLucia, J. 1998. A unified view of polymer, dumbbell, and oligonucleotide DNA nearest-neighbor thermodynamics. *Proc. Natl. Acad. Sci. USA.* 95:1460–1465.
45. Kafri, Y., D. Mukamel, and L. Peliti. 2000. Why is the DNA denaturation transition first order? *Phys. Rev. Lett.* 85:4988.
46. Hanke, A., M. G. Ochoa, and R. Metzler. 2008. Denaturation transition of stretched DNA. *Phys. Rev. Lett.* 100:018106.
47. Kafri, Y., D. Mukamel, and L. Peliti. 2002. Melting and unzipping of DNA. *Eur. Phys. J. B.* 27:135–146.
48. Einert, T. R., P. Naeger, H. Orland, and R. R. Netz. 2008. Impact of loop statistics on the thermodynamics of RNA folding. *Phys. Rev. Lett.* 101:048103.
49. Altan-Bonnet, G., A. Libchaber, and O. Krichevsky. 2003. Bubble dynamics in double-stranded DNA. *Phys. Rev. Lett.* 90:138101.
50. Lifson, S. 1964. Partition functions of linear-chain molecules. *J. Chem. Phys.* 40:3705–3710.
51. Rubinstein, M., and R. H. Colby. 2003. Polymer Physics. Oxford University Press, Oxford, United Kingdom.
52. Kuhner, F., M. Erdmann, L. Sonnenberg, A. Serr, J. Morfill, et al. 2006. Friction of single polymers at surfaces. *Langmuir.* 22:11180–11186.
53. Polanyi, M., and E. Wigner. 1928. Regarding the interference of resonant oscillations as the cause of energy fluctuations and chemical reactions. *Z. Phys. Chem. Abt. A.* 139:439.
54. Hänggi, P., P. Talkner, and M. Borkovec. 1990. Reaction-rate theory: fifty years after Kramers. *Rev. Mod. Phys.* 62:251–342.
55. Bockelmann, U., P. Thomen, and F. Heslot. 2008. Dynamics of the DNA duplex formation studied by single molecule force measurements. *Biophys. J.* 87:3388–3396.
56. Andreatta, D., S. Sen, J. Lustres, S. Kovalenko, N. Ernsting, et al. 2006. Ultrafast dynamics in DNA: ''fraying'' at the end of the helix. *J. Am. Chem. Soc.* 128:6885–6892.
57. Guéron, M., and J. L. Leroy. 1995. Studies of base pair kinetics by NMR measurement of proton exchange. *Methods Enzymol.* 261: 383–413.
58. Butt, H. J., and M. Jaschke. 1995. Calculation of thermal noise in atomic-force microscopy. *Nanotechnology.* 6:1–7.
59. Kühner, F., M. Erdmann, and H. E. Gaub. 2006. Scaling exponent and Kuhn length of pinned polymers by single molecule force spectroscopy. *Phys. Rev. Lett.* 97:218301.
60. Albrecht, C., G. Neuert, R. Lugmaier, and H. E. Gaub. 2008. Molecular force balance measurements reveal that double-stranded DNA unbinds under force in rate-dependent pathways. *Biophys. J.* 94:4766–4774.
61. Birshtein, T. M., and O. B. Ptitsyn. 1966. Conformations of Macromolecules. John Wiley, New York.
62. Rupprecht, A., J. Piskur, J. Schultz, L. Nordenskiöld, Z. Song, et al. 1994. Mechanochemical study of conformational transitions and melting of Li-, Na-, K-, and CsDNA fibres in water-ethanol solutions. *Biopolymers.* 34:897–920.
63. Buhot, A., and A. Halperin. 2000. Extension of rod-coil multiblock copolymers and the effect of the helix-coil transition. *Phys. Rev. Lett.* 84:2160–2163.
64. Hyeon, C., and D. Thirumalai. 2007. Measuring the energy landscape roughness and the transition state location of biomolecules using single molecule mechanical unfolding experiments. *J. Phys. Condens. Matter.* 19:113101.
65. Dudko, O. K., A. E. Filippov, J. Klafter, and M. Urbakh. 2003. Beyond the conventional description of dynamic force spectroscopy of adhesion bonds. *Proc. Natl. Acad. Sci. USA.* 100:11378–11381.

Biophysical Journal, Volume 97

Supporting Material

Force-driven separation of short double stranded DNA

Dominik Ho, Julia L. Zimmermann, Florian A. Dehmelt, Uta Steinbach, Matthias Erdmann, Philip Severin, Katja Falter, and Hermann E. Gaub

MATERIALS AND METHODS

Theoretical calculations were performed using Mathematica version 5.1 (Wolfram Research, Champaign, IL). The experimental data presented in this study was obtained according to Morfill and colleagues [1]. In the following paragraphs we briefly discuss the experimental setup and data analysis.

DNA constructs. DNA oligomers **1**: SH-5'-TTT TTT TTT TTT TTT TTT TTC GTT GGT GCG GAT ATC TCG GTA GTG GGA TAC GAC GAT ACC GAA GAC AGC TCA TGT TAT ATT ATG-3', **2**: SH-5'-TTT TTT TTT TTA TCC CAC TAC CGA GAT ATC CGC ACC AAC G-3' and **3**: SH-5'-TTT TTT TTT TCC GAG ATA TCC GCA CCA ACG-3' were purchased HPLC grade from IBA GmbH (Goettingen, Germany).

Preparation of slides and cantilevers. The used oligonucleotides modified with a thiol group at their 5'-termini were immobilized on amino-functionalized surfaces using a hetero-bifunctional poly(ethylene glycol) (PEG) spacer [2]. Oligonucleotide **1** was immobilized on the cantilever and oligonucleotide **2**, respectively **3**, was coupled to the surface. Before use, the cantilevers (Bio-lever, Olympus) were cleaned as described earlier [3]. After this cleaning procedure, amino-modified cantilevers were prepared using 3-aminopropyldimethylethoxysilane (ABCR GmbH, Karlsruhe, Germany). For the surface-coupling of oligonucleotide **2**, respectively **3**, commercially available amino-functionalized slides (Slide A, Nexterion, Mainz, Germany) were used. From now on, both surfaces (cantilever and slide) were treated in parallel as described previously [4]. They were incubated in borate buffer pH 8.5 for 1 h in order to deprotonate the amino groups to ensure coupling to the N-hydroxysuccinimide (NHS) groups of the heterobifunctional NHS-PEG-maleimide (molecular weigh, 5000 g/mol; Nektar, Huntsville, AL). After dissolving the PEG at a concentration of 50 mM in borate buffer at pH 8.5, this solution was incubated on the surfaces for 1 h. In parallel, the thiol groups of oligonucleotides **1**, **2** and **3** were recovered from disulfide bonds. Oligonucleotides were reduced using tris (2-carboxyethyl) phosphine hydrochloride beads (Perbio Science, Bonn, Germany). After washing the surfaces with ultrapure water, a solution of the oligonucleotides **1** and **2**, respectively **3**, (1.75 mM) was incubated on the cantilever tip and the surfaces for 1 h. During this incubation time, the free functional maleimide group of the PEG was allowed to react with the 5'-thiol end of the respective oligonucleotide, yielding a thioester bond. Finally, the cantilever and the surfaces were rinsed with PBS to remove noncovalently bound oligonucleotides and stored in PBS until use.

Force spectroscopy. The force measurements were performed in PBS containing 150 mM NaCl at room temperature using an MFP-3D AFM (Asylum Research, Santa Barbara, CA). Cantilever spring constants were measured as described previously [5] [6]. During one experiment, the approach and retract velocity were held constant. To obtain measurements over a broad range of different loading rates, several experiments were performed each at a different retract velocity ranging from 50 nm/s to 10 mm/s.

Data Analysis. The obtained data were converted into force-extension curves. From these force-extension curves, the rupture force (the force at which the dsDNA separates into two single strands) and the corresponding loading rate were determined using the software Igor Pro 5.0 (Wavemetrics, Lake Oswego, OR) and a custom-written set of procedures. The rupture force is defined as described previously [7]. To determine the loading rate, the freely jointed chain model was used, according to previous studies [9].

POLYMER MODELS

Herein, we employ polymer extension models for B-DNA, S-DNA and single stranded DNA according to the three-state equilibrium model of Cocco and colleagues [8]. The poly(ethylene-glycol) is modeled according to Oesterhelt and colleagues [9].

Double-stranded B-DNA. B-DNA elasticity is very well described by chain bending fluctuations leading to an entropic elasticity, while elastic stretching of the double helix generates the roughly linear stretching between 20 and 50 pN with a spring constant per base pair of f_B/C_B =1200/0.34 pN/nm. According to previous work [10], the extension per base-pair is

$$x_B(f) = C_B\left(1 - \sqrt{\frac{k_B T}{4 A_B f}} + \frac{f}{f_B}\right),$$

where the persistence length is A_B = 50 nm, the force constant f_B = 1230 pN and the contour length C_B = 0.34 nm. The free energy correspondingly becomes

$$w_B(f) = -\int_{f'=0}^{f} x_B(f')\, df'$$

Double-stranded S-DNA. For S-DNA elasticity a linear response to elongation was suggested [8] with an extension per base pair of

$$x_S(f) = x_1 + \frac{f - f_1}{S}.$$

and a free energy function of

$$w_S(f) = w_B(f_0) - \tfrac{1}{2}\left((x_o + x_1)(f_1 - f_0) + 2x_1(f - f_1) + (f - f_1)^2 / S\right)$$

where the parameters are x_0 = 0.32 nm, x_1 = 0.58 nm, f_0 = 62 pN, f_1 = 68 pN and S = 4700 pN/nm. The values for f_0 and f_1 are salt dependent parameters and given for a salt concentration of 500 mM. They shift down by 5 pN for each decade reduction in NaCl concentration. Thus the above set of parameters is chosen such that experimental data on the B-S transition, the salt dependence [11] and the stretching data for forces between 68 and 150 pN [12] are reproduced well.

Single-stranded DNA. The ssDNA polymer model is phenomenological [8] and includes the logarithmic dependence of extension on force seen at >50 mM NaCl concentration [13] as well as the reduction in contour length generated at low force by self-adhesion ("folding") of the chain. The extension per base pair is

$$x_{ss}(f) = C_{ss}\left(\frac{a_1 \ln\left(f/f_1\right)}{1 + a_3 \mathrm{Exp}\left(-f/f_3\right)}\right),$$

where C_{ss} = 0.34 nm, a_1 = 0.21, a_2 = 0.34, f_1 = 0.0037 pN, f_2 = 2.9 pN and f_3 = 8000 pN. The parameter a_3 = 2.1 ln(M/0.0025)/ln(0.15/0.0025)-0.1 depends on NaCl concentration M (mol). The free energy correspondingly becomes

$$w_{ss}(f) = -\int_{f'=0}^{f} x_{ss}(f')\, df'.$$

Poly(ethylene glycol). For the PEG extension per monomer we used a two state model develop by Oesterhelt and colleagues [1].

$$x_{PEG}(f) = \left(\frac{C_{planar}}{\mathrm{Exp}\left(\Delta G(f)/k_B T\right)+1} + \frac{C_{helical}}{\mathrm{Exp}\left(-\Delta G(f)/k_B T\right)+1}\right)\cdot\left(\coth\left(\frac{f \cdot A_{PEG}}{k_B T}\right) - \frac{k_B T}{f \cdot A_{PEG}}\right) + \frac{f}{K_{PEG}},$$

where C_{planar} = 3.58 A, $C_{helical}$ = 2.8 A, A_{PEG} of 7 A, K_{PEG} = 150 N/m and

$$\Delta G(f) = \Delta G_0 - f\left(C_{planar} - C_{helical}\right),$$

where ΔG_0 = 3.3 $k_B T$. This model takes into account that the PEG monomers appear in two conformations.

PARTITION SUM CORRECTIONS

Boundary Condition. The partition sum of Equation 8 does not account for the boundary conditions at the end of the DNA duplex yet. As boundary conditions, we therefore introduce two additional base-pairs at $i = 0$ and $i = N + 1$, which are single stranded. The partition sum Z' including the two boundary base pairs becomes

$$Z' = \sum_{\substack{all\,matrix\\ elements}} \begin{bmatrix} 0 & 0 & 0 \\ 0 & 0 & 0 \\ \exp\left(-w_{ss}(f) - C_{ds-ss}\right) & \exp\left(-w_{ss}(f) - C_{ds-ss}\right) & \exp\left(-w_{ssDNA}(f)\right) \end{bmatrix} \times Z \times \begin{bmatrix} 0 & 0 & 0 \\ 0 & 0 & 0 \\ 0 & 0 & \exp\left(-w_{ssDNA}(f)\right) \end{bmatrix}.$$

Strand-separated states. All states with less than two remaining base-pairs are already strand separated. We subtract the Boltzmann probabilities of these states from the partition sum such that the partition sum that we use for all further calculations becomes

$$Z'' = Z' - \left(Z_0 + Z_1\right),$$

where $Z_0 = \sum_{\substack{all\,matrix\\ elements}} \begin{bmatrix} 0 & 0 & 0 \\ 0 & 0 & 0 \\ 0 & 0 & \exp\left(-w_{ss}(f)\right) \end{bmatrix} \times \begin{bmatrix} 0 & 0 & 0 \\ 0 & 0 & 0 \\ \exp\left(-w_{ss}(f) - C_{ds-ss}\right) & \exp\left(-w_{ss}(f) - C_{ds-ss}\right) & \exp\left(-w_{ss}(f)\right) \end{bmatrix}^{N+1} \times$

and $Z_1 = \sum_{i=1}^{N} \sum_{\substack{all\,matrix\\ elements}} \begin{bmatrix} 0 & 0 & 0 \\ 0 & 0 & 0 \\ \exp\left(w_{ss}(f) - C_{ds-ss}\right) & \exp\left(w_{ss}(f) - C_{ds-ss}\right) & \exp\left(w_{ss}(f)\right) \end{bmatrix}^{i} \times \begin{bmatrix} 0 & 0 & 0 \\ 0 & 0 & 0 \\ \exp\left(w_{ss}(f) - C_{ds-ss}\right) & \exp\left(w_{ss}(f) - C_{ds-ss}\right) & \exp\left(w_{ss}(f)\right) \end{bmatrix} \times \begin{bmatrix} 0 & 0 & 0 \\ 0 & 0 & 0 \\ \exp\left(w_{ss}(f) - C_{ds-ss}\right) & \exp\left(w_{ss}(f) - C_{ds-ss}\right) & \exp\left(w_{ss}(f)\right) \end{bmatrix}^{N-i} \cdot \begin{bmatrix} 0 & 0 & 0 \\ 0 & 0 & 0 \\ 0 & 0 & \exp\left(w_{ss}(f)\right) \end{bmatrix}$

TRANSITION STATE THEORY

Equilibrium Flux. The equilibrium flux is simply the sum of the Boltzmann probabilities of al states s_{tst} times the base pair opening rate:

$$k(f) = \left\langle \delta\left[n - n_{tst}\right] \dot{n}_+ \right\rangle_{equilibrium}$$

$$= \frac{1}{Z(f)} \sum_{s_{tst}} \dot{n}_+ \exp\left(-\Delta G_{total}(s_{tst}, f)\right)$$

$$k(f) = \frac{1}{Z''} \dot{n}_+ \sum_{k=1}^{N-1} \sum_{\substack{all\,matrix \\ elements}} \begin{bmatrix} 0 & 0 & 0 \\ 0 & 0 & 0 \\ \exp\left(-g_{ss}(f) - C_{ds-ss}\right) & \exp\left(-g_{ss}(f) - C_{ds-ss}\right) & \exp\left(-g_{ss}(f)\right) \end{bmatrix}^{k} \times$$

$$\begin{bmatrix} \exp\left(-g_B(f) + J_k\right) & \exp\left(-g_B(f) + J_k - C_{B-S}\right) & \exp\left(-g_B(f) - C_{ds-ss}\right) \\ \exp\left(-g_S(f) + J_k - C_{B-S}\right) & \exp\left(-g_S(f) + J_k\right) & \exp\left(-g_S(f) - C_{ds-ss}\right) \\ 0 & 0 & 0 \end{bmatrix} \times$$

$$\begin{bmatrix} \exp\left(-g_B(f) + J_{k+1}\right) & \exp\left(-g_B(f) + J_{k+1} - C_{B-S}\right) & \exp\left(-g_B(f) - C_{ds-ss}\right) \\ \exp\left(-g_S(f) + J_{k+1} - C_{B-S}\right) & \exp\left(-g_S(f) + J_{k+1}\right) & \exp\left(-g_S(f) - C_{ds-ss}\right) \\ 0 & 0 & 0 \end{bmatrix} \times$$

$$\begin{bmatrix} 0 & 0 & 0 \\ 0 & 0 & 0 \\ \exp\left(-g_{ss}(f) - C_{ds-ss}\right) & \exp\left(-g_{ss}(f) - C_{ds-ss}\right) & \exp\left(-g_{ss}(f)\right) \end{bmatrix}^{N-k-1} \times \begin{bmatrix} 0 & 0 & 0 \\ 0 & 0 & 0 \\ 0 & 0 & \exp\left(-g_{ss}(f)\right) \end{bmatrix}$$

Thermodynamic Equilibrium Prevails. To appropriately describe the separation of dsDNA employing the canonical transition state theory, thermodynamic equilibrium must prevail within the binding potential. Two scenarios would contradict such an assumption: Either, the changes of state occurred on timescales equal to or slower than the rate of escape or if, in order to reach the transition states, an intermediate free energy barrier needs to be crossed. In the following, we discuss these scenarios and conclude that, for the experimentally observed force range between 0 and 100 pN, the canonical transition state theory is applicable.

The changes in state from dsDNA to ssDNA occur at base-pair opening and closing rates. Within the present work, we assumed that these rates are in the order of 10^8 s^{-1}. From our numerical calculations, we deduce that the base-pair opening rate is about two orders of magnitude faster than the rate at which short dsDNA dissociates for forces below 100 pN. We therefore conclude that the escape process does not critically disturb the thermodynamic equilibrium.

Due to the base-pair heterogeneity the transition state might only be reached by crossing intermediate free energy barriers [8]. In this case, this intermediate barrier crossing would become rate limiting and the

populations of states would not be Boltzmann distributed. In order to investigate this effect, we calculated the free energy as a function of the open base-pairs explicitly for the two dsDNAs used here (Figure S1). Hereby, we neglected the simultaneous formation of more than one DNA bubble. Figure S1b illustrates that no significant energy barriers appear for forces up to 100 pN.

Since the changes in state occur much faster than the separation of the strands and, apart from the transition state, no significant energy barriers arises along the reaction coordinate, we conclude that the canonical transition state theory is appropriate for modeling the rate of strand separation for tens of base-pair long dsDNA. However, for forces significantly higher than 100 pN, the requirements for the canonical transition state theory fail: The rate of escape becomes comparable to the timescale of internal fluctuations, i.e. the base-pair opening and closing rates. Further, rate-dominating barriers apart from the transition state arise. Both effects result in a significant perturbation of the equilibrium distribution and consequently in the breakdown of the canonical transition state theory.

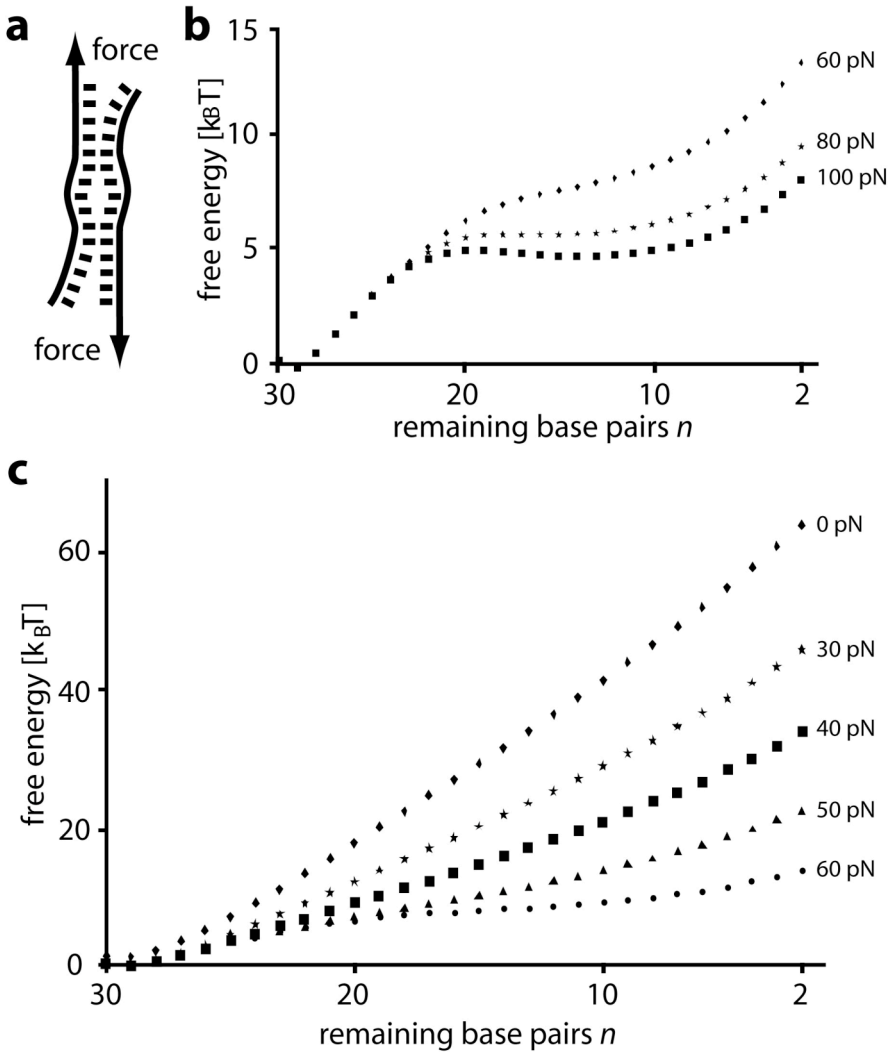

Figure S1. (a) The calculated energy landscape collapsed onto one coordinate *n*, the number of remaining base pairs, is calculated from equilibrium theory. Thereby, we allow the double strand to open up from its ends as well as to form a bubble of ssDNA. In order to speed up the numerical calculations, we do not account for the simultaneous opening of more than one bubble. (b) Free energy landscape of the **1**·**2** DNA duplex at 60, 80 and 100 pN calculated from the partition sum. (c) Free energy landscape of the **1**·**2** DNA duplex at forces smaller than 60 pN. The transition state is located at n_{tst} = 2 and no significant barriers apart from the transition state are observed for forces up to 100 pN.

REFERENCES

[1] Morfill, J., F. Kuhner, K. Blank, R. Lugmaier, J. Sedlmair and H. E. Gaub. 2007. B-S Transition in Short Oligonucleotides. Biophys. J. 93:2400-2409.

[2] Kuehner, F., J. Morfill, R. A. Neher, K. Blank, and H. E. Gaub. 2007. Force-induced DNA slippage. Biophys. J. 92:2491–2497.

[3] Neuert, G., C. Albrecht, E. Pamir, and H. E. Gaub. 2006. Dynamic force spectroscopy of the digoxigenin-antibody complex. FEBS Lett. 580:505–509.35.

[4] Blank, K., J. Morfill, and H. E. Gaub. 2006. Site-specific immobilization of genetically engineered variants of Candida Antarctica lipase B. ChemBioChem. 7:1349–1351.11180–11186.

[5] Butt, H. J., and M. Jaschke. 1995. Calculation of thermal noise in atomic-force microscopy. Nanotechnology. 6:1–7.

[6] Hugel, T., and M. Seitz. 2001. The study of molecular interactions by AFM force spectroscopy. Macromol. Rapid Commun. 22:989–1016.

[7] Evans, E., and K. Ritchie. 1999. Strength of a weak bond connecting flexible polymer chains. Biophys. J. 76:2439–2447.

[8] Cocco, S., J. Yan, J. Léger, D. Chatenay, J. Marko. 2004. Overstretching and force-driven strand separation of double-helix DNA. Phys. Rev. E. 70:011910.

[9] Oesterhelt, F., M. Rief, and, H. E. Gaub. 1999. Single molecule force spectroscopy by AFM indicates helical structure of poly(ethylene- glycol) in water. N. J. Phys. 1:1–11.

[10] Marko, J., and E. Siggia. 1995. Stretching DNA. Macromolecules. 28:8759-8770.

[11] Wenner, J. R., M. C. Williams, I. Rouzina, and V. A. Bloomfield. 2002. Biophys. J. 82:3160.

[12] Leger, J.-F., G. Romano, A. Sarkar, J. Robert, L. Bourdieu, D. Chatenay, and J. F. Marko. 1999. Phys. Rev. Lett. 83:1066.

[13] Y. Zhang, H. J. Zhou, and Z. C. Ou-Yang. 2001. Biophys. J. 81:1133.

Appendix B

Invited Publications

B.1 Publication 5: Molekularer Kraftsensor: Quantifizierung biomolekularer Wechselwirkungen im Parallelformat

Katja Falter and Hermann E. Gaub;
Biospektrum, 2011, Vol. 6, 662-664

Appendix C

Manuscripts

C.1 Manuscript M1: A force-based, parallel assay for the quantification of protein-DNA interactions

Katja Limmer, Diana Pippig, Daniela Aschenbrenner and Hermann E. Gaub;
PLOS one, accepted January 2014

A force-based, parallel assay for the quantification of protein-DNA interactions

Katja Limmer[1,2], Diana Pippig[1], Daniela Aschenbrenner[1] and Hermann E. Gaub[1,3]

[1] Lehrstuhl für Angewandte Physik and Center for Nanoscience (CeNS), Ludwig-Maximilians-Universität, Amalienstraße 54, 80799 München, Germany

[2] Munich Center for Integrated Protein Science (CIPSM)

[3] Corresponding author: Gaub@lmu.de

Abstract

Analysis of transcription factor binding to DNA sequences is of utmost importance to understand the intricate regulatory mechanisms that underlie gene expression. Several techniques exist that quantify DNA-protein affinity, but they are either very time-consuming or suffer from possible misinterpretation due to complicated algorithms or approximations like many high-throughput techniques. We present a more direct method to quantify DNA-protein interaction in a force-based assay. In contrast to single-molecule force spectroscopy, our technique, the Molecular Force Assay (MFA), parallelizes force measurements so that it can test one or multiple proteins against several DNA sequences in a single experiment. The interaction strength is quantified by comparison to the well-defined rupture stability of different DNA duplexes. As a proof-of-principle, we measured the interaction of the zinc finger construct Zif268/NRE against six different DNA constructs. We could show the specificity of our approach and quantify the strength of the protein-DNA interaction.

Introduction

The sequence-specific interaction of certain proteins with the genomic DNA is prerequisite for the complex task of transcriptional regulation. Those transcription factors bind alone or in clusters to the DNA and can thus activate or impede transcription. Many of the transcription factors can bind to several, different DNA sequence motifs with varying strength [1]. Recent studies suggest that not only strong interactions between transcription factors and the DNA influence gene expression, but that weak interactions significantly contribute to transcriptional regulation and are evolutionary conserved [2]. Quantitative models support the importance of weak interactions and show that correct

recapitulation of transcriptional processes is only possible by including low-affinity transcription factor binding sites in their calculations [3]. Hence, in order to get a comprehensive picture of transcriptional regulation, it is essential to quantify the interaction of a broad range of transcription factors with all possible DNA sequences.

Recent developments in high-throughput techniques, for example the *in vivo* method chromatin immunoprecipitation combined with microarray analysis (ChIP-chip) [4,5] or sequencing (ChIP-seq) [6] or *in vitro* techniques like protein binding microarrays (PBM) [7-10] have greatly increased our knowledge about various transcription factor binding sites. However, in most instances these techniques lack the ability to accurately quantify the protein-DNA interaction or require complicated algorithms and approximations to do so. Various methods exist to characterize the protein-DNA interactions by measuring thermodynamic and kinetic constants, for example electrophoretic mobility shift assay (EMSA) or surface plasmon resonance. Yet their common drawback is the low throughput that makes it nearly impossible to analyze a transcription factor against a whole genome. Two techniques have made huge advances in bridging the gap between measuring thermodynamic constants and high throughput, namely mechanically induced trapping of molecular interactions (MITOMI) [11] and high-throughput sequencing - fluorescent ligand interaction profiling (HiTS-FLIP) [12]. Both can determine dissociation constants of several transcription factors against thousands of DNA sequences (MITOMI) or of one protein against millions of DNA motifs (HiTS-FLIP), but require some approximations in order to calculate dissociation constants in a high-throughput format (MITOMI) or need a washing step that interferes with the analysis of transient interactions (HiTS-FLIP).

Importantly, due to the high concentration of DNA in a bacterial cell or eukaryotic nucleus, the dynamic equilibrium between unbound and bound activated transcription factors is shifted towards DNA-protein complexes. Hence, affinity described by the dissociation constant might not be the best measure to characterize the protein-DNA interaction inside a nucleus. The specificity defined as the ability of a transcription factor to discriminate between a regulatory sequence and the vast majority of non-regulating DNA might be a more suitable quantity. But quantification of the specificity in that sense means to determine the complete list of dissociation constants for all possible DNA sequences or a constant calculated from those dissociation constants [13]. Therefore, a method that determines the specificity in a single measurement is highly desirable considering the number of transcription factors and possible genomic sequences. Since the force required to break a bond increases with decreasing

potential width, a more localized interaction between protein and DNA as it is expected for a sequence specific interaction will result in a higher unbinding force. Thus, a possibility for describing the specificity arises out of the binding strength between a protein and a DNA motif that is accessible in force-based measurements. Single-molecule force spectroscopy experiments allow the characterization of a protein-DNA bond in great detail [14-18] but are very time consuming and therefore not the appropriate tool to analyze the binding properties of a transcription factor against a whole genome.

The Molecular Force Assay (MFA) developed in our lab [19,20] parallelizes single-molecule force experiments. It relies on the principle of comparing the interaction in question with a well-defined reference bond. We here describe a new application of the MFA to quantify binding strengths of several DNA-protein complexes directly and in parallel. This should contribute to a more conclusive and complete understanding of transcriptional regulation. In an adaptation of the original setup, we demonstrate in a proof-of principle experiment that we are able to determine the binding strength of a zinc finger protein against several DNA sequences in a single measurement.

Zinc finger motifs are one of the most abundant DNA binding domains in eukaryotic transcription factors [21]. The protein in our experiment Zif268/NRE is an artificial fusion protein of two zinc fingers of the Cys_2-His_2 class [22]. Zif268 is a transcription factor in mouse and a popular model system due to the existence of structural data of the protein-DNA complex [21,23]. NRE is an engineered variant of Zif268 that binds specifically and with high affinity to a nuclear receptor element [24]. Our force-based design allows us to characterize the interaction of this six zinc finger protein with three DNA binding motifs, a high affinity sequence, a low affinity sequence and a no binding sequence, by a single value that can be directly correlated to the binding strength. Additionally, we show that we could gain further information about differences in the binding strength by varying the reference bond between a 20 base pair (bp) DNA sequence and a 40 bp DNA sequence. This demonstrates the possibility to convert the measured binding strength into intuitive units of DNA base pairs binding strength. Hence, this new variant of the MFA can quantify DNA-protein interaction and describe the binding strength in a simple picture by correlating it to the average binding strength of a certain number of DNA base pairs.

Results and Discussion

The standard Molecular Force Assay (MFA) consists of two molecular bonds in series, a reference and a sample bond, clamped between two surfaces. The two surfaces are separated with a constant velocity so that a force builds up in the two molecular bonds until the weaker one ruptures. A fluorophore conjugated to the linker sequence between the two molecular complexes indicates the intact molecular bond. Hence, the ratio of the fluorescence intensity before and after the force loading of the molecular constructs is a measure of the strength of the sample bond in comparison to the reference bond. An alternative view of this assay is that the force greatly enhances the off rate of the bond under investigation and reduces the otherwise extremely long spontaneous dissociation times towards seconds [25]. As every molecular complex is tested against its own reference bond, the measurement is a single-molecule experiment that can be conducted in parallel with several thousand constructs. If oligonucleotide sequences are used for sample and reference complex, different binding sequences for ligands can be introduced in the sample bond so that a strengthening of the sample bond can be detected upon binding. Thus, the dissociation constant for ligands like polyamides [26] or proteins [27] was determined and an ATP-aptamer [28] as well as the interaction of the protein Dicer with double-stranded RNA [29] was characterized. Additionally, the reference bond can be varied in length and thus in the binding strength the sample bond is compared to. Hence, it was possible in former studies to quantify the increase of the sample bond strength upon ligand binding to the stability of 9.5 base pairs for a polyamide and to 27.7 base pairs for the protein EcoRI [30]. In a subsequent experiment integrated in a microfluidic setup, the binding of EcoRI to two sample bonds with different affinity was tested against four different reference bonds in a single measurement and the stabilization of the sample bonds was quantified in units of DNA base pairs. [31].

In the configuration of the MFA used in all former studies, the ligand-DNA interaction is not directly probed, but the ligand stabilizes the molecular bond and is thus detected. We here describe our new variant of the MFA that can probe the protein-DNA interaction directly and compare it to a reference bond. For this purpose, the fusion protein construct consisting of an N-terminal ybbR-tag [32] followed by a superfolderGFP [33] variant and the six zinc finger construct ZIF268/NRE [22] (details can be found in the supplement) is covalently attached via the ybbR-tag to a glass slide coated with Coenzyme A in a 4x4 pattern [34]. The two double-stranded DNA complexes in series are covalently attached to the 16 pillars of a soft PDMS surface with the upper one as reference bond and the lower one as sample bond (see Figure 1A). The DNA sequences in shear geometry are separated by a linker sequence to which a Cy5 fluorophore is conjugated. Due to the macrostructure of the PDMS

stamp (see Figure 1A) a maximum of 16 combinations of different reference sequences as well as sample sequences can be tested within one experiment (Figure 1A). The PDMS surface is carefully brought into contact with the glass slide so that the sample sequence is able to bind to the protein on the glass slide (Figure 1B). This process is controlled via reflection interference contrast microscopy [35]. The GFP signal is used to place the protein spots below the stamp pillars functionalized with the different DNA sequences. After 10 minutes, the PDMS surface is retracted with constant velocity by a Piezo actuator. Thereby, a force is applied to the protein-sample complex as well as to the reference bond until the weaker one ruptures (Figure 1C). The fluorescence Cy5 signal on the glass slide is measured by an inverted epi-fluorescence microscope and indicates the number of intact protein-DNA complexes. Thus, the protein-DNA interaction is directly probed and compared to a well-characterized DNA double strand. In order to approximate the environment in a eukaryotic nucleus we designed our experiments as a competition assay and pre-incubated the zinc finger protein with low-molecular weight DNA from salmon sperm before the contact process. Details on the surface funtionalization, molecular constructs, contact and separation process as well as the fluorescence read-out are described in the supplement.

In a first test of our assay, we determined the binding of the zinc finger protein to a no binding sequence and a high affinity binding motif. The bond strength was compared to two reference sequences, a 20 bp double-stranded DNA and a 40 bp double-stranded DNA, both in shear geometry, by measuring the Cy5 fluorescence intensity of the transferred DNA after the contact and separation process. Figure 2 displays the results for all possible combinations of sample and reference bond. For the no binding sequence, only very little signal is measured. It hardly exceeds the background value of about 1000 – 2000 counts of pixel intensity so that false positives of unspecific interactions between the zinc finger protein with no binding sequences can be excluded in our assay. The high affinity sequence on the other hand clearly bound to the protein and the upper reference bond ruptured in most cases so that Cy5 labeled DNA was transferred to the glass slide. Additionally, a difference between the two reference bonds is evident. The weaker reference of 20 bp ruptured more often, yielding 17000 counts of transferred DNA on the slide. The stronger reference exceeds the binding strength of the protein-high affinity sequence interaction in more cases than the weaker reference, yielding distinctly less fluorescence signal of 13000 counts. These results of our first test confirm the specificity and feasibility of our approach for quantifying DNA-protein binding strength by means of the MFA and varying reference bonds.

In order to calculate a single, comparable number for the binding strength, environmental differences like the binding density of protein and oligonucleotide constructs on the surfaces have to be taken into account. In order to correct for differences in protein density on the glass slide, 0.5µM of a Cy5 labeled 40 bp DNA duplex carrying a high affinity binding site for the protein in question is added subsequent to the force probe experiment to saturate all functional proteins bound to the surface. Calibration measurements confirmed a complete saturation after 30 min incubation time. After removing unbound fluorophores by a washing step, the fluorescence on the glass slide is determined again. It is a measure for the maximum number of functional proteins on the slide. Since the binding density of the DNA complexes on the PDMS always exceeds the number of functional proteins on the glass slide, further corrections are not necessary. The ratio of fluorescence signal on the glass slide directly after the rupture event $F_{transfer}$ to the maximal number of functional proteins $F_{intact\ protein}$ is defined as the Normalized Fluorescence, NF. The NF is calculated by dividing the pictures after background subtraction pixel-by-pixel (see Figure 3A), which cancels out inhomogeneities and renders this method robust. Histograms of the NF picture are generated and fitted by a Gaussian to yield the NF mean and standard deviation (Figure 3B). Thus, every mean value of the NF is the result of several million tested molecular constructs (more details about the statistics can be found in the supplement). This number can be interpreted as the binding strength of the protein-DNA interaction in comparison to a certain reference bond. A variation of the reference bond will result in a different NF and refines the information of the DNA-protein interaction. We tested our zinc finger protein against three DNA double strands incorporating either a high affinity sequence, a low affinity sequence or a no binding sequence against two reference bonds, a 20 bp and a 40 bp DNA double strand and analyzed the data in the way just described (the exact sequences are shown in the supplement in Figure S1). The results of one example experiment are depicted in Figure 3C. Due to the low DNA transfer for the no binding sequence, a calculation of the NF was not possible, so we set these values to zero. Differences are clearly visible for the NF values for the low and high affinity sequences as well as for the variations of the reference bond. As expected, we measured the highest value of 0.65±0.07 for the high affinity sequence against the 20 bp reference bond compared to 0.39±0.15 for the low affinity sequence against the same reference bond. The stronger reference bond lowers the values to 0.32±0.01 and 0.20±0.02 for high and low affinity DNA motifs, respectively. For both DNA binding motifs, the mean NF is reduced by half if the number of reference base pairs is doubled: 0.65 (20bp) to 0.32 (40 bp) for the high affinity motif and 0.39 (20bp) to 0.20 (40bp). Hence, a linear relationship between the number

of reference base pair and the mean NF can be assumed in this range of reference bond length. This result does not mean that the strength of the protein-DNA bond is altered by different reference bonds. The comparison of the protein-DNA bond with different reference bonds yields different NF values that draw a more detailed picture of the protein-DNA interaction and enables to adjust the setup to the biological problem. A linear relationship between the NF and number of base pairs in the reference duplex makes it possible to adjust the reference duplexes until the NF yields a value of 0.5 so that the reference duplex of a certain number of base pairs has the same stability as the protein-DNA bond. Thus, the protein-DNA bond strength can be directly quantified with the stability of a certain number of base pairs. In our proof-of principle experiment, we compare the stability of a protein-DNA interaction with varying affinities to the stability of two DNA duplexes of different lengths. Interestingly, the NF values for the low affinity sequence against the 20 bp reference bond, 0.39, and for the high affinity sequence against the 40 bp reference bond, 0.32, are equal within errors (see Figure 3C). This allows the interpretation of a difference in binding strength of the zinc finger protein with these two DNA motifs that corresponds to the average binding strength of a 20 bp DNA double strand. Thus, we demonstrated that the specificity of DNA-protein interactions can be quantified via the binding strength in a force-based assay in a single measurement. Further, we can characterize the binding strength in a simple picture by correlating it to the average binding strength of a certain number of DNA base pairs.

Conclusion

We described a new variant of the MFA that allows to directly detect the binding strength of protein-DNA interactions. This force-based format can test several DNA sequences against a protein in parallel with good statistics and can characterize the binding strength descriptively by correlating it to the average binding strength of a certain number of DNA base pairs. As a proof-of-principle, we could quantify the interactions of a zinc finger protein with three DNA sequences and compare them against two reference bonds. The resolution of the assay depends on the biological problem and the strength of the reference duplex. It was already demonstrated that the MFA can detect a single nucleotide polymorphism in a 20 base pair DNA duplex [19]. Shorter reference duplexes or a reference duplex in zipper geometry can discriminate between very small differences in the strength of the protein-DNA complexes invoked for example by a single base pair variation in the DNA target sequence. Further experiments will identify the capabilities and limitations of the assay for different DNA-protein

complexes. For a complete characterization of a protein's binding specificity and affinity, it is necessary to probe the interactions with DNA sequences representative of a whole genome. This is, in principle, feasible with our force-based design. We have already shown that much smaller geometries for the DNA spots are sufficient to calculate the NF [27] and the fabrication of DNA microarrays is a standard procedure. Furthermore, our lab succeeded in integrating the MFA in a microfluidic chip [31]. The utilized surface chemistry also allows for the measurement of several proteins in a single experiment. Thus, our force-based assay can quantify protein-DNA interactions in a parallel format. It has the potential, with further developments in miniaturization and parallelization, to improve our understanding of transcriptional regulation.

Acknowledgements

The authors thank Marcus Otten and Mathias Strackharn for helpful discussions. K.L. is grateful to the Elite Network of Bavaria (IDK-NBT) for a doctoral fellowship.

References

1. Badis G, Berger MF, Philippakis AA, Talukder S, Gehrke AR, et al. (2009) Diversity and complexity in DNA recognition by transcription factors. Science 324: 1720-1723.

2. Tanay A (2006) Extensive low-affinity transcriptional interactions in the yeast genome. Genome Res 16: 962-972.

3. Segal E, Raveh-Sadka T, Schroeder M, Unnerstall U, Gaul U (2008) Predicting expression patterns from regulatory sequence in Drosophila segmentation. Nature 451: 535-540.

4. Ren B, Robert F, Wyrick JJ, Aparicio O, Jennings EG, et al. (2000) Genome-wide location and function of DNA binding proteins. Science 290: 2306-2309.

5. V. Iyer CH, C. Scafe, D. Botstein, M.Snyder, P. Brown (2001) Genomic binding sites of the yeast cell-cycle transcription factors SBF and MBF. Nature 409: 533-538.

6. Park PJ (2009) ChIP-seq: advantages and challenges of a maturing technology. Nat Rev Genet 10: 669-680.

7. Bulyk ML, Huang X, Choo Y, Church GM (2001) Exploring the DNA-binding specificities of zinc fingers with DNA microarrays. Proc Natl Acad Sci U S A 98: 7158-7163.

8. Mukherjee S, Berger MF, Jona G, Wang XS, Muzzey D, et al. (2004) Rapid analysis of the DNA-binding specificities of transcription factors with DNA microarrays. Nat Genet 36: 1331-1339.

9. Berger MF, Philippakis AA, Qureshi AM, He FS, Estep PW, 3rd, et al. (2006) Compact, universal DNA microarrays to comprehensively determine transcription-factor binding site specificities. Nat Biotechnol 24: 1429-1435.

10. Berger MF, Bulyk ML (2009) Universal protein-binding microarrays for the comprehensive characterization of the DNA-binding specificities of transcription factors. Nat Protoc 4: 393-411.

11. Fordyce PM, Gerber D, Tran D, Zheng J, Li H, et al. (2010) De novo identification and biophysical characterization of transcription-factor binding sites with microfluidic affinity analysis. Nat Biotechnol 28: 970-975.

12. Nutiu R, Friedman RC, Luo S, Khrebtukova I, Silva D, et al. (2011) Direct measurement of DNA affinity landscapes on a high-throughput sequencing instrument. Nat Biotechnol 29: 659-664.

13. Stormo GD, Zhao Y (2010) Determining the specificity of protein-DNA interactions. Nat Rev Genet 11: 751-760.

14. Steven J. Koch AS, Benjamin C. Jantzen, Michelle D. Wang (2002) Probing protein-DNA Interactions by Unzipping a Single DNA Double Helix. Biophysical Journal 83: 1098-1105.

15. Bartels FW, Baumgarth B, Anselmetti D, Ros R, Becker A (2003) Specific binding of the regulatory protein ExpG to promoter regions of the galactoglucan biosynthesis gene cluster of Sinorhizobium meliloti - a combined molecular biology and force spectroscopy investigation. Journal of Structural Biology 143: 145-152.

16. Kuhner F, Costa LT, Bisch PM, Thalhammer S, Heckl WM, et al. (2004) LexA-DNA bond strength by single molecule force spectroscopy. Biophys J 87: 2683-2690.

17. Bizzarri AR, Cannistraro S (2010) The application of atomic force spectroscopy to the study of biological complexes undergoing a biorecognition process. Chem Soc Rev 39: 734-749.

18. Moy VT, Florin EL, Gaub HE (1994) Intermolecular forces and energies between ligands and receptors. Science 266: 257-259.

19. Albrecht C, Blank K, Lalic-Multhaler M, Hirler S, Mai T, et al. (2003) DNA: a programmable force sensor. Science 301: 367-370.

20. Blank K, Mai T, Gilbert I, Schiffmann S, Rankl J, et al. (2003) A force-based protein biochip. Proc Natl Acad Sci U S A 100: 11356-11360.

21. Nikola P. Pavletich COP (1991) Zinc Finger-DNA Recognition: Crystal Structure of a Zif268-DNA Complex at 2.1 A. Science 252: 809-817.

22. Jin-Soo Kim COP (1998) Getting a handhold on DNA: Design of poly-zinc finger proteins with femtomolar dissociation constant. Proc Natl Acad Sci 95: 2812-2817.

23. Elrod-Erickson M, Rould MA, Nekludova L, Pabo CO (1996) Zif268 protein-DNA complex refined at 1.6 A: a model system for understanding zinc finger-DNA interactions. Structure 4: 1171-1180.

24. Greisman HA, Pabo CO (1997) A general strategy for selecting high-affinity zinc finger proteins for diverse DNA target sites. Science 275: 657-661.

25. Carrion-Vazquez M, Oberhauser AF, Fowler SB, Marszalek PE, Broedel SE, et al. (1999) Mechanical and chemical unfolding of a single protein: a comparison. Proc Natl Acad Sci U S A 96: 3694-3699.

26. Ho D, Dose C, Albrecht CH, Severin P, Falter K, et al. (2009) Quantitative detection of small molecule/DNA complexes employing a force-based and label-free DNA-microarray. Biophys J 96: 4661-4671.

27. Severin PM, Ho D, Gaub HE (2011) A high throughput molecular force assay for protein-DNA interactions. Lab Chip 11: 856-862.

28. Ho D, Falter K, Severin P, Gaub HE (2009) DNA as a force sensor in an aptamer-based biochip for adenosine. Anal Chem 81: 3159-3164.

29. Limmer K, Aschenbrenner D, Gaub HE (2013) Sequence-specific inhibition of Dicer measured with a force-based microarray for RNA ligands. Nucleic Acids Res 41: e69.

30. Severin PM, Gaub HE (2012) DNA-Protein Binding Force Chip. Small.

31. Otten M, Wolf P, Gaub HE (2013) Protein-DNA force assay in a microfluidic format. Lab Chip 13: 4198-4204.

32. Yin J, Lin AJ, Golan DE, Walsh CT (2006) Site-specific protein labeling by Sfp phosphopantetheinyl transferase. Nat Protoc 1: 280-285.

33. Pedelacq JD, Cabantous S, Tran T, Terwilliger TC, Waldo GS (2006) Engineering and characterization of a superfolder green fluorescent protein. Nat Biotechnol 24: 79-88.

34. Wong LS, Thirlway J, Micklefield J (2008) Direct site-selective covalent protein immobilization catalyzed by a phosphopantetheinyl transferase. J Am Chem Soc 130: 12456-12464.

35. Wiegand GN, K.R.; Sackmann, E. (1998) Microinterferometry: three-dimensional reconstruction of surface microtopography for thin-film and wetting studies by interference contrast microscopy (RICM). Appl Opt 37: 6892-6905.

Figures

Figure 1

Description of the Molecular Force Assay (MFA). (A) The geometries of the PDMS stamp and the 4x4 pattern of protein spots on the glass slide are displayed. The zinc finger protein is covalently bound to an amino-coated glass slide functionalized with Coenzyme A via a ybbR-tag. A superfolderGFP acts as an additional spacer and helps to adjust the glass slide beneath the pads of the stamp. Different combinations of reference sequences and DNA binding motifs are attached to each pillar. (B) The PDMS stamp is carefully brought into contact with the glass slide and the DNA sample bonds are allowed to bind to the protein. Subsequently, the PDMS stamp is retracted with constant velocity so that a force builds up in the DNA-protein complexes and the reference bonds until the weaker construct ruptures. (C) After the force probe, the fluorescence signal on the glass slide is a measure for the number of intact protein-DNA bonds.

Figure 2

Transfer of Cy5-labeled DNA to the glass slide. After the contact and separation process, the fluorescence intensity of Cy5 on the glass slide is determined. Histograms of selected areas (without prior background subtraction) show a very modest signal slightly above the background signal (1000-2000 counts) for the DNA harboring the no binding sequences for the protein in question. DNA with a high affinity sequence did bind the protein in question and a transfer signal is clearly visible. The images are optimized in contrast to make the transfer of the no binding sequence as well as the difference in fluorescence signal between the no binding sequence and high affinity motif visible. A first assessment of the binding strength is possible by varying the reference bond. The weaker reference of 20 bp shows a higher fluorescence intensity of 17000 counts compared to the stronger reference of 40 bp with 13000 counts.

Figure 3

Quantification of the binding strength. (A) In order to quantify the binding strength, the flurorescence signal representing the DNA transfer has to be normalized to the number of available protein binding sites. For this purpose, a Cy5-labeled 40bp DNA duplex harboring a high affinity binding motif is added subsequently to the force measurement in order to saturate all functional proteins. Following a washing protocol to remove all unbound DNA strands, the fluorescence intensity

is measured a second time. After background subtraction, the fluorescence intensity of transferred DNA is divided by the signal corresponding to all functional proteins, yielding the Normalized Fluorescence NF. (B) Histograms of every pad on the PDMS stamp sum up the huge number of single-molecule experiments and are fitted by a Gaussian distribution in order to calculate an average NF and the standard deviation. Here, the histogram of the NF displayed in A is shown in detail. (C) One example measurement is displayed as a proof-of-principle. Details to the statistics are described in the supplement. The NF for the no binding sequences is too little to render fitting procedures possible. So we approximate the NF to be zero. Differences between low and high affinity binding motifs are very pronounced. A variation of the reference bond between 20 and 40 bp shear shows that the NF of the low affinity sequence against a 20 bp shear is about the same a the NF of the high affinity sequence against a 40 bp shear. This can be descriptively interpreted such that the difference in binding strength of the zinc finger protein with a low affinity sequence compared to a high affinity sequence corresponds to the stability of 20 bp DNA duplex.

Figure 1

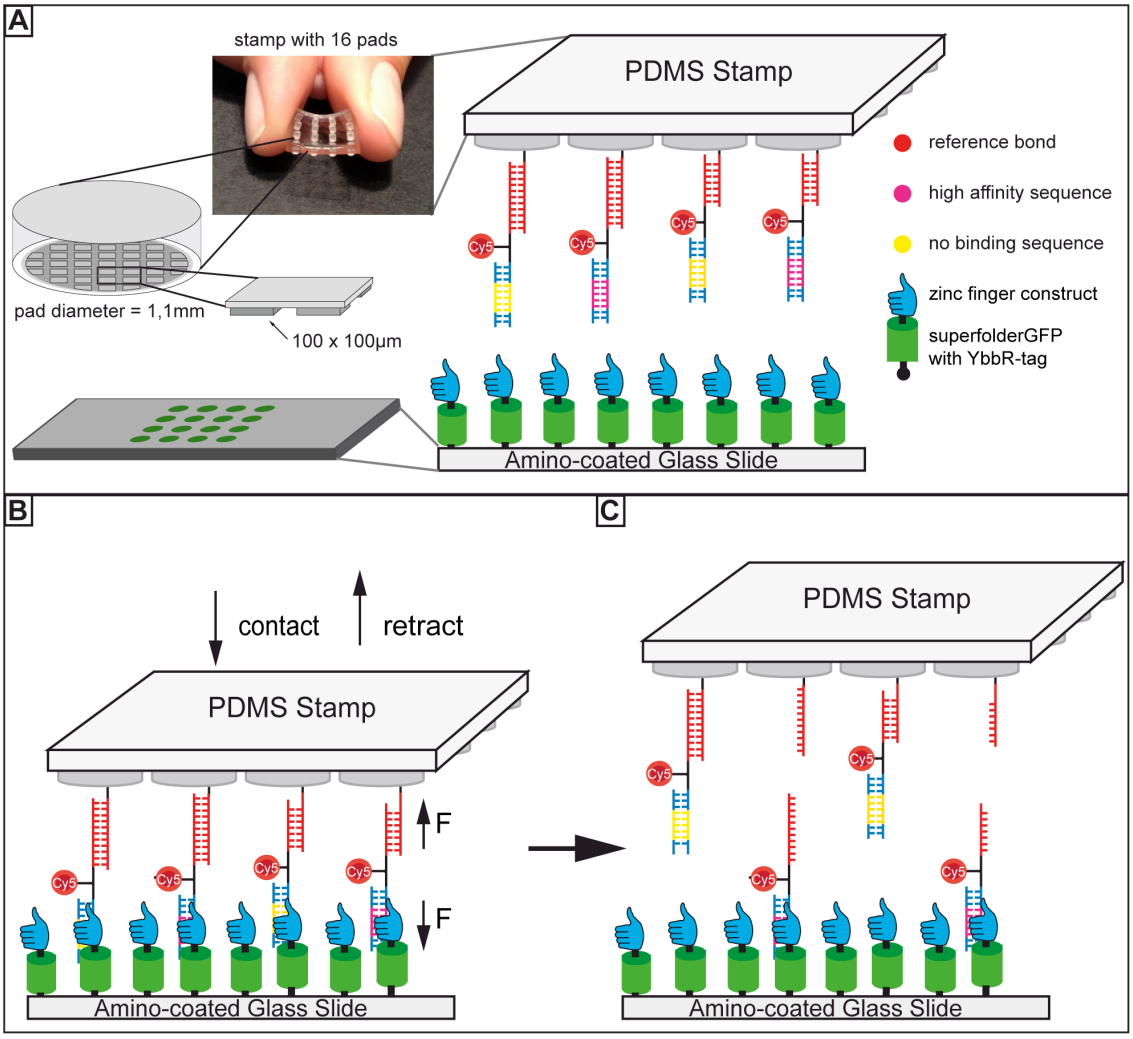
A
stamp with 16 pads
PDMS Stamp
reference bond
high affinity sequence
no binding sequence
zinc finger construct
superfolderGFP
with YbbR-tag
pad diameter = 1,1mm
100 x 100µm
Cy5
Amino-coated Glass Slide
B
contact
retract
PDMS Stamp
F
F
Amino-coated Glass Slide
C
PDMS Stamp
Amino-coated Glass Slide

Figure 2

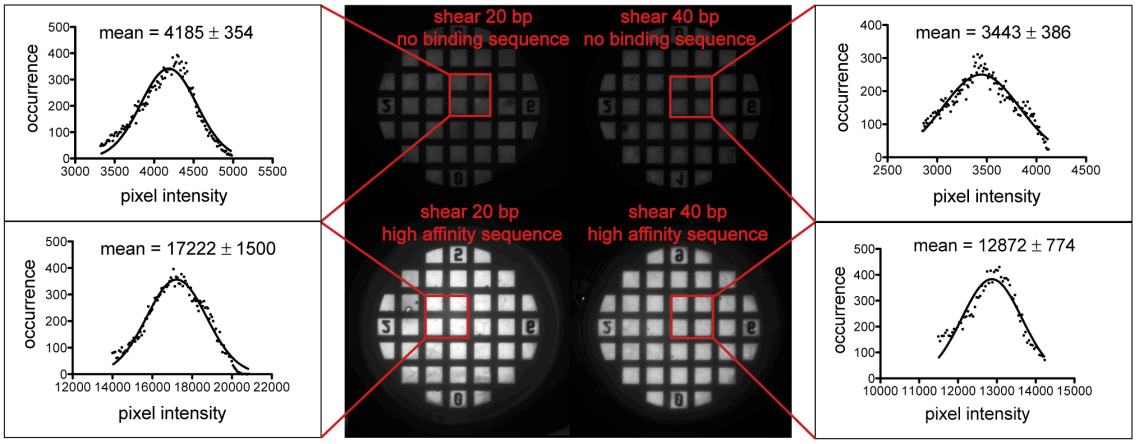
shear 20 bp
no binding sequence
shear 40 bp
no binding sequence
shear 20 bp
high affinity sequence
shear 40 bp
high affinity sequence
mean = 4185 ± 354
mean = 3443 ± 386
mean = 17222 ± 1500
mean = 12872 ± 774
occurrence
pixel intensity

Figure 3

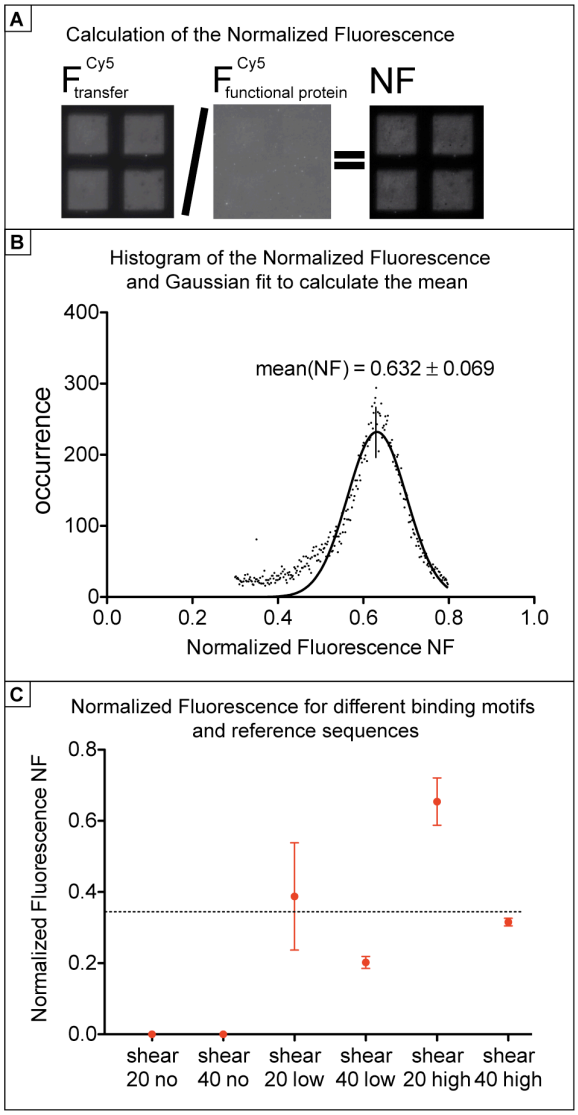
A
Calculation of the Normalized Fluorescence
F Cy5 transfer
F Cy5 functional protein
NF
B
Histogram of the Normalized Fluorescence and Gaussian fit to calculate the mean
mean(NF) = 0.632 ± 0.069
occurrence
400
300
200
100
0
0.0
0.2
0.4
0.6
0.8
1.0
Normalized Fluorescence NF
C
Normalized Fluorescence for different binding motifs and reference sequences
Normalized Fluorescence NF
0.8
0.6
0.4
0.2
0.0
shear 20 no
shear 40 no
shear 20 low
shear 40 low
shear 20 high
shear 40 high

-

Supplement

Methods and Materials

Oligonucleotide constructs

The molecular complexes consist of three strands that are successively hybridized in shear geometry prior to usage. The uppermost strand which is covalently bound to the PDMS stamp is modified with an amino-group. Spacer18, a hexaethylene glycol chain of 18 atoms length, acts as an additional spacer between the amino-group and the oligonucleotides in order to avoid surface effects. Furthermore, poly-T stretches link the double-stranded sequences to the surfaces and each other. The cyanine dye Cy5 is attached by an N-Hydroxysuccinimide ester to the middle strand between the two duplexes.The reference bond is varied in length between 20 and 40 basepairs in order to test the protein-DNA bond against different strengths. The sample bond varies in its sequence in order to analyze the binding behavior of the protein against a high affinity DNA, 5′–caacaggtaac**aagggttca**g**gcgtgggcg**ttcgcgaagg–3', a low affinity DNA, 5'–caacaggtaac**aagtggtca**g**gcgaggtcg**ttcgcgaagg–3', and a no binding sequence, 5'–caacagtaacagagtgcaagccgtgagcttgccgcgaagg–3'. The complete DNA constructs are dispalyed in Figure S1. All oligonulceotide constructs, including modified ones, were obtained from biomers.net GmbH, Germany.

Protein construct

A fusion protein construct consisting of an N-terminal ybbR-tag [1] (DSLEFIASKLA) followed by a superfolderGFP variant [2] and the six zinc finger protein construct Zif268/NRE (with an RQKDGERP linker sequence between the Zif268 and NRE moieties) [3] was cloned into pGEX6P2 between BamHI and XhoI sites similar to [4] . All construct fragments were amplified from synthetic templates (Mr.Gene or Geneart, Lifetechnologies, UK). The resulting fusion protein (ybbR-sfGFP-Zif268/NRE) harbored a GST-tag and was expressed in *E.coli* BL21 DE3 Codon Plus cells (Agilent Technologies, USA). One liter of SB medium was inoculated with 10ml of an overnight culture and grown at 37°C. When an OD_{600} of 0.7 had been reached, over night expression at 18°C was induced by adding 0.25mM IPTG. Cells were lyzed in 50mM TRIS-HCl (pH 7.5, 300 mM NaCl, 2mM DTT, 5% Glycerol, 10µM $ZnCl_2$) by a French pressure cell press. The ybbR-GFP-zinc finger construct was obtained in the soluble fraction

and purified by Glutathione affinity chromatography on GSTrap columns (GE Healthcare, Germany) according to standard procedures. After over night treatment with PreScission protease the GST-tag was removed and the protein further purified by Heparin cation exchange chromatography (HiTrap Heparin, GE Healthcare, Germany). Following preparative size exclusion chromatography on a HiLoad 16/60 Superdex 75 column (GE Healthcare, Germany) in 50mM TRIS-HCl (pH7.5, 150mM NaCl, 2mM DTT, 10µM $ZnCl_2$, 5% Glycerol) the protein construct was concentrated to 10µM by ultrafiltration in Amicon Ultra centrifugal filter units (Merck Millipore, USA) and stored at -80°C until further usage.

Stamp preparation

Micro-and macrostructured poly(dimethylsiloxane) (PDMS) stamps were fabricated by casting 1:10 crosslinker/base (Sylgard, Dow Corning, MI, USA) into a custom-made Pyrex/silicon wafer (HSG-IMIT, Germany) according to standard procedures [5]. The resulting PDMS stamps feature pillars of 1mm diameter and height with a spacing of 3mm in a square pattern on a 3mm thick basis and are cut in pieces of 4x4 pillars. The flat surface of the pillars is microstructured with 100µm x 100µm pads separated by 41µm wide and 5µm deep rectangular trenches enabling the drainage of liquid during the contact and separation process (Figure 1A). For the surface functionalization, the cleaned stamp surface was first activated in 12.5% HCl overnight and derivatized with (3-glycidoxypropyl)-trimethoxysilane (ABCR, Germany) in order to generate epoxide groups. After 30 minutes at 80°C in an Argon atmosphere, the functionalized stamp was allowed to cool down to room temperature. The amino-modified DNA strand, dissolved in water, was diluted 1:10 in a sodium borate-buffer (50mM H_3BO_3, 50mM $Na_2B_4O_7$•10 H_2O pH=9.0; Carl Roth GmbH & Co. KG, Germany) to a concentration of 10µM and 1.5µl was transferred to every pillar on the stamp. Overnight incubation of the stamp under humid conditions allowed the amino-groups to react with the epoxide-groups. Oligonucleotides that did not bind to the stamp were washed off the next day in an aqueous solution of 0.01% SDS (sodium dodecyl sulphate; Sigma-Aldrich GmbH, Germany). The other two DNA strands were pre-incubated in 5x SSC buffer (saline sodium citrate; 750mM sodium chloride, 75mM trisodium citrate; Sigma-Aldrich GmbH, Germany) in a concentration of 0.2µM. 1.5µl was transferred to every pillar of the stamp. After a minimum of 60 minutes incubation time the functionalized stamp was washed with 0.05% Tween 20 (VWR Scientific GmbH, Germany) in 1x SSC and gently dried with N_2 gas.

Slide preparation

Conventional glass slides for microscopy were aminosilanized in our lab: After thorough cleaning by sonication in 50% (v/v) 2-propanol in ddH20 for 15 min and oxidation in a solution of 50% (v/v) hydrogen peroxide (30%) and sulfuric acid for 30 min, they were washed with ddH2O and dried in a nitrogen stream. For the silanization, the glass slides were soaked for 1 h in a solution of 90% (v/v) ethanol, 8% ddH2O and 2% 3-aminopropyldimethylepoxysilane (ABCR, Germany). Subsequently they were washed twice in 2-propanol and ddH2O and dried at 80 °C for 40 min. They can be stored for several weeks in an Argon atmosphere at room temperature.

For further functionalisation, the amino-silanized glass slide was first deprotonated in a sodium borate buffer (50mM H_3BO_3, 50mM $Na_2B_4O_7$•10 H_2O pH=8.5; Carl Roth GmbH & Co. KG, Germany) for 30 minutes, then a heterobifunctional PEG crosslinker with N-hydroxy succinimide and maleimide groups (MW 5000, Rapp Polymere, Germany) was applied for 1 h at 30mM. The slide was thoroughly washed with ddH20 and gently dried with N2, before it was incubated another hour with Coenzyme A (Merck Millipore, USA) dissolved in coupling buffer (50mM $NaHPO_4$, 50mM NaCl, 10mM EDTA at pH=7.2). Again the slide was washed with ddH2O and gently dried with N_2. At this stage, the slide can be stored up to several days.

The Zif268/NRE protein aliquot at a concentration of 10µM is spun down in a table top centrifuge to remove agglomerates and the supernatant was diluted in a 50mM TRIS-HCl buffer (pH=7.5, 150mM NaCl, 10mM $MgCl_2$, 10µM $ZnCl_2$, 2mM DTT) to a final concentration of 2.5µM. Furthermore, low molecular weight DNA from salmon sperm (Sigma-Aldrich GmbH, Germany) was added in a concentration of 1g/ml. After a short incubation time of 15 minutes, 1,5 µl of Phosphopantetheinyltransferase Sfp was added to the sample and 2µl droplets of the mix were transferred to the functionalized glass slide in a 4x4 pattern. Sfp reacted the Coenzyme A on the glass slide to the ybbR-tag of the protein in humid atmosphere at room temperature during three hours incubation time. A PMMA mask with a well for the 4x4 pattern of spotted protein sample was fixed to the glass slide with a silicone lip seal. The mask prevented samples from drying out during following washing procedures and the MFA experiment. All protein that did not bind to the surface was washed off by 25ml 50mM TRIS-HCl buffer (pH=7.5, 150mM NaCl, 10µM $ZnCl_2$), 25ml 100mM TRIS-HCl buffer (pH=7.5, 300mM NaCl, 10µM $ZnCl_2$) and again 25ml 50mM TRIS-HCl buffer (pH=7.5, 150mM NaCl, 10µM $ZnCl_2$). The last buffer was also used for the MFA experiments. After the washing procedure, the samples were measured within 3 hours.

Contact process and fluorescent read-out

The functionalized stamp adhered upside-down to the glass block glued to a closed-loop piezoelectric actuator (PZ 400, Piezo Systems Jena, Germany) and a DC motorized translation stage (Physik Instrumente GmbH, Germany). The slide with the oligonucleotide constructs was fixed beneath the stamp on a stainless steel stage with permanent magnets. The fluorescent signal of the superfolderGFP fused between the ybbR-Tag and the zinc finger protein was used to place every protein spot beneath the right stamp pillar. The whole contact device is mounted on an inverted microscope (Axio Observer Z1, Carl Zeiss MicroImaging GmbH, Germany) with an xy-DC motorized high-accuracy translation stage (Physik Instrumente GmbH, Germany). Contact was made by means of the piezo and care was taken that each individual pillar is not compressed more than 3µm. The planar adjustment of stamp and slide as well as the contact process were controlled by reflection interference contrast microscopy [6]. In order to let the protein bind to the DNA sample sequence on the PDMS stamp, the contact between stamp and slide was maintained for 10 minutes. The piezo retracted the stamp with a velocity of 1µm/s in all experiments. A force buildt up in the molecular complexes until the weaker bond, either the protein-DNA complex or the reference bond, broke with higher probability. A Cy5 fluorophor conjugated to the linker sequence between the two DNA double strands indicated the intact bond. Hence, the Cy5 fluorescent intensity $F_{transfer}$ on the glass slide was measured with a CCD camera (ANDOR iXon, Andor, Northern Ireland) after the contact and separation process. In order to normalize the signal of the intact protein-DNA complexes to the protein density on the glass slide, the sample was subsequently incubated with a 40 bp double-stranded DNA sequence containing the high affinity binding site and labeled with a Cy5 fluorophor in a concentration of 0.5µM for 30 minutes. Unbound dsDNA was removed by the following washing procedure: 25ml 50mM TRIS-HCl buffer (pH=7.5, 150mM NaCl, 10µM $ZnCl_2$), 25ml 100mM TRIS-HCl buffer (pH=7.5, 300mM NaCl, 10µM $ZnCl_2$) and again 25ml 50mM TRIS-HCl buffer (pH=7.5, 150mM NaCl, 10µM $ZnCl_2$). The Cy5 fluorescent intensity was measured again and gives the number of possible protein binding sites. Since the binding density of the DNA complexes on the PDMS always exceeds the number of functional proteins on the glass slide, further corrections are not necessary. The ratio of fluorescence signal on the glass slide directly after the rupture event $F_{transfer}$ to the maximal number of functional proteins $F_{intact\ protein}$ is defined as the Normalized Fluorescence, NF. The NF is calculated by dividing the pictures after background subtraction pixel-by-pixel by a custom-built software written in

Labview. Histograms of the NF picture are generated and fitted by a Gaussian to yield the NF mean and standard deviation.

Statistics

In every experiment, every pillar of the PDMS stamp can be functionalized with a different combination of reference and sample complex. In our proof-of principle measurements we usually bind the same combination of sample and reference bond to at least two pillars for better statistics. The contact area of a pillar is (100x100 μm^2 x 25)= $25x10^4$ μm^2. From the fluorescence signal of the functional protein we can estimate a lower bound for the density of functional protein on the glass slide of 10^3 per μm^2. Thus, every pillar tests around $25x10^7$ molecular complexes and the NF is the mean of $25x10^7$ tested molecular complexes. In order to demonstrate the validity of our approach to quantify the specificity of the protein-DNA interaction in a single measurement with good statistics, we show the result of one example measurement. Every data point is the average of two mean NF values. All NF values in this measurement are very close except the one for the low affinity binding motif against the 20bp reference. Other experiments yielded results in good agreement with the displayed experiment.

References

1. Yin J, Lin AJ, Golan DE, Walsh CT (2006) Site-specific protein labeling by Sfp phosphopantetheinyl transferase. Nat Protoc 1: 280-285.

2. Pedelacq JD, Cabantous S, Tran T, Terwilliger TC, Waldo GS (2006) Engineering and characterization of a superfolder green fluorescent protein. Nat Biotechnol 24: 79-88.

3. Jin-Soo Kim COP (1998) Getting a handhold on DNA: Design of poly-zinc finger proteins with femtomolar dissociation constant. Proc Natl Acad Sci 95: 2812-2817.

4. Strackharn M, Pippig DA, Meyer P, Stahl SW, Gaub HE (2012) Nanoscale arrangement of proteins by single-molecule cut-and-paste. J Am Chem Soc 134: 15193-15196.

5. Xia YaW, George M (1998) Soft Lithography. Annu Rev Mater Sci 28: 153-184.

6. Wiegand GN, K.R.; Sackmann, E. (1998) Microinterferometry: three-dimensional reconstruction of surface microtopography for thin-film and wetting studies by interference contrast microscopy (RICM). Appl Opt 37: 6892-6905.

Figure S1

DNA sequences. The molecular constructs with all modifications are displayed. The reference bond comprises the same sequence for all six constructs, but differs in the length of the middle strand. The ZIF268/NRE high affinity sequence is shown in red. The mutations for the low affinity sequence and the no binding sequence are colored green.

Figure S1

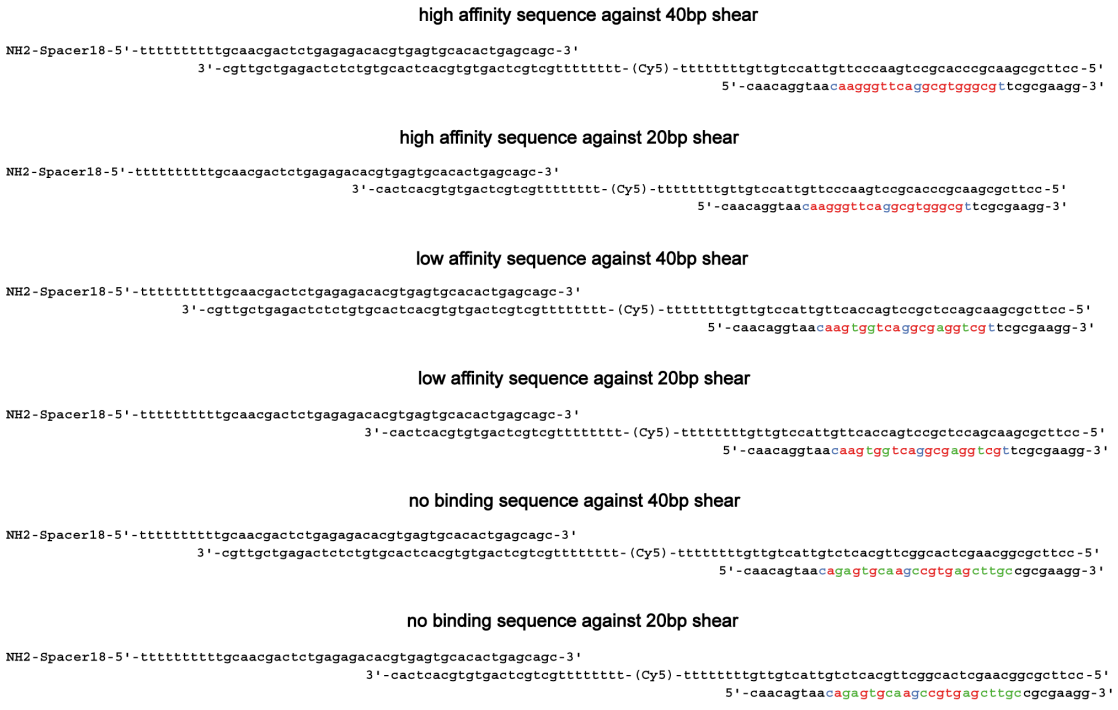

Bibliography

[1] National human genome research institute. http://www.genome.gov, May 2012.

[2] W T Astbury. X-ray studies of nucleic acids. *Symp Soc Exp Biol*, (1):66–76, 1947.

[3] M H F Wilkins and J T Randall. Crystallinity in sperm heads: molecular structure of nucleoprotein in vivo. *Biochim Biophys Acta*, 10(1):192–3, Jan 1953.

[4] J D Watson and F H Crick. Molecular structure of nucleic acids; a structure for deoxyribose nucleic acid. *Nature*, 171(4356):737–8, Apr 1953.

[5] G. Binnig, C. F. Quate, and Ch. Gerber. Atomic force microscope. *Phys. Rev. Lett.*, 56:930–933, Mar 1986.

[6] G U Lee, L A Chrisey, and R J Colton. Direct measurement of the forces between complementary strands of DNA. *Science*, 266(5186):771–3, Nov 1994.

[7] M Rief, H Clausen-Schaumann, and H E Gaub. Sequence-dependent mechanics of single DNA molecules. *Nat Struct Biol*, Jan 1999.

[8] J Morfill, F Kuhner, K Blank, R. A Lugmaier, J Sedlmair, and H. E Gaub. B-S transition in short oligonucleotides. *Biophysical Journal*, 93(7):2400–2409, May 2007.

[9] E L Florin, V T Moy, and H E Gaub. Adhesion forces between individual ligand-receptor pairs. *Science*, 264(5157):415–7, Apr 1994.

[10] V T Moy, E L Florin, and H E Gaub. Intermolecular forces and energies between ligands and receptors. *Science*, 266(5183):257–9, Oct 1994.

[11] J Fritz, A G Katopodis, F Kolbinger, and D Anselmetti. Force-mediated kinetics of single p-selectin/ligand complexes observed by atomic force microscopy. *Proc Natl Acad Sci U S A*, 95(21):12283–8, Oct 1998.

[12] Paul J Bujalowski and Andres F Oberhauser. Tracking unfolding and refolding reactions of single proteins using atomic force microscopy methods. *Methods*, 60(2):151–60, Apr 2013.

[13] M Benoit, D Gabriel, G Gerisch, and H E Gaub. Discrete interactions in cell adhesion measured by single-molecule force spectroscopy. *Nat Cell Biol*, 2(6):313–7, Jun 2000.

[14] Martin Benoit and Hermann E Gaub. Measuring cell adhesion forces with the atomic force microscope at the molecular level. *Cells Tissues Organs*, 172(3):174–89, 2002.

[15] S K Kufer, E M Puchner, H Gumpp, T Liedl, and H E Gaub. Single-molecule cut-and-paste surface assembly. *Science*, 319(5863):594–6, Feb 2008.

[16] Stefan K Kufer, Mathias Strackharn, Stefan W Stahl, Hermann Gumpp, Elias M Puchner, and Hermann E Gaub. Optically monitoring the mechanical assembly of single molecules. *Nature Nanotech*, page 5, Nov 2008.

[17] Mathias Strackharn, Diana A Pippig, Philipp Meyer, Stefan W Stahl, and Hermann E Gaub. Nanoscale arrangement of proteins by single-molecule cut-and-paste. *J Am Chem Soc*, 134(37):15193–6, Sep 2012.

[18] Mario B Viani, Tilman E Schäffer, Ami Chand, Matthias Rief, Hermann E Gaub, and Paul K Hansma. Small cantilevers for force spectroscopy of single molecules. *Journal of Applied Physics*, 86(4):5, Jul 1999.

[19] Keir C Neuman and Attila Nagy. Single-molecule force spectroscopy: optical tweezers, magnetic tweezers and atomic force microscopy. *Nat Methods*, 5(6):491–505, Jun 2008.

[20] Christian Albrecht, Kerstin Blank, Mio Lalic-Mühltaler, Siegfried Hirler, Thao Mai, Ilka, Susanne Schiffmann, Tom Bayer, Hauke, and Hermann E Gaub. DNA: A programmable force sensor. *Science*, 301(5631):367–370, Jul 2003.

[21] K Blank, T Mai, I Gilbert, S Schiffmann, J Rankl, R Zivin, C Tackney, T Nicolaus, K Spinnler, F Oesterhelt, M Benoit, H Clausen-Schaumann, and H E Gaub. A force-based protein biochip. *Proc Natl Acad Sci USA*, 100(20):11356–60, Sep 2003.

[22] Christian Dose, Dominik Ho, HermannE. Gaub, PeterB. Dervan, and ChristianH. Albrecht. Recognition of "mirror-image" DNA by small molecules. *Angew. Chem. Int. Ed.*, 46(44):8384–8387, Nov 2007.

[23] Dominik Ho, Christian Dose, Christian H Albrecht, Philip Severin, Katja Falter, Peter B Dervan, and Hermann E Gaub. Quantitative detection of small molecule/DNA complexes employing a force-based and label-free DNA-microarray. *Biophysj*, 96(11):4661–4671, Mar 2009.

[24] Philip M. D Severin, Dominik Ho, and Hermann E Gaub. A high throughput molecular force assay for protein–DNA interactions. *Lab Chip*, 11(5):856, Jan 2011.

[25] Philip M. D Severin and Hermann E Gaub. DNA-protein binding force chip. *Small*, pages n/a–n/a, Aug 2012.

[26] Craig C Mello and Darryl Conte, Jr. Revealing the world of RNA interference. *Nature*, 431(7006):338–42, Sep 2004.

[27] Jeffrey M Friedman and Peter A Jones. MicroRNAs: critical mediators of differentiation, development and disease. *Swiss Med Wkly*, 139(33-34):466–72, Aug 2009.

[28] A Tanay. Extensive low-affinity transcriptional interactions in the yeast genome. *Genome Research*, 16(8):962–972, Jun 2006.

[29] Eran Segal, Tali Raveh-Sadka, Mark Schroeder, Ulrich Unnerstall, and Ulrike Gaul. Predicting expression patterns from regulatory sequence in drosophila segmentation. *Nature*, 451(7178):535–540, Jan 2008.

[30] Victor A. Bloomfield, Donald M. Crothers, and Ignacio Tinoco. *Nucleid Acids: Structures, Properties and Functions*. University Science Books, 2000.

[31] http://de.wikipedia.org/wiki/Desoxyribonukleinsäure and http://en.wikipedia.org/wiki/DNA, November 2013.

[32] Paul W K Rothemund. Folding DNA to create nanoscale shapes and patterns. *Nature*, 440(7082):297–302, Mar 2006.

[33] Shawn M Douglas, Hendrik Dietz, Tim Liedl, Björn Högberg, Franziska Graf, and William M Shih. Self-assembly of DNA into nanoscale three-dimensional shapes. *Nature*, 459(7245):414–8, May 2009.

[34] B Yurke, A J Turberfield, A P Mills, Jr, F C Simmel, and J L Neumann. A DNA-fuelled molecular machine made of DNA. *Nature*, 406(6796):605–8, Aug 2000.

[35] Yamuna Krishnan and Friedrich C Simmel. Nucleic acid based molecular devices. *Angew Chem Int Ed Engl*, 50(14):3124–56, Mar 2011.

[36] Jiří Sponer, Judit E Sponer, Arnošt Mládek, Petr Jurečka, Pavel Banáš, and Michal Otyepka. Nature and magnitude of aromatic base stacking in DNA and RNA: Quantum chemistry, molecular mechanics and experiment. *Biopolymers*, Jun 2013.

[37] S B Smith, Y Cui, and C Bustamante. Overstretching B-DNA: the elastic response of individual double-stranded and single-stranded DNA molecules. *Science*, 271(5250):795–9, Feb 1996.

[38] T Strunz, K Oroszlan, R Schäfer, and H J Güntherodt. Dynamic force spectroscopy of single DNA molecules. *Proc Natl Acad Sci U S A*, 96(20):11277–82, Sep 1999.

[39] C. H Albrecht, G Neuert, R. A Lugmaier, and H. E Gaub. Molecular force balance measurements reveal that double-stranded DNA unbinds under force in rate-dependent pathways. *Biophysical Journal*, 94(12):4766–4774, Mar 2008.

[40] Rupert Krautbauer, Matthias Rief, and Hermann E. Gaub. Unzipping DNA oligomers. *Nanoletters*, 3(4):493–496, 2003.

[41] Neocles B Leontis, Jesse Stombaugh, and Eric Westhof. The non-watson-crick base pairs and their associated isostericity matrices. *Nucleic Acids Research*, 30(16):3497–531, Aug 2002.

[42] http://en.wikipedia.org/wiki/Thymidine and http://en.wikipedia.org/wiki/Uridine, November 2013.

[43] R Stoltenburg, C Reinemann, and B Strehlitz. Selex—a (r)evolutionary method to generate high-affinity nucleic acid ligands. *Biomolecular Engineering*, 24(4):381–403, Oct 2007.

[44] A D Ellington and J W Szostak. In vitro selection of RNA molecules that bind specific ligands. *Nature*, 346(6287):818–22, Aug 1990.

[45] Craig Tuerk and Larry Gold. Systematic evolution of ligands by exponential enrichment: RNA ligands to bacteriophage t4 dna polymerase. *Science*, 249:6, Aug 1990.

[46] A D Ellington and J W Szostak. Selection in vitro of single-stranded DNA molecules that fold into specific ligand-binding structures. *Nature*, 355(6363):850–2, Feb 1992.

[47] Marie-Laure Caparros C. David Allis; Thomas Jenuwein, Danny Reinberg. *Epigenetics*. Cold Spring Harbor Laboratory Press, 2009.

[48] Bruce Alberts, Alexander Johnson, Julian Lewis, Martin Raff, Keith Roberts, and Peter Walter. *The Molecular Biology of The Cell, Fith Edition*. Garland Science, 2008.

[49] Pick-Wei Lau, Keelan Z Guiley, Nabanita De, Clinton S Potter, Bridget Carragher, and Ian J Macrae. The molecular architecture of human dicer. *Nature Publishing Group*, 19(4):436–440, Dec 2167.

[50] A Vermeulen. The contributions of dsRNA structure to dicer specificity and efficiency. *RNA*, 11(5):674–682, May 2005.

[51] Annika Röhl. Cellular processes dependent on the RNAi machinery. http://www.nobelprize.org/nobel_prizes/medicine/laureates/2006/advanced.html.

[52] Haruhiko Siomi and Mikiko C Siomi. On the road to reading the RNA-interference code. *Nature*, 457(7228):396–404, Jan 2009.

[53] Richard W Carthew and Erik J Sontheimer. Origins and mechanisms of miRNAs and siRNAs. *Cell*, 136(4):642–655, Feb 2030.

[54] David P Bartel. MicroRNAs: genomics, biogenesis, mechanism, and function. *Cell*, 116(2):281–97, Jan 2004.

[55] S Vasudevan, Y Tong, and J. A Steitz. Switching from repression to activation: MicroRNAs can up-regulate translation. *Science*, 318(5858):1931–1934, Dec 2007.

[56] U.A. Orom, F.C. Nielsen, and A.H. Lund. MicroRNA-10a binds the 5'utr of ribosomal protein mRNAs and enhances their translation. *Mol Cell*, 30:460–471, May 2008.

[57] M Carrion-Vazquez, A F Oberhauser, S B Fowler, P E Marszalek, S E Broedel, J Clarke, and J M Fernandez. Mechanical and chemical unfolding of a single protein: a comparison. *Proc Natl Acad Sci U S A*, 96(7):3694–9, Mar 1999.

[58] G Wiegand, K R Neumaier, and E Sackmann. Microinterferometry: Three-dimensional reconstruction of surface microtopography for thin-film and wetting studies by reflection interference contrast microscopy (RICM). *Applied optics*, 37(29):6892–905, Oct 1998.

[59] Th. Förster. Zwischenmolekulare Energiewanderung und Fluoreszenz. *Annalen der Physik*, 6(2):55–75, 1948.

[60] Zachary A Gurard-Levin and Milan Mrksich. Combining self-assembled monolayers and mass spectrometry for applications in biochips. *Annu Rev Anal Chem (Palo Alto Calif)*, 1:767–800, 2008.

[61] Ningsheng Shao Yan Yan Jijun Tang, Jianwei Xie. The DNA aptamers that specifically recognize ricin toxin are selected by two in vitro selection methods. *Electrophoresis*, 27(7):1303–1311, 2006.

[62] D E Huizenga and J W Szostak. A DNA aptamer that binds adenosine and ATP. *Biochemistry*, 34(2):656–65, Jan 1995.

[63] C H Lin and D J Patel. Structural basis of DNA folding and recognition in an AMP-DNA aptamer complex: distinct architectures but common recognition motifs for DNA and RNA aptamers complexed to AMP. *Chemistry & Biology*, 4(11):817–32, Nov 1997.

[64] M N Stojanovic, Paloma de Prada, and Donald W Landry. Fluorescent sensors based on aptamer self-assembly. *J. Am. Chem. Soc.*, 122:2, 2000.

[65] D. L. Nelson and M. M. Cox. *Lehninger Principles of Biochemistry*. W. H. Freeman and Company, 2005.

[66] D Fourmy, M I Recht, S C Blanchard, and J D Puglisi. Structure of the a site of escherichia coli 16s ribosomal RNA complexed with an aminoglycoside antibiotic. *Science*, 274(5291):1367–71, Nov 1996.

[67] Peter C Anderson and Sandro Mecozzi. Minimum sequence requirements for the binding of paromomycin to the rRNA decoding site A. *Biopolymers*, 86(2):95–111, Jun 2007.

[68] M I Recht, D Fourmy, S C Blanchard, K D Dahlquist, and J D Puglisi. RNA sequence determinants for aminoglycoside binding to an A-site rRNA model oligonucleotide. *Journal of Molecular Biology*, 262(4):421–36, Oct 1996.

[69] Brian P Davies and Christoph Arenz. A homogenous assay for microRNA maturation. *Angew. Chem. Int. Ed.*, 45(33):5550–5552, Aug 2006.

[70] N P Pavletich and C O Pabo. Zinc finger-DNA recognition: crystal structure of a zif268-DNA complex at 2.1 a. *Science*, 252(5007):809–17, May 1991.

[71] J S Kim and C O Pabo. Getting a handhold on DNA: design of poly-zinc finger proteins with femtomolar dissociation constants. *Proc Natl Acad Sci U S A*, 95(6):2812–7, Mar 1998.

[72] M Elrod-Erickson, M A Rould, L Nekludova, and C O Pabo. Zif268 protein-DNA complex refined at 1.6 a: a model system for understanding zinc finger-DNA interactions. *Structure*, 4(10):1171–80, Oct 1996.

[73] H A Greisman and C O Pabo. A general strategy for selecting high-affinity zinc finger proteins for diverse DNA target sites. *Science*, 275(5300):657–61, Jan 1997.

[74] Jun Yin, Alison J Lin, David E Golan, and Christopher T Walsh. Site-specific protein labeling by SFP phosphopantetheinyl transferase. *Nat Protoc*, 1(1):280–5, 2006.

[75] Jean-Denis Pédelacq, Stéphanie Cabantous, Timothy Tran, Thomas C Terwilliger, and Geoffrey S Waldo. Engineering and characterization of a superfolder green fluorescent protein. *Nat Biotechnol*, 24(1):79–88, Jan 2006.

[76] Marcus Otten, Philip Wolf, and Hermann E Gaub. Protein-DNA force assay in a microfluidic format. *Lab Chip*, 13(21):4198–204, Oct 2013.

Danksagung

In dieser Arbeit stecken neben vielen Stunden im Labor und Herzblut auch unglaublich viel Unterstützung meiner Kollegen, Freunde und Familie. Diesen allen möchte ich an dieser Stelle Danke sagen.

Zu allererst möchte ich mich bei meinem Doktorvater Hermann Gaub bedanken, der mich mit spannenden Projekten gefördert hat und mich in vielen lehrreichen Diskussionen inspiriert und motiviert hat. Besonders hervorheben möchte ich die Unterstützung während und nach der Elternzeit.

Der ganzen Gambicrew gilt mein Dank für die unglaublich gute Atmospähre nicht nur im Labor sonder auch bei Ausflügen, beim gemeinsamen Grillen oder anderen Kochevents. Besonderes möchte ich mich bedanken bei

... Dominik Ho, der mich als Betreuer meiner Diplomarbeit für das Thema begeistert hat, und eine generell super Zeit in jeder Hinsicht.

... Philip Severin und Uta Wienken für interessante Diskussionen und viele gemeinsam verbrachte, nette Stunden auch außerhalb des Labors.

... Daniela Aschenbrenner, meine Super-Diplomandin, die mir nicht nur wissenschaftlich eine unglaublich große Hilfe war, insbesondere in den Schwangerschaften, sondern auch eine gute Freundin geworden ist.

... Anita Ladenburger für ihr großes Engagement in ihrer Bachelorarbeit.

... Mathias Strackharn für viele, hilfreiche Diskussionen, die große Hilfsbereitschaft und gemeinsame Unternehmungen.

... Diana Pippig für die gute Zusammenarbeit beim zinc finger Projekt und die Unterstützung im Chemielabor.

... Katy Ehrlich für ihre Hilfsbereitschaft, besonders bei Problemen mit der englischen Sprache.

... Philip Tinnefeld für die Hilfe und Ratschläge bei Farbstoffproblemen

... Ralf David, Angelika Kardinal und Thomas Nicolaus für die immer freundliche

Unterstützung im Chemielabor

... Matthias Erdmann, Hubert Krammer, Stefan Kufer, Marcus Otten, Ingo Stein, Stefan Stahl, Jan Vogelsang, Franz Weinert, Julia Zimmermann für die gute Zusammenarbeit, viele gemeinsame Mittagessen, lustige Abende und die gute Zeit.

Nicht vergessen werden darf meine Familie, die mich immer unterstützt hat, sei es mit viel Verständnis, Geduld oder Babysitter-Diensten und ohne die das Fertigstellen dieser Arbeit nicht möglich gewesem wäre,

... besonders mein Mann Thomas Limmer, auch für die langen Abende, die wir mit Korrekturlesen verbracht haben.

...meine Eltern Maria und Erwin Falter, die oft eingesprungen sind und sich um Antonia gekümmert haben.

....meine Schwiegereltern Maria und Josef Limmer für das Überlassen des Arbeitszimmers und die große Hilfe bei der Betreuung von Antonia.